

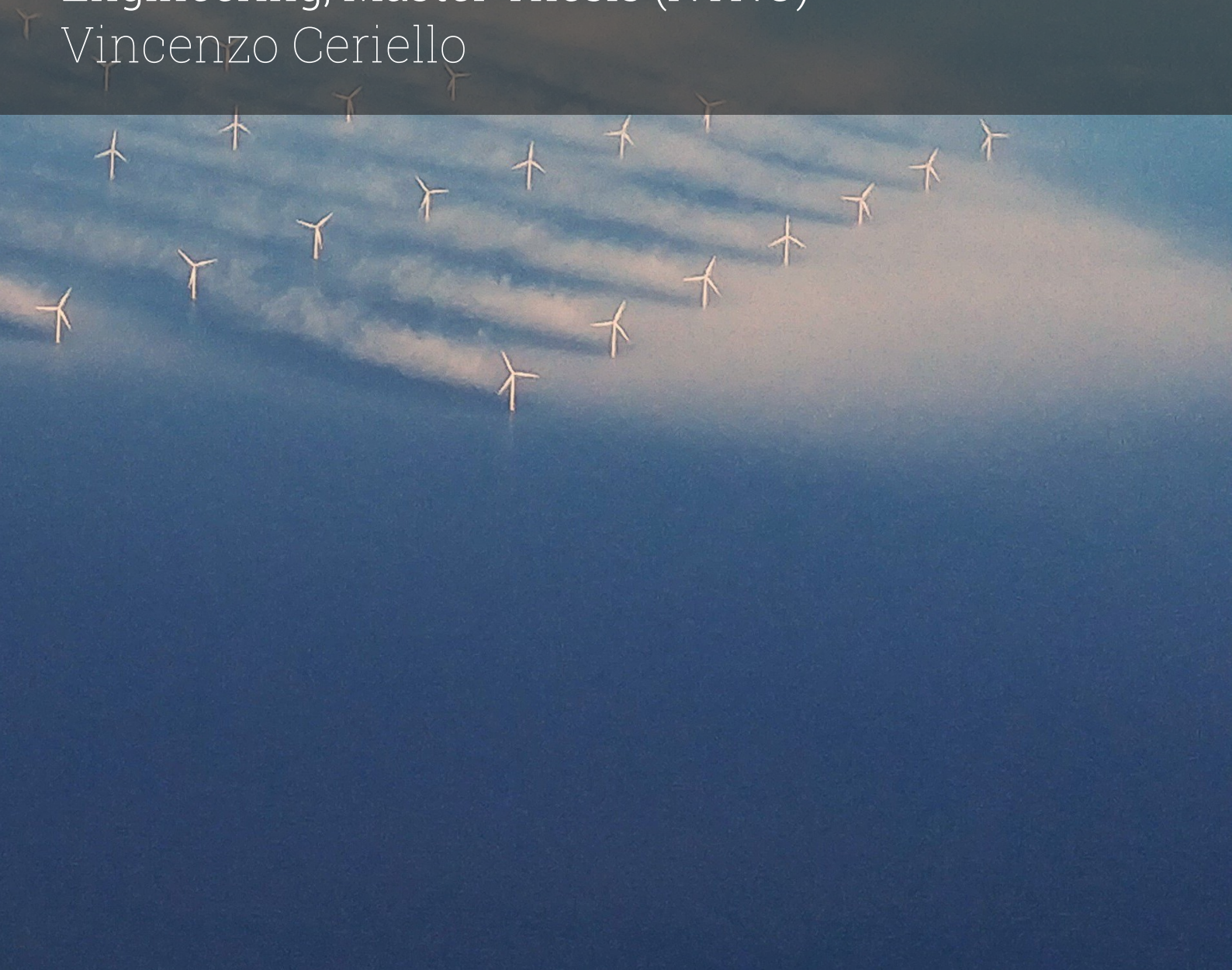
Wake Effect Mitigation of Floating Offshore Wind Farms

Combining Layout Optimization, Turbine
Repositioning and Yaw-based Wake Redirection

OE54030: Master Thesis (TU Delft)

TMR5950: Wind Turbine Energy - Offshore
Engineering, Master Thesis (NTNU)

Vincenzo Ceriello



Wake Effect Mitigation of Floating Offshore Wind Farms

Combining Layout Optimization, Turbine Repositioning and Yaw-based Wake Redirection

by

Vincenzo Ceriello

University	Student Number
TU Delft	5622271
NTNU	582211

Supervisors:

Dr. ir. M. B. Zaaijer

Delft University of Technology

Dr. ir. A. C. Viré

Delft University of Technology

Prof D. T. Nguyen

Norwegian University of Science and Technology

Prof. E. E. Bachynski-Polic

Norwegian University of Science and Technology

The code used for the content provided in this Master's thesis is available at:
<https://github.com/Vincer99/VCeriello-Thesis-Code>

Cover Image: Aerial picture of Horns rev wind farm in Denmark by Vattenfall



Preface

I am humbled to submit this master's thesis as a fulfilment of the requirements for obtaining a master's degree in Offshore and Dredging Engineering from Delft University of Technology, as well as a master's degree in Technology-Wind Energy from the Norwegian University of Science and Technology (NTNU), pursued under the European Wind Energy Master program.

My heartfelt gratitude goes out to my dedicated daily supervisors: Michiel, Erin, and Dong. Your unwavering support, clear guidance, and insightful suggestions have been invaluable. Without your contributions, this project would not have reached its fruition. Your patience and boundless kindness in helping me overcome challenges are deeply appreciated. The extensive coaching sessions have held greater significance to me than standard thesis meetings.

This master's thesis report marks the culmination of my journey within the European Wind Energy Master program. These two years represent a pivotal juncture in my personal and intellectual growth.

Through this journey, I have expanded the horizons of my mind, collaborated with individuals from across the globe, and traversed Europe, experiencing its diverse landscapes. My gratitude knows no bounds for my fellow EWEM students, who have shared in the same challenges, victories, and uncertainties. Our shared experiences have been instrumental in adapting to numerous changes, and I am certain that our bonds will endure as lifelong friendships. Thank you for creating an environment where I felt at home wherever we journeyed together.

I extend my heartfelt appreciation to my father, mother, and sister for their unwavering support and love. I recognize and thank you for the sacrifices you've made, affording me the opportunity to pursue my chosen path.

To Ludovica, your love and support have been my guiding light. Your encouragement in making decisions that align with my best interests, even if they take us apart, is cherished beyond words.

*Vincenzo Ceriello
Delft, July 2023*

Abstract

Floating wind turbines despite the potential to harness energy from deep offshore areas where higher average wind speeds face challenges in terms of competitiveness. One approach to raising the competitiveness of a wind farm is to mitigate efficiency losses resulting from the wake effect. This report focuses on the combination of three notable wake effect mitigation strategies: layout optimization, yaw-based wake redirection, and turbine repositioning.

A preliminary analysis of the combined effect of wind turbine repositioning and yaw-based wake redirection on power performance for the case of two turbines only is performed. Above rated wind speeds, upstream turbine yawing reduces downstream turbine movement, with reductions of around 1 to 4 rotor diameters longitudinally and 0.2 to 0.5 times the rotor diameter laterally, keeping the same level of power efficiency.

Nextly, an optimization problem that integrates layout optimization with yaw-based wake steering and turbine repositioning for power maximization across an extended wind farm is formulated. The optimization frame followed a sequential approach. The results on a case study confirmed that the effect of adding yaw-based wake redirection to turbine repositioning remains significant for multiple turbines, with several percent-point efficiency improvements for small movable ranges. For larger ranges, the contribution of yaw control diminishes rapidly to one percent-point or less. Yaw control enables movable range reductions of 10% to 50%, preserving wind farm efficiency. Yet, reductions are more pronounced in smaller, less effective movable ranges. Below rated conditions, the effectiveness of yaw control diminishes swiftly.

Furthermore, the study delves into the implications of integrating position mooring for turbine repositioning and yaw-based wake mitigation strategies on mooring system performance. This examination employs a proposed methodology aimed at minimizing the position error across most points within the movable range. Both the tension of the mooring lines and the static stiffness of the floater showed to be sensitive to the position of the floater, the direction of the wind load and the yaw of the wind turbine. It results that the orientation of the mooring lines with correspondence of the prevailing wind direction, as well as that restrictive constraints on the tension and stiffness should be taken into account when designing a mooring system for turbine repositioning.

Overall, combining, yaw-based wake redirection, and turbine repositioning allows for greater wind farm AEP, with gains contingent on turbine movable range and upcoming wind speeds. Designing position mooring systems must factor in the influence of yaw-based wake redirection and turbine repositioning on mooring system tension and stiffness. More advanced analyses, including dynamic assessments, are essential for comprehending the mooring lines system's response to position mooring for turbine repositioning, and yaw-based wake redirection.

Contents

Preface	i
Abstract	ii
1 Introduction	1
1.1 Background	1
1.1.1 Global investments in energy transition technologies: trends, challenges, and opportunities	1
1.1.2 Status of wind energy	2
1.1.3 Floating offshore wind energy	3
1.1.4 Levelized cost of energy	4
1.1.5 The wake effect	5
1.2 Wind farm layout optimization	5
1.3 Wind farm control	6
1.3.1 Introduction to wind farm control	6
1.3.2 Wind turbine repositioning	6
1.3.3 Repositioning mechanism	7
1.3.4 Yaw-based wake mitigation strategies	8
1.3.5 Yaw-based wake redirection	8
1.4 Problem analysis	9
1.5 Objectives	10
1.6 Approach	10
1.7 Organization of thesis	10
2 Position and yaw influence on the wake effects applied to a two turbine case	12
2.1 Two turbines preliminary analyses objectives	13
2.2 Methodology	14
2.2.1 Nested for-loop configuration	14
2.2.2 Simulation set-up	14
2.2.3 Power production calculation using PyWake	15
2.2.4 Definition of the wind turbine efficiency for the case study	16
2.3 Wind Turbine under yaw misalignment in pywake	16
2.3.1 Wake models	17
2.4 Case study definition	20
2.4.1 Wind turbines coordinates and yaw angles range of variability	20
2.4.2 Wind turbine selection	20
2.4.3 Wind resource	21
2.5 Simulation results analyses	23
2.5.1 Upwind turbine efficiency	23
2.5.2 Downwind turbine efficiency	24
2.5.3 Wind farm efficiency	26
3 WFLO combined with turbine repositioning and yaw-based wake redirection for an extended wind farm case study	29
3.1 The wind farm layout optimization problem	29
3.1.1 General optimization problem	29
3.1.2 Wind farm layout optimization	30
3.1.3 WFLO combined with turbine repositioning	30
3.1.4 WFLO combined with yaw-based wake redirection	32
3.2 Methodology	33
3.2.1 Scenarios	33

3.2.2	Sequential optimizations	33
3.2.3	Optimization function: the AEP	34
3.2.4	Optimization Framework	35
3.2.5	AEP calculations in Pywake	39
3.2.6	Wind farm efficiency	40
3.3	Case study definition	41
3.3.1	Wind farm case study	41
3.3.2	Wind farm site	41
3.3.3	Wind turbine selection	42
3.3.4	Wind resource selection	43
3.3.5	Definition of the wind turbines' movable range size	43
3.3.6	Optimization strategy selection	44
3.3.7	Wake models selection	45
3.4	Results analyses	46
3.4.1	Comparison of the wind farm efficiency	46
3.4.2	Effect of the wind direction on the yaw optimization	48
3.4.3	Effect of the wind speed on the yaw optimization	49
3.4.4	Effect of the movable range size on the yaw optimization	50
4	Mooring lines analyses	52
4.1	Introduction to position mooring movability and station-keeping performances assessment	52
4.1.1	Selection of the repositioning mechanism	52
4.1.2	Position Mooring for turbine repositioning	53
4.1.3	The impact of the yaw on the translational equilibrium of the turbine	54
4.1.4	Problem analyses	54
4.2	Methodology for position mooring performance assessment	56
4.2.1	Workflow and general structure	56
4.2.2	Definition of the position of the FOWT and of the mooring lines parameter	57
4.2.3	Mooring lines length optimization loop	58
4.2.4	MoorPy for mooring lines performance calculation	60
4.2.5	General Hypotheses	60
4.3	Case study definition	61
4.3.1	Wind turbine selection	61
4.3.2	Floater selection and movable range shape	62
4.3.3	Wind resource selection	63
4.3.4	Implementation of the methodology in the case study	64
4.4	Case study results	67
4.4.1	Station keeping performances: position error	67
4.4.2	Impact of the thrust force on the horizontal tension at the fairlead	70
4.4.3	Effect of the wind direction and turbine yaw on the surge stiffness term	75
5	Discussion	79
5.1	Preliminary Analyses	79
5.1.1	The interpretations and implications of key findings	79
5.1.2	Limitations	79
5.2	Optimized Combined Layout	80
5.2.1	The interpretations and implications of key findings	80
5.2.2	Limitations	80
5.3	Mooring Lines System	81
5.3.1	The interpretations and implications of key findings	81
5.3.2	Limitations	81
6	Conclusion and Further Analyses	83
6.1	Conclusion	83
6.2	Further Analyses	84
	References	85

- A Additional results for position mooring of UMaine VoltturnUS-S 90**
- A.0.1 Sway stiffness terms 91
- A.0.2 Yaw stiffness terms 92

1

Introduction

This Master's Thesis Project aims to provide valuable insights into enhancing the efficiency of wind farms with floating offshore wind turbines (FOWTs), with a specific focus on addressing the aerodynamic interaction among the turbines. This chapter will first provide background information regarding the overall wind energy sector. Subsequently, the potential solutions for mitigating the wake effect will be investigated, including wind farm layout optimization, the use of movable floating offshore wind turbines, and redirecting the wake generated by a wind turbine through its nacelle yaw misalignment. Subsequently, a thorough analysis of the drawbacks associated with the aforementioned strategies, as well as their potential benefits, will be conducted. These reflections will form the basis for defining the objectives of the thesis and determining the approach adopted to achieve them. The final section of the introduction will outline the organization of this Master's thesis report, providing an overview of the subsequent chapters and their content.

1.1. Background

In this section, the necessary background information is provided to comprehend the components involved in this Master's thesis project. Subsection 1.1.1 outlines the motives behind investing in energy transition technologies, emphasizing the significance of investing in wind energy. Subsection ?? offers an overview of the current state of wind energy, including its growing utilization and the investment trends in both onshore and offshore wind energy. Lastly, subsection 1.1.3 introduces the concept of floating wind energy.

1.1.1. Global investments in energy transition technologies: trends, challenges, and opportunities

The global investment in energy transition technologies, such as renewable energy, energy efficiency, electrified transport and heat, energy storage, hydrogen, and carbon capture and storage (CCS), has reached a remarkable milestone in 2022. According to reports [74, 73, 38], the total investment in these technologies reached a record high of USD 1.3 trillion. To stay on track with the objectives outlined in the Paris Agreement, annual investments in energy transition technologies would need to at least quadruple [38]. The Paris Agreement aims to limit the global mean temperature increase to below 2 degrees Celsius above pre-industrial levels. This substantial increase in investments is necessary to accelerate the deployment of clean and sustainable energy solutions.

Despite the challenges posed by macroeconomic conditions, geopolitical factors, and supply chain disruptions, global investments in energy transition technologies have shown remarkable growth. The USD 1.3 trillion invested in 2022 represents a 19% increase from the previous year and nearly 70% increase from pre-pandemic levels in 2019. This upward trend reflects a growing recognition of the urgent need to address the climate crisis and mitigate the risks associated with fossil fuel dependence [38].

To achieve the desired energy transition a significant redirection of financial resources is necessary, moving away from fossil fuel investments and towards energy-transition-related technologies. While fossil fuel investments experienced a temporary decline in 2020 due to the impact of the COVID-19 pandemic on global energy markets, they rebounded in 2021 and are estimated to have nearly returned to pre-pandemic levels in 2022. This resurgence in fossil fuel investments indicates that substantial funding is still being allocated to new oil and gas fields rather than renewable energy projects, as it is shown in Figure 1.1.

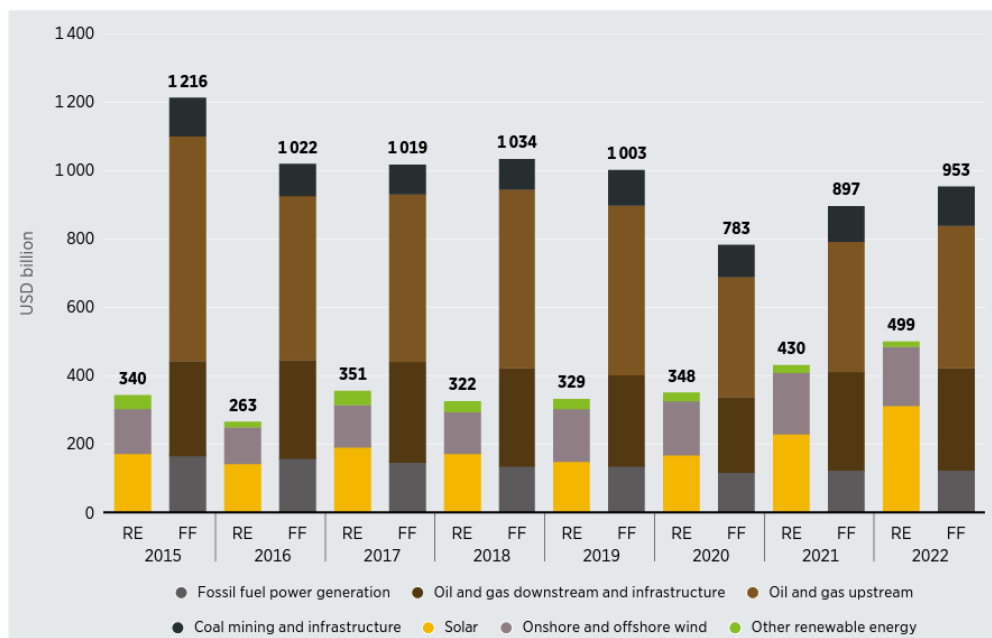


Figure 1.1: Annual investment in renewable energy (RE) vs. fossil fuels (FF), 2015-2022 [38].

While there has been progress in global investments in energy transition technologies, there is still a significant need to redirect financial resources away from fossil fuels and towards renewable energy and sustainable technologies in order to effectively address the energy transition and mitigate climate change.

In addition, investment in wind energy not only addresses environmental concerns but also brings various social, political, and economic benefits. One of the key advantages is the diversification of national energy portfolios, which enhances energy security and reduces the risk of global conflicts related to limited natural resources [46]. Additionally, wind energy plays a significant role in achieving Sustainable Development Goals by cutting operational costs, mitigating climate change and environmental damage, enhancing employee engagement and morale, and reducing learning gaps [61]. The development of wind energy promotes innovation and creates job opportunities, driving economic growth in the renewable energy sector. These multiple benefits make wind energy investment a promising avenue for sustainable development and a catalyst for positive change at both local and global levels [4].

1.1.2. Status of wind energy

These environmental and economic benefits, along with government mandates and support, have generated remarkable growth in wind energy exploitation in recent years, becoming a leading source of renewable power generation. In 2021, wind electricity generation witnessed a substantial increase of 273 TWh, reflecting a significant growth rate of 17% compared to the previous year [36]. This growth outpaced other renewable power technologies and underlines the tremendous potential of wind energy. To meet the ambitious goals of the Net Zero Emissions by 2050 Scenario, further efforts are required to expand wind capacity [36].

As evidenced by Figure 1.2, the interest in offshore wind farms has been growing steadily. These offshore installations offer numerous advantages over their onshore counterparts. Firstly, offshore wind turbines reduce environmental impact by eliminating the requirement for transportation roads. Additionally, they mitigate visual and noise disturbances in urban areas as the turbines are positioned far away from residential zones. Secondly, acquiring land permits for offshore projects is generally easier, and the proximity of many major coastal cities allows for shorter transmission lines. Furthermore, offshore wind benefits from stronger and less turbulent wind resources due to the absence of obstructions and uneven terrain [2].

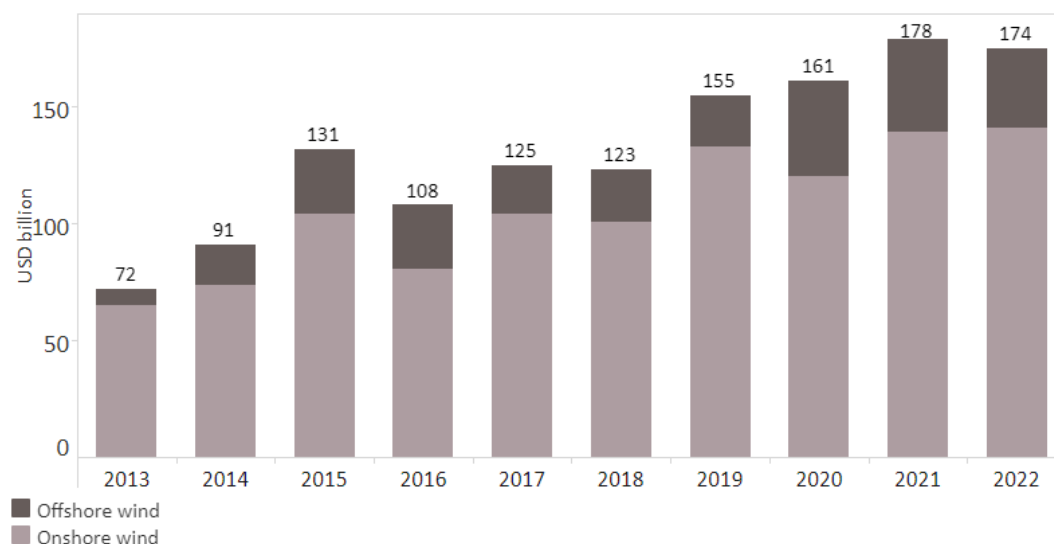


Figure 1.2: Annual Financial Commitments in Wind Energy Industry [38].

The superior wind conditions offshore result in higher electricity generation compared to onshore wind turbines. In fact, the global average capacity factor for offshore wind power in 2017 was found to be 30% higher than that of onshore wind power, indicating its higher efficiency and productivity. However, a cautious approach is warranted when interpreting these statistics. It is important to consider that a significant portion of onshore turbines currently in operation are characterized by older technology and smaller sizes. Furthermore, it is crucial to acknowledge that the capacity factor, which is commonly employed as a metric for assessing wind resource potential, is contingent upon the specific turbine model chosen for installation at a particular site. Therefore, the selection of turbine technology significantly influences the resulting capacity factor and should be taken into account when evaluating wind resource availability.

To achieve widespread adoption of wind power, enhancing its competitiveness is crucial. This objective has become a top priority within the wind energy research community [9, 75]. Thus, overcoming the challenges associated with offshore wind and driving technological advancements are essential for realizing its full potential and establishing a sustainable and economically viable energy source.

1.1.3. Floating offshore wind energy

Floating wind turbines have garnered significant attention in the offshore wind energy sector due to their unique characteristics and advantages. They are similar to conventional offshore wind turbines in many aspects [1]. One of the key advantages of floating wind turbines is their ability to operate in areas with more consistent and stronger winds, generally resulting in higher capacity factors compared to conventional offshore wind turbines. This was demonstrated by the Hywind Scotland pilot project, which achieved the highest capacity factor among UK offshore wind farms for three consecutive years, with an average capacity factor of 54% in the first two years and a record of 57.1% in a single year [21].

Despite the higher initial cost of floating wind turbines compared to conventional turbines, they can

lower the overall energy system costs. This is due to their access to a more constant and efficient wind resource, reducing the need for storage and balancing in the system [58]. Additionally, emerging floating wind energy technologies offer unquantified benefits such as positive environmental impact and socio-economic advantages, further strengthening the business case for floating wind turbines [28].

Accurate estimation of energy production for floating wind turbines can be achieved by leveraging the knowledge and experience gained from existing offshore wind turbines. Economic potential is typically assessed in terms of cost development rather than system performance. Expert elicitation conducted by Wisser et al. [87] predicted a 37-49% cost reduction for wind energy by 2050.

1.1.4. Levelized cost of energy

To enhance the competitiveness of floating wind turbines compared to other renewable energy resources, it is crucial to reduce the Levelized Cost of Energy (LCOE). The LCOE is a significant metric used to evaluate the economic feasibility of energy projects, especially in the context of the transition to sustainable energy sources. Accurate calculation of the LCOE for wind power projects is essential for decision-making processes and enables policymakers to design effective support mechanisms and incentivize investments in wind power.

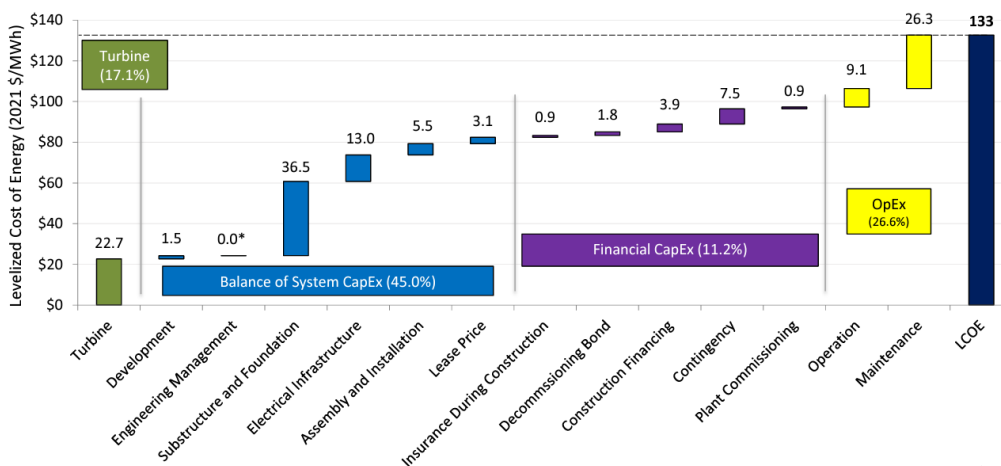


Figure 1.3: Levelized Cost Breakdown for Reference Floating Offshore Wind Plant. [79].

Figure 1.3 provides a visual representation of the levelized cost breakdown for a standard floating offshore wind plant. The primary obstacles to the installation of floating wind turbines are the significant capital and operating expenditures (CAPEX, OPEX). The former comprises the initial investment costs associated with procuring wind turbines, their installation, grid connection, and infrastructure development. This category encompasses a substantial portion of the capital expenses for crucial components such as the wind turbine itself, substructures, foundations, and electrical infrastructure. On the other hand, O&M costs pertain to ongoing expenses related to inspections, repairs, replacements, and general maintenance.

On the other hand, the power production of the project is described by the Annual Energy Production (AEP), representing the total energy output of the wind farm over a year.

Clearly, to enhance the competitiveness of wind farms, and thus reduce the LCOE of a project, there are two main strategies: either minimize the CAPEX and OPEX or increase the overall power production. One of the approaches to do so involves tackling the efficiency decline caused by aerodynamic interactions among individual turbines. This phenomenon is commonly referred to as the wake effect and will be explored further in the subsequent section.

1.1.5. The wake effect

When two turbines are aligned with the prevailing wind, as shown in Figure 1.4 a turbine generates a wake (i.e. a downstream region characterized by reduced velocity and heightened turbulence intensity). This wake significantly impacts the downstream turbine's power production and increases fatigue damage [10, 52]. This phenomenon is known as the wake effect. Effectively mitigating these effects is crucial for optimizing wind farm performance.

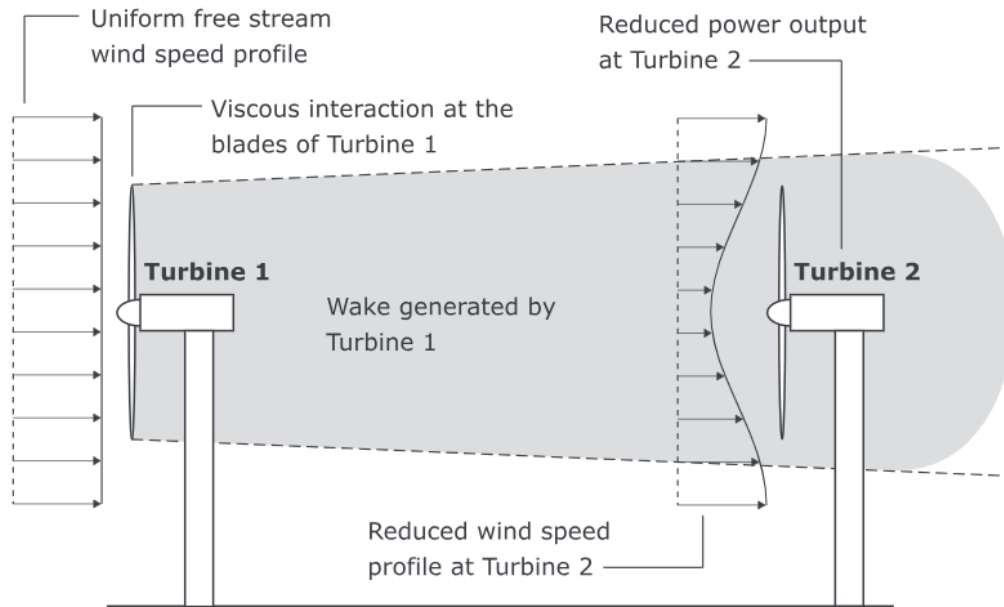


Figure 1.4: The phenomenon of aerodynamic coupling between two wind turbines aligned with the free stream wind [45].

Researchers and industry experts have proposed several strategies to minimize the negative impact of wake effects on energy production. The first approach involves optimizing the spacing between turbines, allowing for sufficient distance in the direction of the dominant wind. By increasing the gap, the turbulent mixing process can be optimized, resulting in a decrease in velocity deficit within the wake. Although widely utilized, this method presents a trade-off, as it conflicts with the cost-saving objective of clustering turbines together. Clustering wind turbines in wind farms provides several advantages. Firstly, by sharing infrastructure and resources, such as access roads and maintenance facilities, clustering reduces construction, operation, and maintenance costs, improving cost efficiency. Secondly, this approach optimizes land utilization, minimizing the land footprint and reducing land leasing expenses. Concentrating turbines in designated areas also helps minimize environmental impact. Furthermore, the integration of clustered turbines with the electrical grid is streamlined, ensuring a stable and reliable power supply. Lastly, operational efficiency is improved as maintenance and monitoring activities are centralized, leading to easier access and proactive maintenance.

Consequently, alternative approaches that can mitigate revenue losses while minimizing spatial requirements are gaining increased attention [12, 52]. Among the alternative approaches, wind farm control and wind farm layout optimization stand out as prominent methods. The subsequent subsections explore the two strategies implemented in this master's thesis. Section 1.2 focuses on wind farm layout optimization, while section 1.3 delves into wind farm control.

1.2. Wind farm layout optimization

The second strategy employed in this master thesis project to mitigate the wake effect is Wind Farm Layout Optimization (WFLO).

The wind farm layout optimization problem involves determining the optimal positions of turbines within a two-dimensional plane in order to maximize energy capture while minimizing costs associated

with various factors. Energy capture for a turbine is influenced by several considerations, including the wind climate (distribution and terrain), the power curve of the turbines (which relates the power generated to the wind input), and the effects of wake interactions between turbines. These factors collectively contribute to the overall objective of maximizing energy production while minimizing associated costs [17, 49].

The primary objectives of wind farm layout optimization typically revolve around minimizing power losses caused by wake effects or maximizing power production. Researchers have identified various factors and considerations to consider during the optimization process. Various objective functions have been identified in the literature, as described by Tesauro [82], and readers are encouraged to refer to that work for more detailed information.

Despite extensive academic research in this field, operational wind farms commonly employ gridded layouts with appropriate spacing between turbines along the prevailing wind direction [13, 46]. However, ongoing advancements in layout optimization techniques hold the potential for more efficient wind farm configurations in the future.

The significance of wind farm layout optimization lies in its ability to improve the performance and efficiency of wind power generation. By finding the optimal layout, wind farms can increase electricity production using the same number of turbines or achieve the same level of electricity production with fewer turbines. This can lead to cost savings and higher returns on investment for wind farm developers and operators. Furthermore, layout optimization can contribute to minimizing the environmental impacts of wind farms, including aspects such as noise and visual pollution [45].

1.3. Wind farm control

In the following sections, an introduction is provided for the concepts of wind farm control in section 1.3.1. Section 1.3.2 offers an analysis of turbine repositioning, while section 1.3.5 introduces yaw-based wake redirection.

1.3.1. Introduction to wind farm control

Wind farm control has emerged as a promising approach to address revenue losses caused by the wake effect. This strategy involves implementing individual turbine control to achieve desired objectives at the wind farm level. It can be applied to existing wind farm layouts, whether they are gridded or optimized. In essence, a wind farm controller utilizes the degrees of freedom available in each wind turbine to achieve a wind farm-level objective [45]. These objectives can include maximizing power production, tracking power set-points to reduce loads, or improving grid interaction by adjusting the power output of turbines to match grid demand [9]. Often, these objectives are interconnected, and certain wake management strategies can optimize multiple objectives simultaneously, although trade-offs may need to be considered.

Researchers have identified four primary strategies for wind farm control: power de-rating/axial induction-based control, yaw-based wake redirection, tilt-based wake redirection, and real-time repositioning of floating wind turbines. While the first two strategies have received significant attention, the concept of real-time repositioning of floating turbines is relatively new and holds the potential for minimizing wake effects and reducing costs [45, 47, 70, 15].

1.3.2. Wind turbine repositioning

The use of floating offshore wind turbines introduces supplementary degrees of freedom (DOFs) to the platform, enabling it to undergo translational and rotational movements in response to wind and wave forces. The turbine repositioning strategy explores the opportunity to relocate floating wind turbines in real-time to mitigate wake effects [22]. In simple terms, the downstream turbine is repositioned to avoid or minimize the wind velocity deficit caused by the wake of the upstream turbine, as is shown in Figure 1.5.

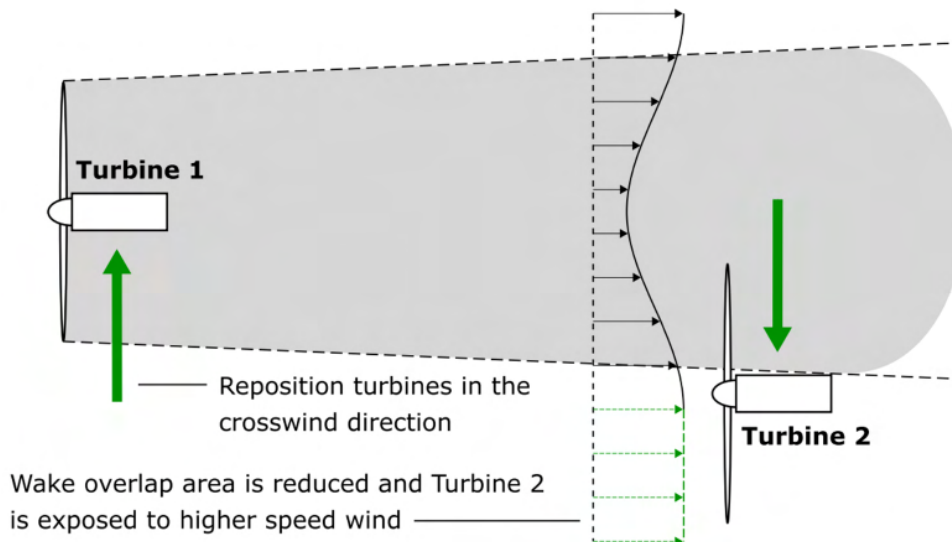


Figure 1.5: Top view of two wind turbines aligned with the incoming free stream associated with turbine repositioning [45].

This wake mitigation strategy presents both challenges and opportunities in terms of controlling the wind turbine system [71, 46]. Overcoming design challenges, such as heave vibration suppression, resonance avoidance, and the complexities associated with system modelling [69, 14], becomes crucial for both the moved wind turbine and the repositioning mechanism. Consequently, the repositioning mechanism can be designed with two primary control objectives in mind: effectively relocating the wind turbine to a desired position and maintaining it in that position once achieved.

While the concepts of power de-rating and yaw-based wake redirection have received considerable attention from wind farm control studies, publications investigating the potential of wind turbine repositioning are limited [45]. Clearly, the applicability of this concept is limited to floating wind turbines, which are at an early stage of development. On the other hand, compared to the other two mentioned wind farm control strategies, turbine repositioning does not necessarily involve reducing the power output of the upstream turbine to increase the overall production, but potentially both downstream and upstream turbines would be operating at the optimum setting.

The economic feasibility of wind farm layouts incorporating movable FOWTs hinges on whether the increase in annual energy production (AEP) justifies the costs associated with achieving turbine mobility. The expenses related to turbine repositioning, including capital expenditure (CapEx) and operational expenditure (OpEx), may also increase depending on the required technology.

The literature on dynamic Wind Farm Layout Optimization (WFLO), where wind farm layouts are optimized for varying wind directions considering turbine repositioning, has reported significant AEP gains and potential reductions in the Levelized Cost of Energy (LCOE) [47, 70].

The costs associated with such a mechanism depend on factors like the type of actuator used and the desired range of turbine movement. Evaluating the investment required for implementing a turbine repositioning mechanism is challenging, but it is reasonable to expect a substantial impact on the initial investment.

1.3.3. Repositioning mechanism

Among different repositioning mechanisms, the one that seems to be more promising compared to the others is the Position Mooring (PM) for turbine repositioning. PM entails altering the length of the mooring lines using winches, resulting in the movement of the wind turbines by several meters. The modification in line length causes an imbalance in mooring line tensions, leading to the displacement

of the turbine. PM proves to be an energy-efficient technique with a large movable range, although it comes with increased capital and operational costs.

The reader is referred to chapter 4 for a wider discussion of the other repositioning mechanism in literature and for the election of PM for turbine repositioning.

The groups of positions that the turbine can move to and maintain are commonly addressed as the movable range. The shape and the size of the movable range is directly influenced by the mooring system configuration.

1.3.4. Yaw-based wake mitigation strategies

The overall objective of yawing the wind turbine is significant, as it fundamentally alters the approach to yaw control. There are two primary applications of the turbine's nacelle yaw in wind farm control:

1. **Yaw-Based Wake Redirection:** If the yaw angle is used to redirect the wake of the upstream wind turbine and optimize power production, the wind farm control method falls under the category of yaw-based wake redirection.
2. **Yaw and Induction-Based Turbine Repositioning (YITuR):** On the other hand, when nacelle yaw is employed to manipulate aerodynamic forces and control the positions of floating platforms, the wind farm control method is defined as YITuR.

These two applications are interrelated, as both are triggered by the yaw of the turbine. Consequently, interference between them is unavoidable. For example, when the turbine is yawed to deflect the wake, the thrust force changes its direction (perpendicular to the rotor plane of the turbine). As a result, the thrust force accelerates the Floating Offshore Wind Turbine (FOWT) in the new direction, leading to an undesired relocation effect, typical of YITuR.

Furthermore, it is important to note that for both yaw-based methods to be effective, the turbine needs to be yawed in two opposite directions. For instance, if the wake needs to be relocated to the right, the turbine must be yawed to the right as well. However, the resulting thrust force will attempt to relocate the turbine to the left, reducing the effectiveness of wake redirection. This occurs because the source of the wake (and the wake itself) will be relocated closer to the original configuration.

1.3.5. Yaw-based wake redirection

Yaw-based wake redirection is a technique used to control the direction of the wake generated by a wind turbine. By using yaw control, the direction of the wake can be adjusted to reduce this interference [41].

To redirect the wake, the turbine's nacelle, which houses the rotor and generator, is rotated, or yawed, to align (or misalign) the rotor plane with the incoming wind. This causes the blades of the rotor to experience different aerodynamic loads, leading to an imbalance in the loads along the rotor plane. This imbalance imparts forces that cause the wind to gain momentum in the crosswind direction, redirecting the wake [41].

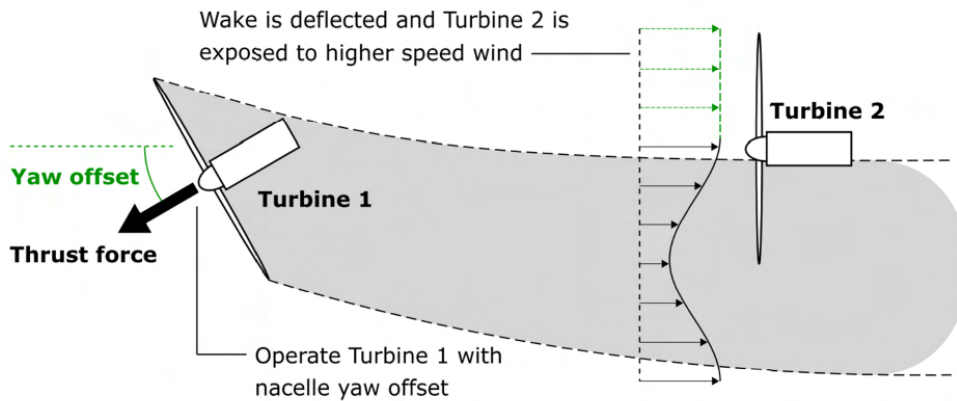


Figure 1.6: Top-view of two wind turbines aligned with the incoming free stream associated with Yaw-based wake redirection [45]

Figure 1.6 illustrates the deflection of the wake generated by a wind turbine when operated with a yaw offset. The deflected wake deviates from its original path, resulting in reduced overlap with the rotor of a downstream turbine. Consequently, a portion of the downstream rotor is exposed to higher-speed and less disturbed wind, leading to an increase in its power output that can exceed the power loss of the upstream turbine caused by the yaw misalignment [22].

Yaw-based wake redirection has proven effective in reducing wake interference and improving the overall power output of wind farms [23, 22, 9]. However, it should be noted that yaw-based redirection also reduces the power output of the individual yawed turbine, necessitating careful balancing to achieve desired results [3].

Furthermore, a yawed turbine's wake is narrower than that of a non-yawed turbine and is shifted away from its axis in the opposite direction of the yaw misalignment angle. Thus, the benefits of wake steering stem from both the deflection and the narrower width of the wake [3].

1.4. Problem analysis

As previously discussed, the introduction of turbine repositioning in floating offshore wind farms may not result in significant increases in Annual Energy Production (AEP) that would justify the considerable capital expenditure associated with designing the repositioning mechanism for the platform. Consequently, the potential reduction in the Levelized Cost of Energy (LCOE) might be limited.

In order to minimize initial investment and overall costs, it may be necessary to impose restrictions on the range of turbine movement for repositioning purposes, which can impact the investment needed for the mooring line system. One possible approach is integrating the turbine repositioning strategy with the yaw-based wake redirection, as both strategies involve adjustments in the geometric positioning of the wake and downstream turbine.

The combination of these two strategies can effectively address the limitations associated with employing each strategy independently:

- Utilizing an actuator for turbine movement reduces the necessity for high yaw angles to significantly steer the wake. This allows each turbine to operate closer to its maximum aerodynamic efficiency, thereby minimizing the power losses associated with yawing the wind turbine.
- When employing a repositioning mechanism other than YITuR (such as position mooring), active compensation for the undesired influence of yaw on the turbine's position and the effectiveness of yaw deflection can be achieved, avoiding the undesired interconnection between yaw-based wake redirection and YITuR discussed in section 1.3.4.

- This combination enables higher power production compared to using only turbine repositioning. In other words, it can achieve the same power production with a smaller range of movement and ideally lower initial costs.

Due to the limited availability of data and research on turbine repositioning, assessing its impact on the overall LCOE of a wind farm is challenging. Therefore, it is prudent to examine the individual components of the LCOE separately.

Initially, the combined impact of the two wake-effect mitigation strategies on the overall power production of a wind farm should be evaluated.

Subsequently, the focus can be directed towards comprehending the influence of these strategies on the repositioning mechanism and its station-keeping performance.

1.5. Objectives

Considering the issues identified in the problem analysis, the objectives of this Master's Thesis Project are twofold:

- To provide insights into the potential enhancement of AEP and the overall efficiency of a wind farm by combining wind turbine repositioning, yaw misalignment for wake misalignment, and layout optimization;
- To gain an understanding of how the combination of yaw misalignment and turbine repositioning impact the parameters and station-keeping performances of the selected repositioning mechanism of floating offshore wind turbines.

1.6. Approach

To fulfil the primary objective stated in Section 1.5, the following steps were undertaken:

- Analyse the combined effect of wind turbine repositioning and yaw-based wake redirection on power performance for the case of two turbines only, to comprehend the effects of integration of these two strategies.
- Define an optimization problem for Wind Farm Layout Optimization (WFLOP), incorporating the implementation of yaw-based wake steering and turbine repositioning for power maximization.
- Choose a suitable wind farm case study to represent an extended wind farm scenario.
- Perform and analyze the optimization results for the selected case studies.

To evaluate the impact of the two wind farm control methods on the repositioning mechanism :

- Define and select a repositioning mechanism in order to perform the analyses;
- Propose a methodology to assess the movability and station-keeping performance of the chosen repositioning mechanism when modifying the direction and thrust force to maximize wind farm power production in conjunction with platform repositioning.
- Perform and analyse the results of the proposed methodology for the selected case study.

1.7. Organization of thesis

This report is structured as follows:

- Chapter 2: This chapter outlines the methodology employed for conducting preliminary analyses on a two-turbine case study. It presents and discusses the obtained results.
- Chapter 3: In this chapter, the methodology is described for investigating the integration of turbine repositioning and the formulation of optimization problems for each applied wake mitigation strategy. The proposed methodology is applied to selected extended wind farm case studies, providing insights and analysis of the results.

-
- Chapter 4: This chapter introduces a methodology to evaluate the impact of combining position mooring for turbine repositioning and yaw-based wake mitigation strategies on the performance of the mooring system. The methodology is then implemented in a specific case study, presenting the findings and their implications.
 - Chapter 5: Here, the discussions from chapter 3 and chapter 4 are recalled individually and then integrated together.
 - Chapter 6: The final conclusions are presented in this chapter, along with proposed avenues for further research on the combination of the discussed wake mitigation strategies utilized in this Master Thesis Project.

2

Position and yaw influence on the wake effects applied to a two turbine case

This chapter of the thesis presents and discusses the preliminary analyses conducted on a two-turbine case study.

In Section 2.1, a comprehensive overview is provided, focusing on the combination of wind turbine repositioning and yaw-based wake steering. The objectives of these preliminary analyses are outlined, highlighting the key aspects and goals of the preliminary study.

Moving forward, Section 2.2 presents the methodology and the calculation tools used to perform the analyses.

Hereafter, Section 2.4 offers a detailed description of the specific two-turbine case study employed in this Master's Thesis Project. This section provides relevant information regarding the characteristics, specifications, and operational parameters of the turbines used in the analysis, as well as of the different upcoming wind scenarios.

Subsequently, simulations are performed for two different repositioning cases, and the outcomes are presented and discussed in Section 2.5. The results obtained from these simulations are analyzed, compared, and interpreted, shedding light on the effects of turbine repositioning and yaw-based wake steering on the overall performance of the two-turbine wind farm.

Through these preliminary analyses, the chapter aims to lay the groundwork for further investigation and optimization of extended wind farm cases involving more than two turbines. The findings presented in this chapter serve as a basis for the subsequent in-depth analysis and exploration of different optimization strategies in the subsequent chapters.

2.1. Two turbines preliminary analyses objectives

The yaw-based wake steering and wind turbine repositioning control methods both rely on manipulating the geometric misalignment of the wake generated by upstream turbines in relation to downstream turbines. Therefore, it is essential to carefully consider the coordination between the yaw control of the upstream turbines and the repositioning of the downstream turbines to ensure that the wake redirection strategies work synergistically and result in improved wind farm efficiency.

Ideally, aligning the turbine rotor perpendicular to the incoming wind speed is preferred to maximize power production, thereby minimizing the nacelle yaw angle. Minimizing turbine movement offers distinct advantages, as it results in reduced energy consumption and cost of the repositioning mechanism. The increment in the magnitude of turbine movements generally correlates with higher energy and repositioning expenses.

Due to the complex nature of wind farm power production, which depends on various factors, a series of simulations were performed on a two-turbine scenario before introducing a methodology to assess the potential power gains in an extended wind farm case. In fact, the choice to limit the number of turbines to two serves two purposes. Firstly, having only two turbines enables a focused examination of the mechanics involved in combining the two strategies for wake redirection. Secondly, it helps reduce computational time, as the number of cases to be evaluated would eventually become computationally burdensome if a larger number of turbines were considered.

The objectives of these two-turbine simulations are twofold:

- To gain an understanding of the mechanism and interconnection between yaw-based wake redirection and turbine repositioning wake strategies.
- To gain insight into the range of variability of inputs for the extended wind farm scenario, such as wind speeds, upper and lower boundaries of turbine yaw, boundary limits for turbine movement, and the influence of different wake models.

2.2. Methodology

The subsequent section presents a comprehensive overview of the methodology and simulation setup employed to conduct the analyses. Firstly, in section 2.2.1, the general architecture of the simulation process is outlined, while section 2.4 focuses on defining the simulation setup. The tool used to obtain the simulation results is discussed in section 2.2.3, and finally, in section 2.2.4, the wind turbine efficiency is clearly defined.

2.2.1. Nested for-loop configuration

As delineated in Section 1.5, the primary aim of this preliminary analysis is to gain insights into the influence of turbine position and yaw angles on the power production of a wind farm. It is important to note that the objective of this study is not to determine the optimal combination of these parameters, but rather to comprehend their impact and potential for mitigating wake effects, as well as their combinatory possibilities.

The flow chart of the proposed methodology for the preliminary assessment of combining turbine repositioning and yaw-based wake misalignment on the wakes within a wind farm and its consequent power production is depicted in Figure 2.1. The wind turbine's yaw and position are manipulated to evaluate their effects on the power production of a two-turbine wind farm. Instead of optimizing the turbine coordinates and yaw angles, simulations are performed to calculate the power production while considering turbine coordinates and yaw angles as fixed inputs to the simulation setup.

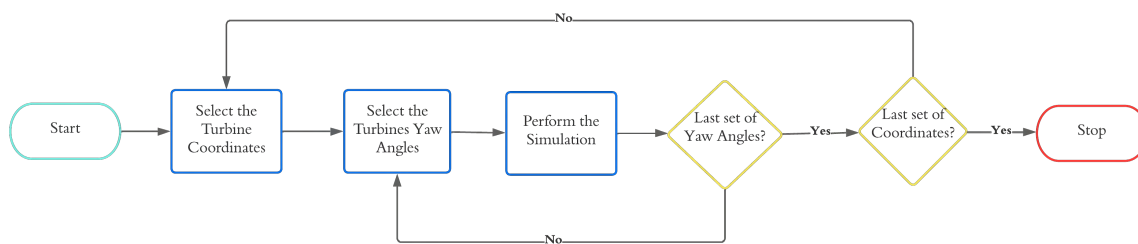


Figure 2.1: Workflow chart of the preliminary two turbine case.

A wide range of turbine coordinate and yaw angle combinations is investigated to fully comprehend their combined effect. The selection of the range of variability is described in Section 2.4.1. Initially, the turbine coordinates are chosen within the specified range, followed by the selection of the turbine yaw angle within the range. The simulation is then executed, and the turbine yaw angles are sequentially changed to the next value within the predefined array (range of variability) until all the yaw angles are explored for the selected turbine coordinates. Once all the turbine yaw angles are investigated with a particular set of turbine coordinates, the turbine coordinates are modified to the next pair, and the process is repeated. When all combinations of yaw angles and turbine coordinates are examined (with corresponding simulation results recorded), the overall process concludes.

2.2.2. Simulation set-up

Figure 2.2 depicts the simulation setup, which includes the configurations and degrees of freedom considered for the turbines in this study. Two turbines are aligned in the flow of the upcoming wind. The upstream turbine denoted as T0, is subjected to changes in its nacelle yaw angle, while the position of the downstream turbine, denoted as T1, is adjusted. The position of T0 was fixed at the origin of the simulation domain's reference system, while the yaw angle of the nacelle of T1 was set to zero.

Two distinct cases of repositioning are examined: Case 1 focuses on repositioning solely in the downstream (longitudinal) direction, while Case 2 involves repositioning exclusively in the lateral direction, perpendicular to the incoming wind speed.

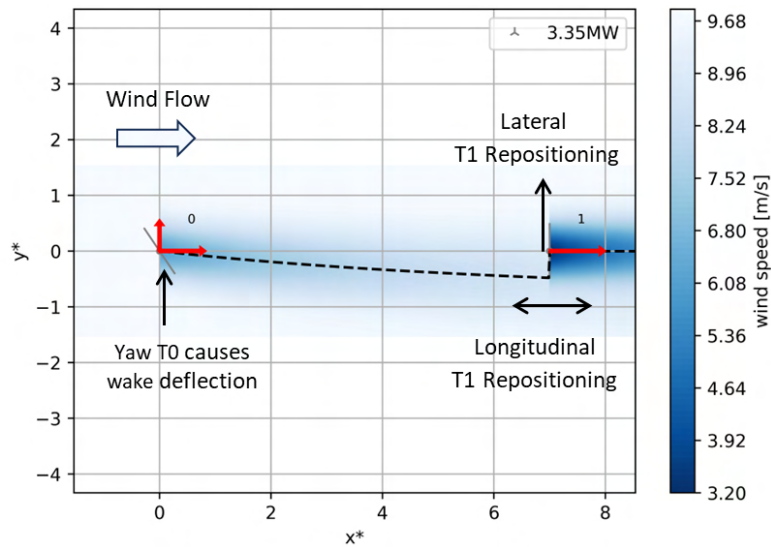


Figure 2.2: Topview of the simulation setup for the two turbine wind farm case.

The primary output of the simulation was the power production of the overall wind farm, as well as the power production of each individual wind turbine. These power production values were functions of the downstream turbine’s position and the yaw angle of the upstream turbine, as well as the upcoming wind speed.

The following subsection provides a detailed description of the simulation setup, including the inputs and outputs, as well as the model used for the calculations.

2.2.3. Power production calculation using PyWake

Figure 2.3 provides an overview of the inputs, including variables and wake effect models utilized, as well as the outputs and the computational tool necessary to perform the calculations. The simulations are carried out using PyWake, a software tool specifically designed for wind farm analysis.

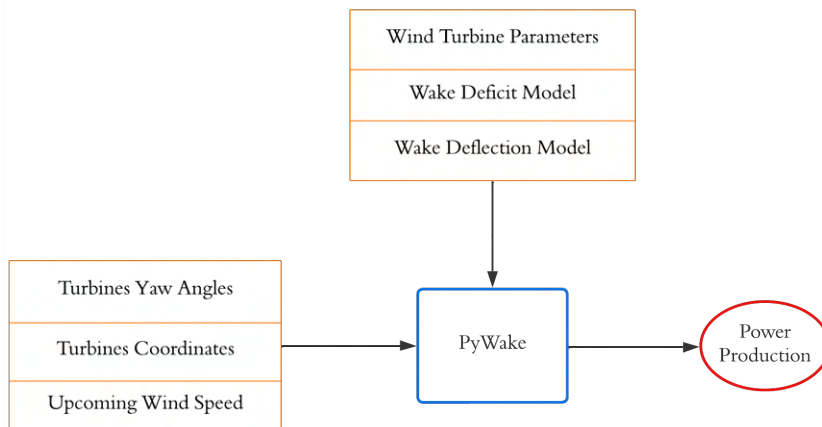


Figure 2.3: Overview of the PyWake workflow to calculate the power production.

PyWake is an open-source wind farm simulation tool used for studying the interaction between turbines within a wind farm and its influence on the farm’s flow field and power production. Based on Python, PyWake is capable of accurately computing the physics behind wind farms as well as obtaining their AEP. It provides a unified interface to wind farm models of different fidelities, e.g., different

engineering models and CFD-RANS. Given its heavy vectorization and use of numerical libraries, PyWake is a very fast tool that can handle many variables at once [55].

2.2.4. Definition of the wind turbine efficiency for the case study

In order to understand the trade-offs involved in the yaw-based wake redirection, including the power losses of the upstream turbine and the power gains of the downstream turbine, it was decided to use wind turbine efficiency as the key metric to display the results.

As is shown in equation 2.1, the reference for computing the turbine efficiency was not the rated power of the selected turbine, but rather the maximum power that the turbine could produce at that specific wind speed, based on the upcoming wind speed. The wind turbine efficiency was computed as follows:

$$\eta_{wt}([x, y, \psi], u) = \frac{P([x, y, \psi], u)}{P([0, 0, 0], u)} \quad (2.1)$$

where:

- P is the power produced by the wind turbine;
- η_{wt} is the efficiency of the wind turbine;
- x is the x-coordinate of the wind turbine;
- y is the y-coordinate of the wind turbine;
- ψ is the yaw angle of the wind turbine;
- u is the upcoming wind speed.

It is worth noting that in the particular simulation scenario described in section 2.4, where only a constant wind speed was examined, the reference for computing the wind farm efficiency at that wind speed (with 0 yaw angle and turbine positions) was actually the power production of a single turbine with its rotor aligned to the wind flow (free stream condition) multiplied by two.

2.3. Wind Turbine under yaw misalignment in pywake

When the wind turbine rotor is not perpendicular to the inflow, its operation and its impact on the flow field exhibit differences. Figure 2.4 shows the effect of the reduced inflow velocity modelled due to the wind turbine yaw by PyWake. To handle these effects in PyWake, the software considers four sub-effects individually:

1. Change of operation due to reduced inflow wind speed: The wind turbine operation (pitch and rotor speed settings) is modeled in terms of Power and CT curves. If these curves are specified in terms of the wind speed normal to the rotor, then the wind speed must be multiplied by $\cos(\theta)$ before looking up the power and CT. PyWake applies this model as the default.
2. Reduced *deficit_{downwind}* due to reduced inflow wind speed: The wake deficit is caused by a reaction to the thrust force, which slows down the inflow. In non-aligned inflow, the thrust force that slows down the flow in the mean wind direction is given by $T_x = \frac{1}{2}\rho C_{T,x}(A \cos \theta)U^2$. The relationship between the thrust coefficient in the rotor-normal direction, $C_{T,n}$, and the thrust coefficient in the down-wind direction, $C_{T,x}$, can be expressed as $C_{T,x} = C_{T,n} \cos^2 \theta$. PyWake models this effect as the default.
3. Reduced deficit *deficit_{normal}* due to misalignment between thrust and downwind direction: Most engineering models calculate the deficit normal to the rotor plane, while the deficit impacting downstream wind turbines is in the downstream direction. In case of yaw misalignment, PyWake maps the deficit to the downstream direction by using $\text{deficit}_{\text{downwind}} = \text{deficit}_{\text{normal}} \cos \theta$.
4. Deflection of wake deficit *deficit_{deflected}* due to transversal thrust component reaction: This effect is modeled by a deflection model that modifies the downwind, horizontal crosswind, and vertical distance between wind turbines. The specific deflection model used is described in Section 3.3.7.

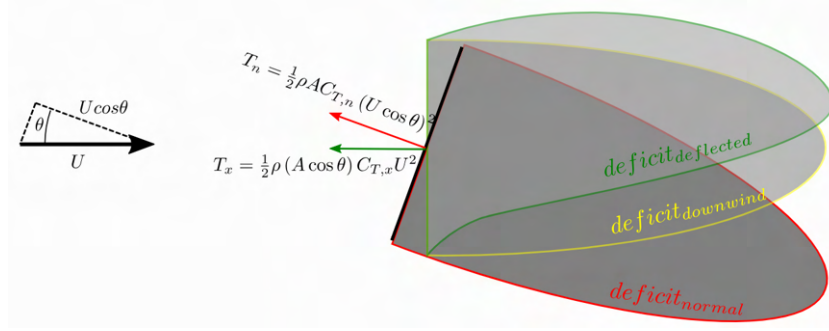


Figure 2.4: Overview of the PyWake modelling of a yawed wind turbine [55].

2.3.1. Wake models

Analytical models in wind energy are mathematical models that utilize analytical solutions to simulate the behaviour of wake flow. These models are typically based on theoretical equations and assumptions, enabling them to provide accurate predictions of wake behaviour under specific conditions [3]. However, due to their simplified nature, they may not be capable of accurately representing the complex, real-world behaviour of wakes in all scenarios.

The main strengths of analytical wake models lie in their simplicity and ability to deliver accurate predictions under certain conditions. These characteristics make them valuable tools, particularly in the initial stages of wind farm planning and design. Analytical wake models are well-suited for wind farm layout problems [85], as they allow for evaluating numerous layouts and optimizing them to meet the constraints of the problem while maintaining computational efficiency [64].

There exists a wide range of wake models, each designed to capture specific aspects of wake behaviour with varying levels of fidelity and complexity. While the output of these models typically includes parameters like wind speed deficit and wake diameter, the specific inputs can vary. Figure 2.5 illustrates the input parameters employed by eleven different analytical wake models.

Parameter	Symbol	Jensen	Katic et al.	Larsen	Ishihara et al.	Frandsen et al.	Bastankhah and Porté-Agel	Tian et al.	Xie and Archer	Gao et al.	Ishihara and Qian	Dhiman et al.
Upstream wind speed	U	✓	✓	✓	✓	✓	✓	✓	✓	✓	✓	✓
WT rotor radius (or diameter)	r_0 (or D_0)	✓	✓	✓	✓	✓	✓	✓	✓	✓	✓	✓
Downstream distance	x (or s)	✓	✓	✓	✓	✓	✓	✓	✓	✓	✓	✓
Wake expansion (or decay) coefficient	k	✓	✓				✓	✓	✓	✓		✓
Thrust coefficient	C_T		✓	✓	✓	✓	✓	✓	✓	✓	✓	✓
Axial induction factor	a					✓		✓		✓		
Ambient turbulence	I_a			✓	✓						✓	
WT-generated turbulence	I_w				✓							
WT hub height	h			✓			✓	✓	✓	✓	✓	
Surface roughness	z_0							✓		✓		
Spanwise coordinate	z						✓		✓		✓	
Vertical coordinate	y						✓		✓		✓	
Wake model-specific coefficients	-				✓	✓					✓	

Figure 2.5: Input parameters of eleven wake models[42].

There is a high number of wake models, designed to capture different aspects of the wake with different degrees of fidelity and complexity [42]. Generally, tFor the sake of this master project This,

two different categories has relevance regarding the wake models: the wake deficit models and the wake deflection models.

Wake Deficit Model: Simplified Bastankhah's Gaussian

Numerous analytical wake models have been developed to estimate the velocity deficit within the wake [44, 50, 40, 24, 8, 84, 18, 39, 25, 89]. For detailed descriptions of these models, readers are referred to the original publications. Archer et al. [3] and Kaldellis et al. [42] provide comprehensive reviews and evaluations of several wake deficit models. Among these models, the Jensen wake model stands out as the most widely recognized and utilized due to its simplicity and widespread adoption in both industry and academia [64].

The wake model employed in the case of a wind farm with two turbines is an adapted version of Bastankhah's Gaussian wake model [7, 83]. The selection of this wake deficit model aligns with similar investigations related to wake mitigation strategies, such as layout optimization and wind turbine repositioning [37, 47, 83]. This model proves to be well-suited for general layout optimization problems, striking a balance between accuracy and computational cost [7].

The governing equations that describe the velocity deficit in the wake regions are presented in Equation 2.2. Two distinct cases are considered in the wake velocity equation, as wakes are assumed to solely impact points downstream.

$$\frac{\Delta V}{V_\infty} = \begin{cases} \left(1 - \sqrt{1 - \frac{C_T}{8\sigma_y^2/D^2}}\right) \exp\left(-0.5 \left(\frac{y_i - y_g}{\sigma_y}\right)^2\right), & \text{if } (x_i - x_g) > 0 \\ 0, & \text{otherwise} \end{cases} \quad (2.2)$$

Where:

- Normalized wake velocity deficit ($\frac{\Delta V}{V_\infty}$), defined by Eq. 2.2.
- Thrust coefficient (C_T).
- Standard deviation of the wake deficit (σ_y), defined by Eq. 2.2.
- Distance from the hub generating the wake (x_g) to the hub of interest (x_i) along the freestream, given by $(x_i - x_g)$.
- Distance from the hub generating the wake (y_g) to the hub of interest (y_i) perpendicular to the freestream, given by $(y_i - y_g)$.
- Turbine Diameter (D), which has a value of 130 m.

In this study, a combination of the simplified Bastankhah's Gaussian wake model and the rotor-average model is employed. The rotor-average model determines the average wind speed at one or multiple points on the downstream wind turbine rotors by calculating the velocity deficit at these points. On the other hand, the rotor centre model utilizes only a single point, specifically the rotor centre, to estimate the average wind speed of the rotor. Ideally, using multiple points distributed across the rotor would provide a more accurate approximation of the rotor's average wind speed. However, incorporating more points also increases computational costs.

Wake Deflection Model: Jimenez Wake Deflection model

The wake deflection models are employed to calculate the redirection of wakes resulting from factors such as yaw misalignment and sheared inflow. These models consider the downwind and crosswind distances between the source wind turbines and the destination turbines/sites, enabling the computation of new deflected downwind and crosswind distances. Deflection modelling plays a crucial role in simulations involving changes in the angle between the incoming flow and the rotor, as observed in active yaw control or wake steering optimization scenarios [55, 41, 51]. Numerous wake deflection models have been developed to capture the deflection of wake flow resulting from the yaw induction of wind turbine nacelles [55, 41, 26, 65].

In this two-turbine simulation scenario, the Jimenez Wake Deflection model is employed. This model is widely used in PyWake and has been shown to provide a reasonable representation of the skewed

inflow behind the turbine rotor [55, 41]. The implementation of the Jimenez Wake Deflection model follows the methodology outlined by Jiménez et al. [41]. The authors conducted Large Eddy Simulations (LES) to characterize the turbulence behind a wind turbine under different yaw angle and thrust coefficient settings, in order to derive the model. Furthermore, compared to other wake deflection methods available in PyWake, the Jimenez Wake Deflection model demonstrates good computational efficiency, making it suitable for conducting a large number of simulations.

2.4. Case study definition

This section presents a detailed description of the inputs utilized in the methodology outlined in Section 2.2. Firstly, the range of variability for the turbine coordinates and yaw angles is specified in Section 2.4.1. Next, the specific turbine model employed in the simulations is selected in Section 2.4.2, and the wake models utilized in the calculations are discussed in Section 2.3.1.

2.4.1. Wind turbines coordinates and yaw angles range of variability

As previously mentioned in Section 2.2.1, the operational parameters that are modified to assess their impact on the power production of the wind farm are the turbine coordinates (position) and yaw angles. To thoroughly investigate their influence on power production, a wide range of operational parameters was considered.

For each combination of turbine coordinates, the yaw angle of the first turbine (T0) was varied within its designated domain. The lower and upper boundaries of the yaw operating parameter were determined based on existing literature [23], ranging from $+35^\circ$ to -35° with increments of 1° .

When the yaw angle of the upstream turbine (T0) deviates from alignment with the wind direction, the resulting wake flow is modified in the opposite direction of the yaw angle [33, 30, 34]. This means that if T0 is yawed to the right, the wake is deflected to the left, and vice versa. In the case of lateral repositioning of the downstream turbine (T1), it is crucial to displace T1 in the direction opposite to the wake deflection caused by T0. This specific direction of displacement ensures that there is no negative interference between the repositioning and yaw control strategies of the turbines. Misalignment between the displacement of T1 and the opposite wake deflection direction could lead to detrimental consequences for the overall performance of the wind farm.

As a consequence, regarding lateral displacement, the downstream turbine's (T1) y-coordinate was varied within a range from 0 (aligned perfectly downstream with T0) to 1.2 times the rotor diameter (D), ensuring no overlap between the two rotors. The displacement steps were set at 0.1D. The distance in the x-direction between the two turbines was fixed at 7D, a commonly used guideline for downwind spacing in wind farms, providing results that align with realistic scenarios.

In terms of longitudinal displacement, the downstream turbine's range of variability was set from 2 rotor diameters (as the lower boundary) to 9 rotor diameters, where T1 is positioned almost completely out of the wake region. Also, in this case, the displacement steps were set at 0.1D.

2.4.2. Wind turbine selection

The turbine used in the simulation process is the IEA37 3.35 MW onshore reference turbine [11]. The IEA 3.35-MW specifications are open source, and the turbine is designed as a baseline for onshore wind turbine specifications. Table 2.1 shows the turbine specifications.

Description	Symbol	Value	Unit
Hub height	h_{hub}	110	[m]
Rotor diameter	D	130	[m]
Cut-in wind speed	V_{cut-in}	4	[m/s]
Rated wind speed	V_{rated}	9.8	[m/s]
Cut-out wind speed	$V_{cut-out}$	25	[m/s]

Table 2.1: IEA37 3.35MW wind turbine characteristics [11]

It is noteworthy that the IEA37 3.35 MW onshore reference turbine is designed solely for land-based applications.

Offshore wind turbines typically exhibit larger hub heights, rotor diameters, and rated power compared to their onshore counterparts. However, incorporating an onshore turbine is unlikely to alter the essence of the outcomes. In essence, the conclusions derived from the two-turbine simulations for an

onshore wind turbine are expected to align closely with those obtained for an offshore wind turbine. It should be noted that the combination of the two wake mitigation strategies, yaw-based wake steering and turbine repositioning, is independent of any specific wind turbine type and is solely utilized as an input for the simulation process.

2.4.3. Wind resource

Regarding wind resources, it typically encompasses two features: wind direction and wind velocity. In the context of this study focusing on an idealized wind farm case, the analysis was limited to the scenario where the wind direction is perpendicular to the rotor of the two turbines when no yaw is applied. This implies that the flow aligns with the direction in which the turbines are aligned before the potential lateral displacement of turbine T1..

For the wind velocity, the choice was made to investigate four different wind speed cases to examine the effects of the upstream turbine's yaw on power production, both at the individual turbine level and for the overall wind farm. The four wind speed cases considered are as follows:

- Below rated wind speed: For the specific turbine, a wind speed of 7 m/s was chosen.
- Rated wind speed: The wind speed for this case corresponds to 9.8 m/s, which represents the rated wind speed for the specific turbine.
- Slightly above rated wind speed: The wind speed selected for the specific turbine is 10 m/s.
- Far above-rated wind speed: A wind speed of 11 m/s was chosen for the specific turbine.

These choices can be better understood by referring to Figures 2.6 and 2.7, which illustrate the impact of yawing the nacelle of the selected wind turbine on the power curve. Yawing the turbine results in a reduction of the effective wind speed by a factor proportional to the yaw angle, causing a shift of the actual power curves to the right. This indicates that, compared to the zero yaw case, the power production at the same wind speed is lower until the new rated wind speed, which is higher.

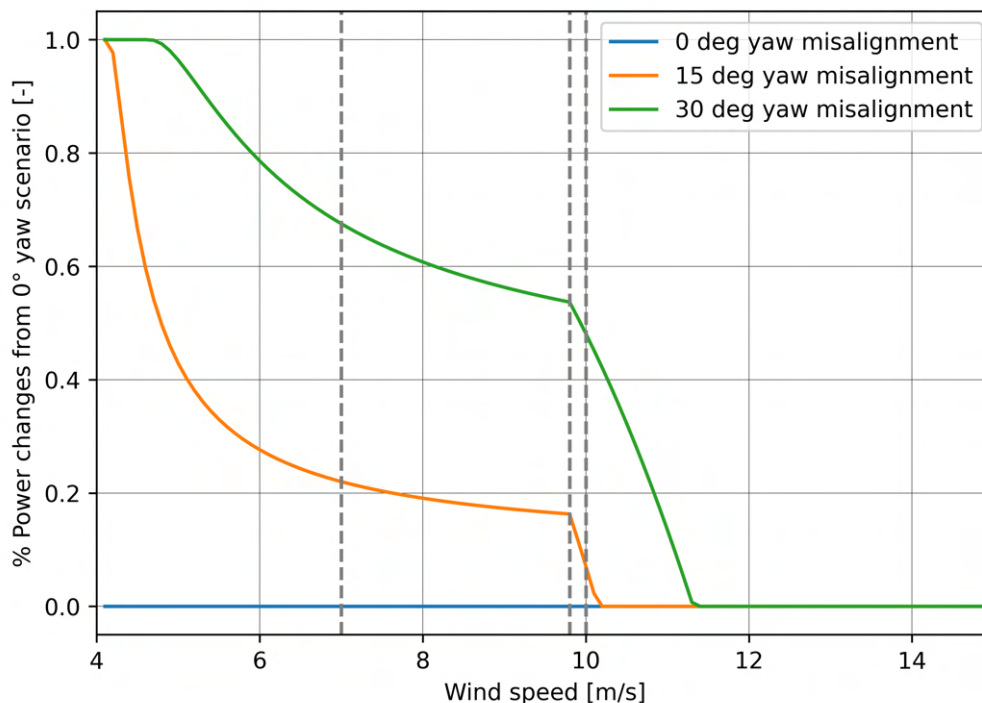


Figure 2.6: Relative changes of the power curves for different nacelle's yaw angles for 0° yaw angle case.

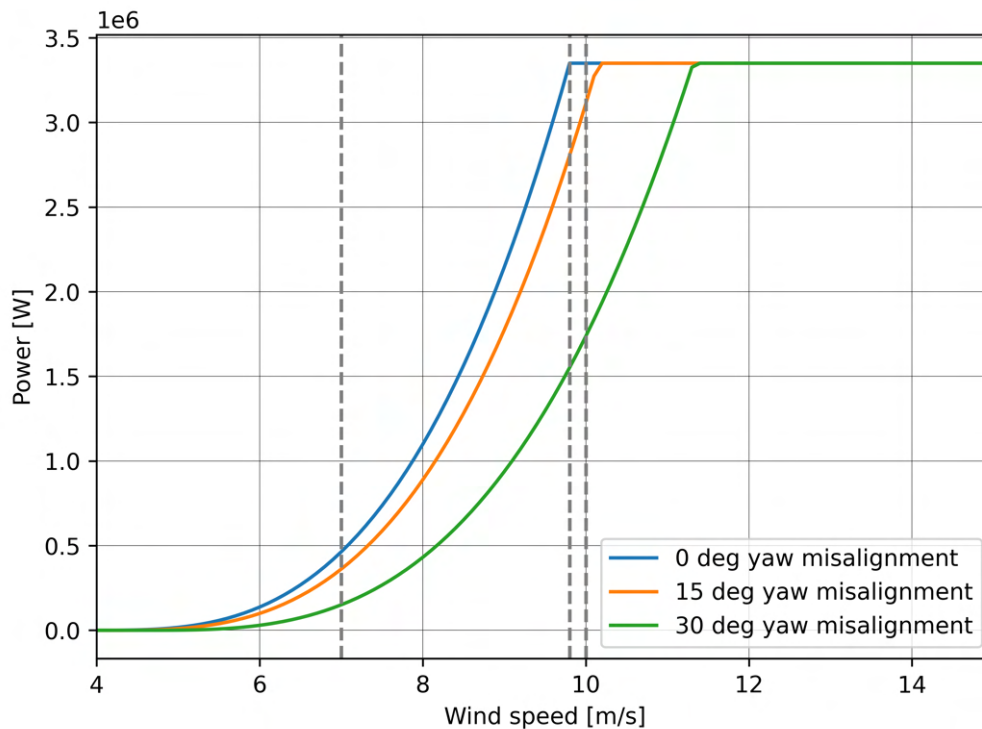


Figure 2.7: Power curves for different nacelle's yaw angles.

Figure 2.7 highlights three distinct regions:

- Below rated wind speed: In this region, the power decrease follows an exponential curve.
- From the rated wind speed to the new rated wind speed (which depends on the nacelle yaw angle): Here, the power curve shows a linear decrease.
- Above the new rated wind speed: In this region, the percentage changes in power compared to the zero yaw case are negligible.

Therefore, the chosen wind speeds are representative of these regions, including the rated wind speed. Specifically, a wind speed of 7 m/s represents the region below rated wind speed, 9.8 m/s represents the rated wind speed, 10 m/s lies within the transitional zone for moderate yaw angles, and 11 m/s falls within the zone where there are no significant changes for moderate yaw angles.

It is essential to note that the power curves depicted in Figure 2.6 are considered ideal, as they exhibit a sudden transition from the region below the rated wind speed to the region above it. This sharp transition, while not reflecting realistic scenarios, is expected to influence the results significantly. Even a marginal difference of 0.2 m/s between wind speeds of 10 m/s and 9.8 m/s can have a substantial impact on the potential power production benefits resulting from yawing the wind turbine. However, it is crucial to recognize that the main objective of these preliminary analyses is to gain insights into general trends and phenomena that occur when employing turbine repositioning and yaw-based wake redirection strategies. The focus is on understanding the overall behaviour rather than capturing detailed real-world conditions.

2.5. Simulation results analyses

The subsequent sections will begin by presenting the findings related to the efficiency of the upstream turbine in section 2.5.1, followed by the examination of the efficiency of the downstream turbine in section 2.5.2. Furthermore, the overall efficiency of the wind farm will be analyzed in section 2.5.3. These results will be presented for two simulation scenarios: one involving longitudinal turbine repositioning and the other involving lateral repositioning.

2.5.1. Upwind turbine efficiency

This subsection presents the efficiency contours of the upwind wind turbine. Since the simulator does not consider the blockage effects of the downstream turbine, the repositioning of the downstream turbine does not have any impact on the power production and efficiency of the upwind wind turbine. Therefore, the changes in turbine positions primarily affect the downstream turbine and its interaction with the wake, while the upstream turbine's performance remains unaffected by the repositioning. Nevertheless, the plots are shown including turbine position to help the interpretation of the downwind and wind farm efficiency, as the sum of the effects are visible in these plots and the plots of the sections 2.5.2 and 2.5.3.

Figure 2.8 demonstrates that the efficiency contours exhibit the same shape across all wind speeds. Notably, these contours align with the power curves associated with a yawed wind turbine displayed in section 2.4.2. It was observed that the efficiency of the turbine decreased as the yaw angle of the first turbine increased, regardless of the wind speed.

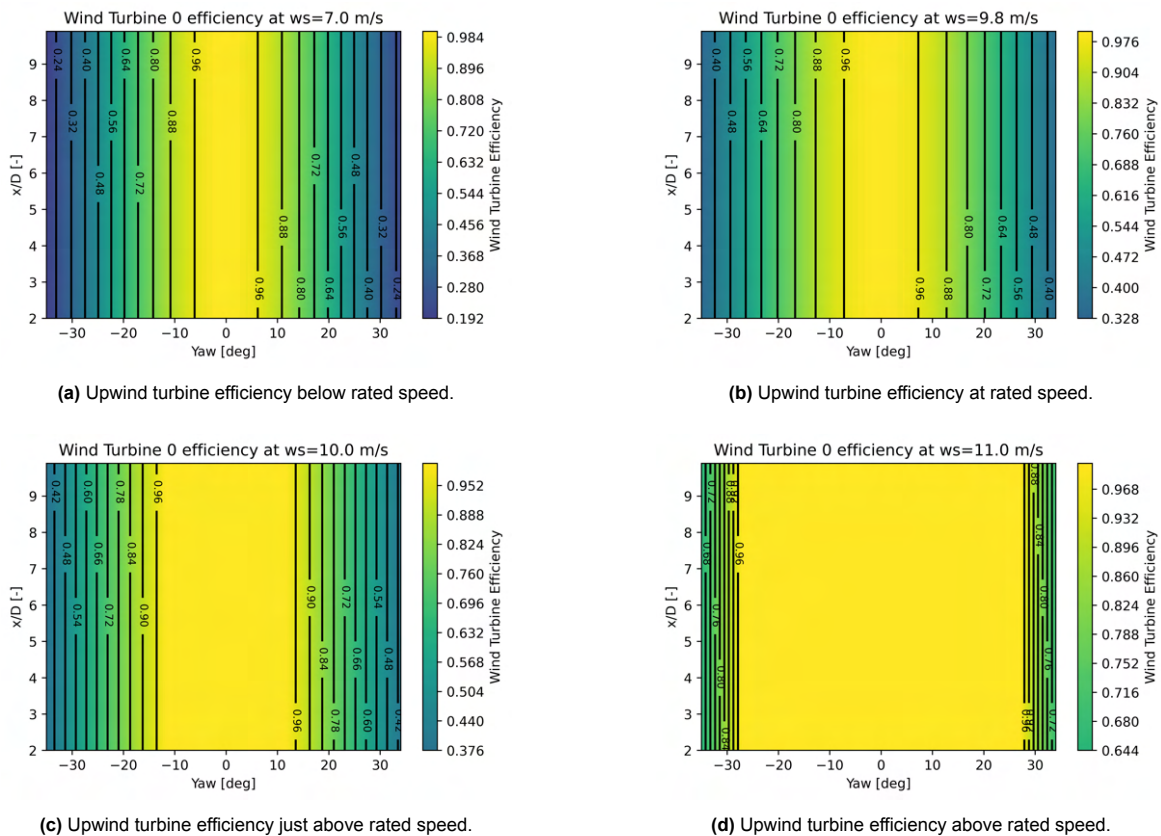


Figure 2.8: Contour plot of the Upwind turbine's efficiency for various desired positions and yaw angles at various wind speeds.

However, as the wind speed increased, it was observed that even with the yawed position, the turbine's efficiency remained relatively high before experiencing a sharp drop. The highest is the wind speed, and the highest is the yaw angle at which the drop in efficiency occurred. This behaviour can be attributed to the fact that for higher wind speeds, the component of the wind speed normal to the rotor, known as the effective wind speed, remained above the rated wind speed until very high yaw

angles. As a result, the turbine continued to produce power at the rated level, effectively mitigating or even nullifying the drawbacks associated with yaw-misalignment for wake redirection.

2.5.2. Downwind turbine efficiency

In this section, the efficiency contours of the downstream wind turbine are presented. The section is divided into two parts: one focusing on the case where the turbine is repositioned in the x-direction, and the other examining the case where the turbine is repositioned in the y-direction.

Case 1: Longitudinal repositioning

Figure 2.9 reveals that the efficiency contours exhibit the same shape across all wind speeds. When the turbine is repositioned downstream, its efficiency increases. Similarly, at the same relative position, when the upstream turbine is yawed, the efficiency of the downstream turbine also increases. This demonstrates the tangible benefits of implementing both control strategies to maximize power production by mitigating the effects of the wake. By yawing the upstream turbine, it is possible to achieve the same turbine efficiency while reducing the required downstream repositioning compared to the case where the upstream turbine is not yawed.

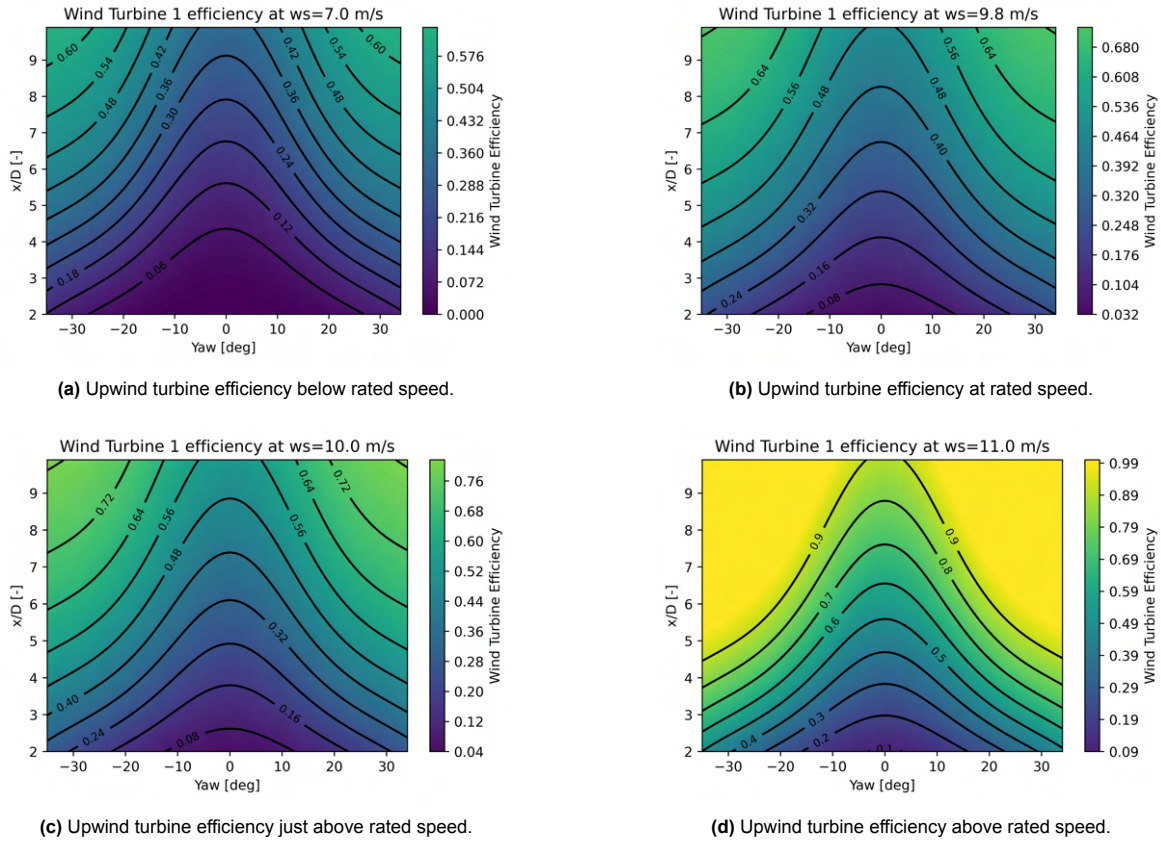


Figure 2.9: Contour plot of the downwind turbine's efficiency for various desired positions and yaw angles at various wind speeds.

Considerations can be made regarding the magnitude of the efficiency gains. It is evident that at all wind speeds, particularly at low wind speeds, yawing the upstream turbine appears to be more convenient in increasing efficiency compared to repositioning the downstream turbine. In fact, even if the costs associated with the mechanism to reposition the turbine are unclear, is it reasonable to expect that the effort to yaw the turbine is more economical and technically simple to achieve compared to the effort required to reposition the turbine, as the yaw mechanism on the turbine's nacelle is a consolidated part of the state-of-art wind turbine [1, 72]. The contribution of each mechanism in enhancing efficiency

varies depending on the actual distance between the two turbines. As the wind speed increases, the gains in efficiency become more significant, and both mitigation strategies become more effective. At wind speeds well above the rated wind speed, as shown in Figure 2.9d, it is apparent that the maximum efficiency can be achieved either by moving the downstream turbine at a distance of 10D or by moving it at a shorter distance of 5D while yawing the upstream turbine. This example well illustrates the potential of combining turbine repositioning and yaw-based wake redirection strategies.

It can be noted that the simulator used for this analysis does not account for the effect of Coriolis acceleration on the wind field as the contours are perfectly symmetric around the vertical axis passing through the origin of the axes.

Case 2: Lateral repositioning

This section presents the contour results for the downstream turbine when it is repositioned laterally. Figure 2.9 demonstrates that the efficiency contours exhibit consistent shapes across all wind speeds. When the turbine is laterally repositioned, its efficiency shows an increase. Similarly, at the same relative position, when the upstream turbine is yawed, the efficiency of the downstream turbine also increases.

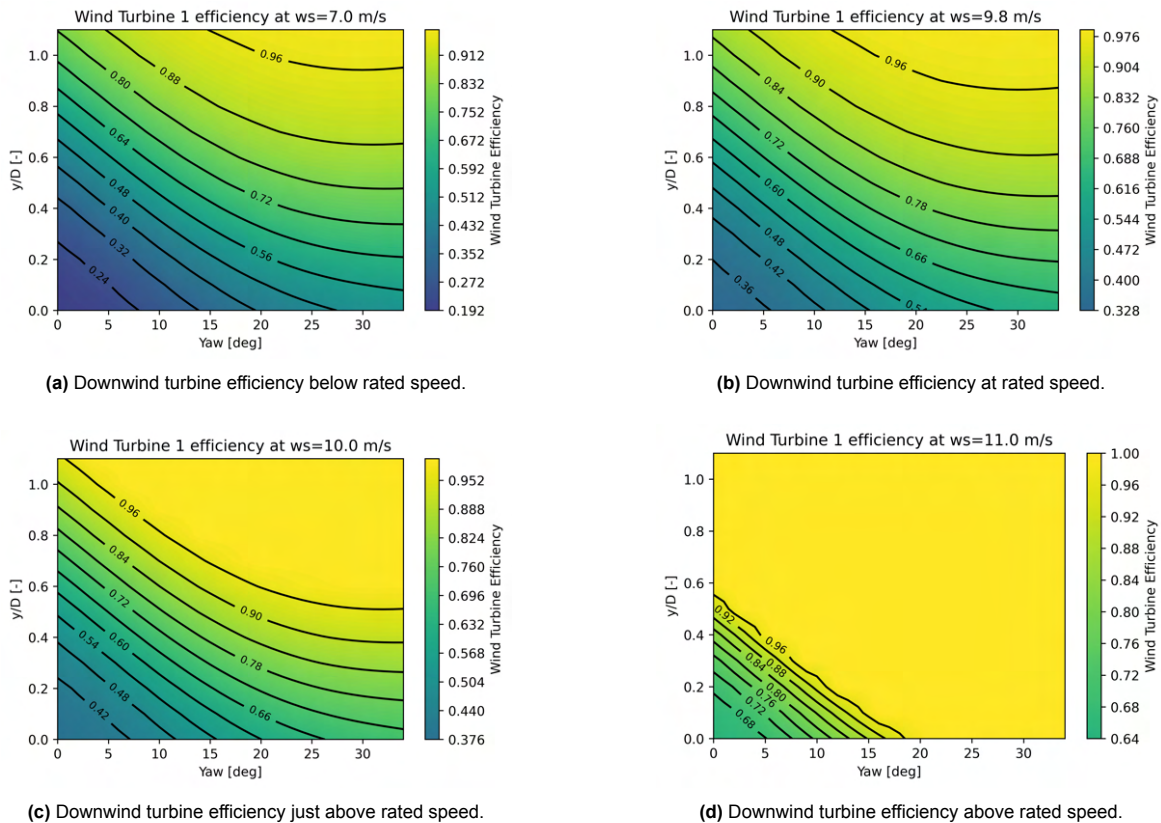


Figure 2.10: Contour plot of the downwind turbine's efficiency for various desired positions and yaw angles at various wind speeds.

In contrast to the case when the turbine is longitudinally repositioned, it becomes evident that the benefits of repositioning in the lateral direction outweigh the benefits derived from the yaw control mechanism. Across all wind speeds, the lateral displacement is much more effective compared to the longitudinal displacement, as it physically moves the turbine away from the wake region, partially or completely reducing the overlap between the downstream rotor and the upstream wake. Significant efficiency gains can be achieved by simply moving the turbine by 0.25D.

It is interesting to note that when the upstream turbine is yawed and repositioning occurs the same efficiency gains observed for larger displacements can also be achieved with smaller displacements.

This is the same as in the case of longitudinal movement. Furthermore, when the turbine is fully moved out of the wake region, reaching its maximum efficiency, it is evident that either repositioning or yawing has an impact on its power production.

Again, it is worth noting that as the wind speed increases, the efficiency also increases.

2.5.3. Wind farm efficiency

This section presents the results of the Wind Farm Efficiency for various wind speed scenarios, considering different yaw angles and positions of the downstream turbine. The section is divided into two parts, each focusing on a specific case of repositioning direction, namely lateral and longitudinal.

It can be noted that the overall efficiency of the wind farm is determined by the combined efficiencies of the individual wind turbines. Specifically, in the examined wind scenario characterized by a single wind speed and direction, the wind farm efficiency results as the average of the efficiencies of both turbines. Alternatively, the contour plots presented in this section can be obtained by overlapping the contours displayed in the sections dedicated to the individual turbines.

Case 1: Longitudinal Repositioning

Figure 2.11 illustrates the contours of Wind Farm Efficiency for various wind speed scenarios.

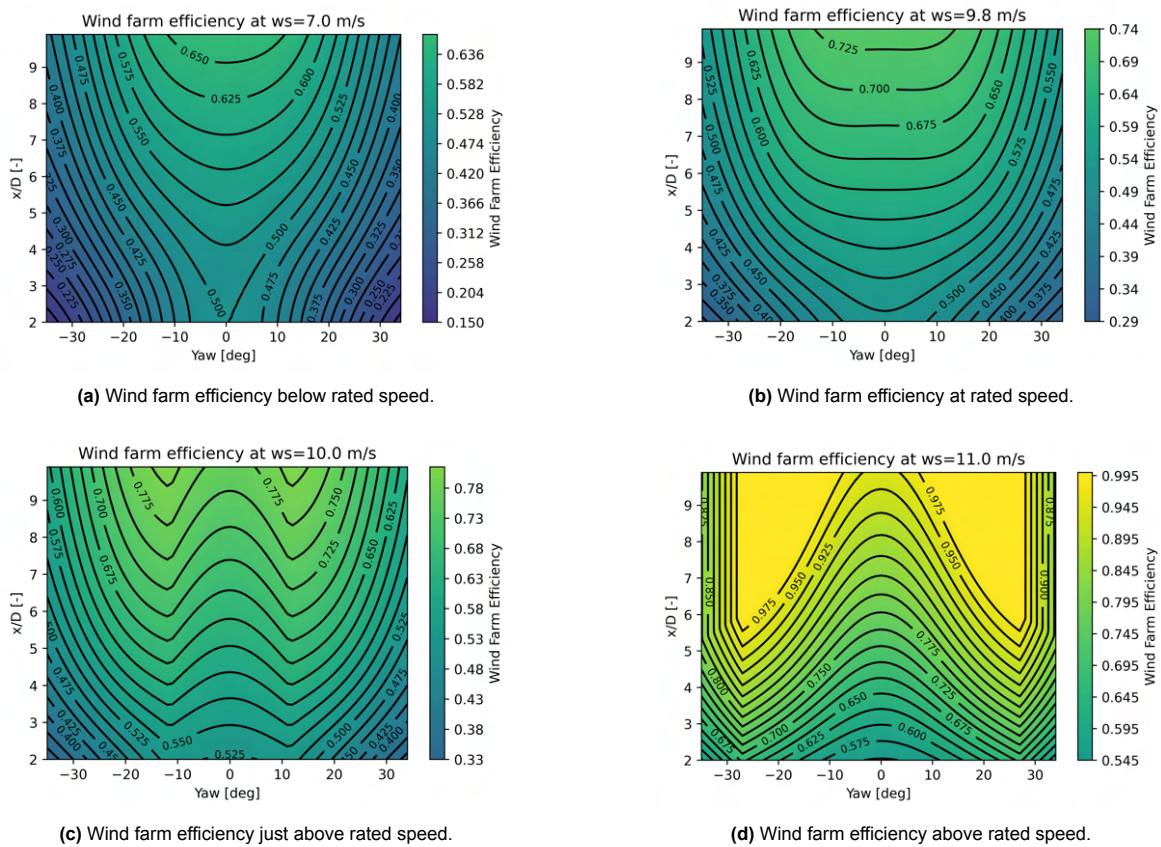


Figure 2.11: Contour plot of the efficiency wind farm for various desired positions and yaw angles at various wind speeds.

Examining Figure 2.11a, it was observed that below the rated wind speed (at 7 m/s), the increase in Turbine 1’s efficiency resulting from downstream repositioning and yaw angles was smaller than the decrease in Turbine 0’s efficiency. Hence, the effect of yaw control on the wind farm was not beneficial. However, this trend changed as the wind speed increased.

At the rated wind speed, as depicted in Figure 2.11b, the beneficial combination of downstream repositioning and yaw angles on Turbine 1 was observed for x/D values greater than $5D$. Turbine 1’s

power gains compensated for the loss in Turbine 0's efficiency up to an angle of 11 degrees. However, as Turbine 1 was positioned further downstream from Turbine 0, the range of yaw angles where the combination of yaw and repositioning was beneficially decreased. This occurred because Turbine 1 was placed almost outside of Turbine 0's wake, or alternatively, the wake had sufficiently recovered at that distance.

Slightly above the rated wind speed (at 10 m/s), as shown in Figure 2.11c, the beneficial effect of yaw control became more pronounced. Turbine 0 continued to produce at its rated power up to an angle of 11 degrees, resulting in a constant efficiency. Meanwhile, the overall wind farm efficiency at a fixed downstream distance increased, reaching an optimum value at 11 degrees. The beneficial effects continued even at higher yaw angles. It should be noted that the farther the downstream turbine was from the upstream turbine, the greater the potential gain from the combination of yaw and repositioning. Conversely, as the downstream turbine was positioned farther away, the operating range of yaw angles for the upstream turbine to maintain a beneficial effect became narrower.

Similar effects were observed at a wind speed of 11 m/s but with higher yaw angles. The combination of downstream repositioning and yaw angles allowed for a reduction of up to 4D in the necessary movement of the downstream turbine to achieve maximum wind farm efficiency. The optimum angle could be reached at very high angles, but the transition from the beneficial zone to the non-beneficial zone was sharp rather than gradual.

Case 2: Lateral Repositioning

Figure 2.11 depicts the contours representing the Wind Farm Efficiency across different wind speed scenarios. The figures reveal a strong correlation between upcoming wind speeds and the impact of wind farm control methods on overall wind farm efficiency. As wind speeds increase, it appears that yaw-based wake steering, combined with repositioning, has a beneficial effect.

Across all wind speeds, the combination of the two methods exhibits an optimum yaw angle at which the highest performances are achieved. The magnitude of the optimum yaw angle depends on both the position of the downstream turbine and the upcoming wind speeds.

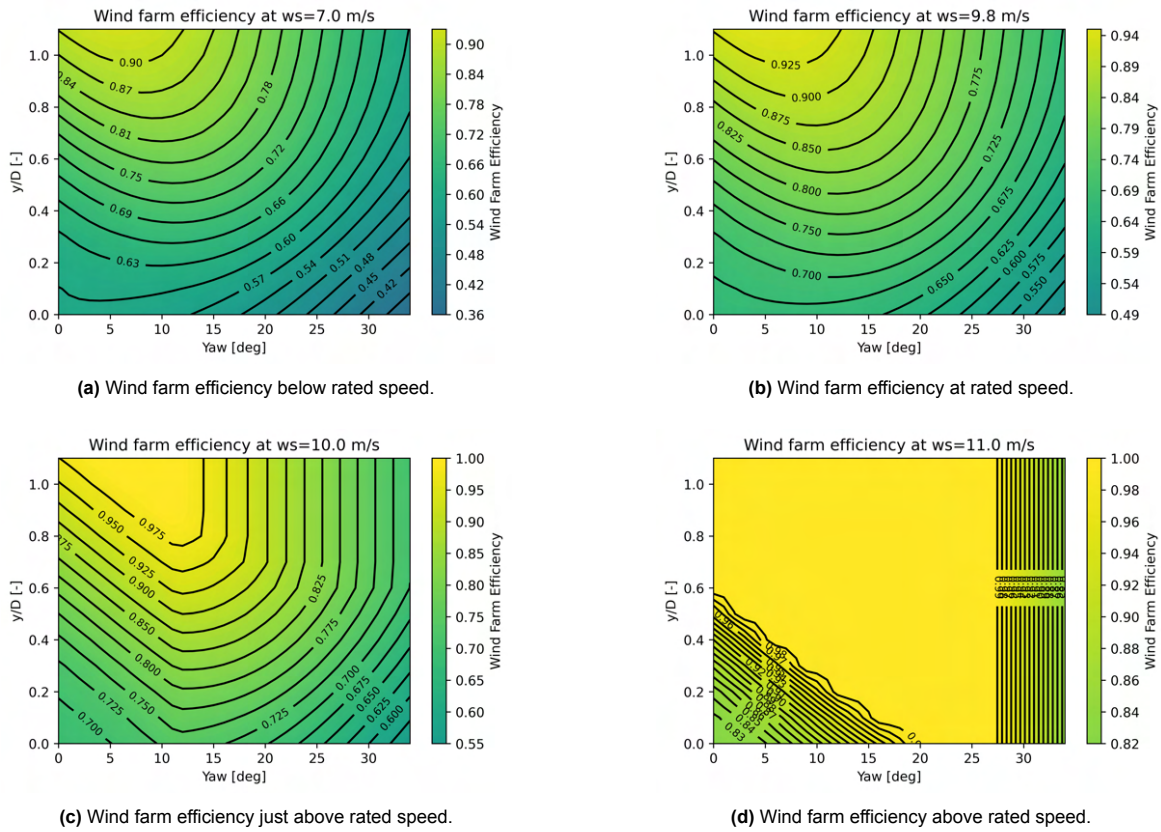


Figure 2.12: Contour plot of the efficiency wind farm for various desired positions and yaw angles at various wind speeds.

At wind speeds of 7 m/s and 9.8 m/s, shown in Figure 2.12a and 2.12b, below rated wind speed and at rated wind speed, the contour shapes are very similar. The beneficial effect of yaw control is less pronounced compared to other wind speeds. Furthermore, there is a smooth transition zone where the combination yields power gains. The optimal yaw angles lie in the range of 10° to 15°.

Just above rated wind speed, at 10 m/s, displayed in Figure 2.12c, the combination of yaw and repositioning significantly enhances efficiency gains compared to applying the two methods independently. There is a linear transition zone of increasing efficiency from 0° up to the optimal yaw angles, which again lie in the range of 10° to 15°. Beyond these angles, the efficiency drops. This behaviour can be explained by examining the power curve of a yawed wind turbine and the contours related to the efficiency of the individual wind turbine.

When the first wind turbine is yawed, the efficiency remains elevated until a certain critical angle is reached, after which the efficiency declines. This transition occurs from a beneficial situation for wind farm production to a situation where the power losses of the upstream turbine are not offset by the power gains of the second turbine. This mechanism is more evident for wind speeds above the rated level, as the effective wind speeds may not differ significantly from the rated level. For high wind speeds, such as 11 m/s, as can be seen from Figure 2.12d, this phenomenon becomes even more apparent.

3

WFLO combined with turbine repositioning and yaw-based wake redirection for an extended wind farm case study

This chapter presents and applies on a case study a methodology for assessing the impact of different wake mitigation strategies when applied individually and in combination within an extended wind farm scenario.

Firstly, section 3.1 introduces the wind farm layout optimization problem and its combination with turbine repositioning and yaw-based wake redirection strategies present in the literature. Next, section 3.2 presents the methodology and workflow used to assess the impact on power production of the aforementioned wake mitigation strategies. It also describes the calculation tools employed in this Master's thesis project. Furthermore, in section 3.3, the specific extended wind farm case chosen to apply the methodology is carefully selected and described. Lastly, in section 3.4, the results are presented and analyzed.

3.1. The wind farm layout optimization problem

This section provides an overview of the existing literature regarding the wind farm layout optimization problem, as well as its combination with turbine repositioning and yaw-based wake redirection. Section 3.1.1 offers a general description of an optimization problem, while section 3.1.2 specifically defines the wind farm layout optimization problem. Following that, section 3.1.3 explores literature studies focusing on the combination of turbine repositioning and layout optimization problem. Lastly, in section 3.1.4, a representative study illustrating the combination of wind farm layout optimization and yaw-based wake redirection is presented.

3.1.1. General optimization problem

Optimization problems are fundamental mathematical problems that involve finding the best possible solution to maximize or minimize an objective function while satisfying a set of constraints. According to Martins and Ning (2021) [57], optimization problems consist of three essential components: design variables, objective function, and constraints. The design variables are the variables that describe the system being optimized, and the dimensionality of the problem is determined by the number of design variables, denoted as n_x . Each design variable, denoted as x_i , is subject to an upper bound \bar{x}_i and a lower bound \underline{x}_i . These bounds restrict the range of values that the variables can take.

The objective function, denoted as $f(x)$, quantifies the quantity that is to be either minimized or maximized. A careful definition of the objective function is crucial, as it determines the aspect of the

problem that will be optimized. It is important to ensure that the objective function properly captures the problem's objectives, as an inappropriate formulation can lead to suboptimal solutions from an engineering standpoint.

Constraints are another critical element in optimization problems and typically involve functions of the design variables. Constraints can be categorized into two types: inequality constraints, expressed as $g_j(x) \leq 0$, and equality constraints, expressed as $h_l(x) = 0$. Inequality constraints impose conditions that the variables must satisfy, while equality constraints define relationships that must be fulfilled.

Mathematically, the optimization problem can be formulated as follows:

$$\begin{aligned}
 & \text{minimize} && f(x) \\
 & \text{by varying} && \underline{x}_i \leq x_i \leq \bar{x}_i \quad i = 1, \dots, n_x \\
 & \text{subject to} && g_j(x) \leq 0 \quad j = 1, \dots, n_g \\
 & && h_l(x) = 0 \quad l = 1, \dots, n_h.
 \end{aligned} \tag{3.1}$$

The optimization problem statement serves as the foundation for the wind farm layout optimization problems, which will be defined in the subsequent sections.

3.1.2. Wind farm layout optimization

Wind Farm Layout Optimization (WFLO) in literature usually refers to the placement of wind turbines within a specified area. The objective of wind farm layout optimization is to determine the positions of wind turbines within the wind farm, with the aim of maximizing energy production and minimizing costs while considering various constraints. These constraints may include the wind farm boundary, proximity between turbines, noise emission levels, and investment limitations. In most cases, wind farm layout optimization involves a multi-objective mixed-integer-discrete-continuous nonlinear constrained optimization problem that lacks an analytical formulation, making it mathematically complex [66].

Over the past two decades, there has been a growing interest in addressing this complex problem. Researchers have proposed different problem formulations and utilized various optimization algorithms to tackle wind farm layout optimization. Previous works have employed simplified formulations, such as equally spaced turbine arrays [80, 16], unequally spaced turbine arrays [43], aligned or staggered grid-like layouts [43, 5], pre-divided discrete grid points [59], and continuous searching spaces [56, 62]. These formulations have been conducted with a range of optimization algorithms, including Monte Carlo [80, 68], Genetic Algorithms (GA) [5, 56], Simulated Annealing (SA) [56], Particle Swarm Optimization (PSO) [27], and local search algorithms [86].

Different objectives have been considered in wind farm layout optimization studies, such as power maximization [43], annual energy production (AEP) maximization [56, 86], profit maximization [80, 56], net present value (NPV) optimization [43], and cost minimization, including the cost of energy (CoE) [59, 68, 27]. For a more comprehensive survey of published works in this area, several papers provide detailed overviews [20, 67, 81].

3.1.3. WFLO combined with turbine repositioning

In the context of this Master's thesis project, the wind farm layout can be classified as either static or dynamic based on the positioning of the turbines. The static layout assumes that the turbine positions remain fixed throughout the operational duration of the wind farm, while the dynamic layout considers the repositioning of turbines over the lifetime of the wind farm. This division was established by Kilinic [47].

The turbine repositioning strategy, as discussed in section 1.3.2, explores the opportunity to relocate floating wind turbines in real-time to mitigate wake effects [22]. In simpler terms, the downstream turbine is moved to avoid or minimize the wind velocity deficit caused by the wake of the upstream turbine.

Motion	Movable range shape	Mooring configuration(s)
Stationary	none	
Linear		
Planar (triangular)		
Planar (rectangular)		
Planar (circular)		

Figure 3.1: Movable range shapes for movable floating offshore wind turbines for various mooring configurations [47].

The range of positions that a turbine can move to and maintain is commonly referred to as the movable range. The shape and size of the movable range are directly influenced by the configuration of the mooring system, as depicted in Figure 3.1. Both linear and triangular shapes of the movable range have been investigated by Rodrigues et al. [70], while Kilinc [47] explored the circular shape of the movable range in his Master's Thesis Project. The following subsections will discuss the most notable research in this area.

Circular movable range

In Kilinc's Master's Thesis Project [47], an investigation was conducted to explore the potential of repositioning wind turbines within a wind farm to enhance the annual energy production (AEP). As discussed in section 3.1.3, the author assumed that the wind turbines had a circular movable range, enabling the examination of various movable range sizes, ranging from small values (resulting in minimal movement) to large values (allowing turbines to relocate anywhere within the wind farm).

Several key observations emerged from this study. Firstly, increasing the movable range leads to enhanced wind farm efficiency. Secondly, the most substantial improvement in wind farm efficiency occurs when the radius of the movable range is up to two times the rotor diameter, while beyond that movable range size, the improvement in wind farm efficiency reaches a plateau. The most important result is that dynamic wind farm layouts exhibit significant potential for enhancing wind farm efficiency.

The author highlights that when the movable range size of the turbines is at least two times the rotor diameter the specific installation position of the turbines (i.e. the centre of the movable range) becomes less significant in layout optimization when turbines are free to move. This is due to the relevant size of the movable range, which determines the magnitude of the allowed turbine movement, offering greater flexibility in the optimization process and making the installation position not relevant.

Among the objectives of this Master's thesis, there is to explore whether the advantages of position mooring for turbine repositioning, in terms of improved wind farm efficiency, can be attained with smaller movable ranges when combined with another wind farm control technique, such as yaw-based wake repositioning.

Linear and triangular movable range

S.F. Rodrigues et al. (2015) proposed an optimization framework [70] for optimizing the layout of a floating offshore wind farm by utilizing a novel type of floating turbine developed by IDEOL. This turbine has the ability to move along its mooring lines, offering increased flexibility in turbine positioning. The basic version of the turbine allows linear movements in one direction, making it simpler to operate since the turbine position is determined by a single parameter: the distance from an anchoring position. In contrast, the more complex design enables the turbine to cover a triangular area and move in two directions, providing enhanced manoeuvrability but also introducing greater control complexity as two coordinates must be set to position the turbine.

In their work, S.F. Rodrigues et al. (2015) propose a nested optimization framework [70] to optimize the positioning of turbines with a movable triangular range. The outer loop of the optimization framework determines the anchor positions for the turbines, while the inner loop optimizes the locations of the turbines for each wind direction. The optimization variables in the outer loop are the central point of the anchoring locations and the rotation angle that describes the orientation of the anchors, with the angle within the mooring lines fixed at 120° . The inner loop takes the position and angles of the anchoring locations as input and optimizes the turbine locations within the footprint area defined by the anchors.

3.1.4. WFLO combined with yaw-based wake redirection

In the study conducted by Fleming (2016) [23], an active approach is proposed to enhance the performance of wind power plants by integrating wake redirection through intentional yaw misalignment with plant layout optimization. The primary aim is to compare the outcomes of this optimization strategy, considering various cost metrics such as power density, maximum cabling length, and the wind farm boundary. This comparison involves the original wind power plant configuration as well as configurations where control or layout optimization is performed separately or sequentially.

The investigation considers three main cases: layout optimization alone, individual application of yaw-based wake redirection, and the combined optimization of layout and control. Within these cases, four distinct scenarios are analyzed: baseline (fixed turbine positions with rotors perpendicular to the incoming wind direction), optimized yaw (fixed positions with turbines optimally yawed for each wind direction), optimized location (optimized positions with turbines yawed in the mean wind direction), and combined optimization (simultaneous optimization of yaw and position).

Among the cases, the combined optimization outperforms both the control-only and layout-only cases in terms of key metrics. Notably, the combined optimization results in a significantly smaller plant area while maintaining a similar mean power output, leading to an approximately 40% increase in power density compared to layout optimization alone.

Furthermore, the study compares all three combined yaw-position optimization cases with a sequential approach, where the layout is optimized first and then the yaw angles are optimized based on the selected layout. The sequential optimizations require significantly less computational power compared to coupled ones. The results demonstrate that the coupled optimization approach is more effective in maximizing power density compared to the sequential optimization approach.

3.2. Methodology

This section presents the different scenarios and corresponding algorithms analysed in this Master's thesis project chosen to capture the impact of the different wake mitigation strategies. Firstly, the scenarios are introduced in section 3.2.1. Then, the choice of the sequential optimization approach is justified and motivated in section 3.2.2. Subsequently, the optimization function used in the process is defined in section 3.2.3. Hereafter, the workflow for each case is outlined in section 3.2.4. Finally, the tools used to do the calculations and the main metrics used to compare the results, the wind farm efficiency, are presented respectively in section 3.2.5 and section 3.2.6.

3.2.1. Scenarios

As mentioned in section 1.5, the objective of this thesis is to investigate the impact of different wind farm control strategies on maximizing power production. To demonstrate the significance of each strategy and its contributions, six distinct scenarios are compared:

1. Baseline: Fixed (original) turbine positions with all turbines yawed in the mean wind direction.
2. Yaw optimization: Fixed (original) turbine positions with turbines optimally yawed for each wind direction.
3. Static layout optimization: Position optimized considering all wind directions, with all turbines yawed in the mean wind direction.
4. Combined static optimization: position optimized for all wind directions and yaw sequentially optimized for each wind direction.
5. Dynamic layout optimization: Position optimized for each wind direction, with all turbines, yawed in the mean wind direction.
6. Combined dynamic optimization: position optimized for each wind direction and yaw sequentially optimized for each wind direction.

The scenarios will be analysed for a wind farm with a circular area. This means that the possible locations for wind turbine placement will conform to the circular shape of the domain, and the mathematical formulation of the constraints on the positions will align with this circular configuration.

The definition of the turbine movable range, which represents the positions where the turbine can be moved and maintained, has a significant impact on the optimization problem for dynamic optimization scenarios. It establishes the constraints that need to be applied to the turbine coordinates during the repositioning optimization process. In all the scenarios assuming that the turbines are repositioned, a circular shape was employed for the movable range. This choice eliminated the need to consider the orientation of the movable range as a variable.

Following the approach of Kilinic [47], adopting a circular movable range reduces the problem's complexity and computational time. This enables the investigation of how different movable range sizes affect the potential gains in wind farm Annual Energy Production (AEP).

It is essential to emphasize that the analysis assumes the turbine's capability to maintain its position irrespective of its nacelle yaw angle. Referring to Section 1.3.5, this means that when the turbine is yawed to redirect the wake, any undesired repositioning effect caused by the alteration in the direction of the thrust force, falling under the purview of the Yaw and Induction-Based Turbine Repositioning (YITuR) control method, is disregarded.

3.2.2. Sequential optimizations

Among the scenarios presented in section 3.2.1, scenarios 4, 5, and 6 involve multiple wake mitigation strategies. scenario 4 considers static wind farm layout optimization and yaw-based wake redirection, scenario 5 involves wind farm layout optimization and turbine repositioning (i.e., dynamic wind farm layout optimization), and Scenario 6 considers dynamic wind farm layout optimization and yaw-based wake redirection strategy.

For all these combined scenarios, it was decided to sequentially combine the different wake mitigation strategies. The reasons behind this choice can be divided into two main aspects: general aspects and case-specific aspects. Generally, the sequential approach is faster compared to simultaneous or nested approaches [47, 6, 22, 23]. Given the high number of uncertainties and design variables involved in the problems, this choice allowed for a larger number of simulations across different scenarios, covering a wider range of topics. It provided insights into the potential benefits of combining these three wake mitigation strategies. On a more specific level, the following observations can be made.

On one hand, regarding the combination of wind farm layout optimization and turbine repositioning with a circular movable range, Kilinic [47] investigated both sequential and nested approaches in his Master's Thesis. He concluded that the nested approach yielded better efficiency gains, especially when the movable range size was relatively small (i.e., below 1.5 D). However, this slightly better performance just demonstrates that it is possible to increase power production by using a more computationally expensive strategy. Therefore, since no additional relevant information could be extracted, a coarser approach was chosen, conducting simulations that sequentially included wind farm layout optimization and turbine repositioning.

On the other hand, regarding the combination of yaw-based wake redirection with (static or dynamic) wind farm layout optimization, Fleming et al. [23], as reported in section 3.1.4, conducted a series of simulations that combined turbine nacelle yawing and layout optimization to optimize power density, cable length, and wind farm boundary. The study compared a series of combined yaw-position optimization cases with a sequential approach, where the layout was optimized first, followed by the optimization of yaw angles based on the selected layout.

However, even though the simultaneous approach yielded better results in terms of power density for the selected extended wind farm case study, where the wind farm boundaries were fixed, the simultaneous optimization did not outperform the sequential one in similar cases studied by Fleming et al. [23]. Moreover, due to the large number of cases analyzed in this Master's Thesis project, the sequential approach was chosen again to reduce the required computational power and time when considering the yaw-based wake redirection strategy.

3.2.3. Optimization function: the AEP

The primary metric for optimization in all scenarios is the Annual Energy Production (AEP), which serves as a surrogate metric for the Levelized Cost of Energy (LCOE). As highlighted in section 1.2, numerous uncertainties are associated with the impact of turbine repositioning on the wind farm's Capital Expenditure (Capex) and Operational Expenditure (Opex). Therefore, it is reasonable to first assess the potential gains in wind farm power production. The trade-offs between balance-of-station costs and annual energy production are specific to each site, and this Master's thesis project aims to explore solutions across various conditions.

The cost and feasibility of altering the overall layout of a wind farm will vary depending on the site, as will the costs associated with the wind turbines' mooring system. Instead of using specific numerical values for a particular site, the decision was made to consider the annual energy production as a metric that captures the trade-offs. Although this metric may not be directly applicable as an absolute value to completely capture all the potential benefits and drawbacks of the different wake mitigation strategies investigated, it is valuable for comparing relative changes in power production among them, which is aligned with the goals of this Master's thesis project.

Additionally, the cost components of Capex and Opex appear to be largely unaffected by design variables such as turbine position, turbine repositioning, and yaw control. For instance, the number of turbines and floater type are typically fixed parameters, which serve to stabilize a considerable portion of the Capex and Opex. Nevertheless, variations in cable costs may arise in response to turbine positions, yet since the area of the site is constrained, the anticipated alterations are projected to be minor. It should be noted, however, that there may be some cost discrepancies between different scenarios. For example, repositioning necessitates a more intricate mooring system, and yawing may contribute to higher loads. Although this does not impact the optimization for a specific scenario, it warrants care-

ful consideration when comparing diverse scenarios.

According to Baker et al. [7], the Annual Energy Production (AEP) can be calculated using the following equation:

$$\text{AEP} = \left(\sum_{k=1}^{n_{\text{wd}}} \sum_{l=1}^{n_{\text{ws}}} f_k w_{k,l} P_{k,l} \right) 8760 \frac{\text{hrs}}{\text{yr}} \quad (3.2)$$

where:

- n_{wd} represents the number of wind direction bins.
- n_{ws} denotes the number of wind speed bins.
- f_k signifies the frequency of occurrence of a wind direction bin.
- $w_{k,l}$ represents the frequency of occurrence of a wind speed bin for each wind direction bin.
- $P_{k,l}$ indicates the total wind farm power output at the midpoint value of a wind direction bin.
- 8760 represents the number of hours in a year.

3.2.4. Optimization Framework

In this section, the optimization framework adopted for each scenario is presented.

Scenario 1: Baseline

The baseline case serves as an initial measurement for comparing changes in wind farm efficiency across various scenarios where a wake mitigation strategy is employed. In this regard, the baseline scenario does not involve any optimization and does not necessitate the use of a specific framework.

The locations of the wind turbines are adopted from the literature [7] and will be labelled as "original" within the context of this Master's thesis project.

Scenario 2: Yaw optimization

The yaw angle of each turbine was optimized to maximize power production for every wind direction. Due to the assumption of yaw control, the optimizations for each wind direction were treated as independent problems and could be optimized separately. This resulted in independent optimization problems, with each problem corresponding to a specific wind direction bin. The general optimization problem can be formulated as follows:

$$\begin{aligned} &\text{maximize} && P_i(x_j, y_j, \psi_j) && j = 1, \dots, n_{\text{wt}}, i = 1, \dots, n_{\text{wd}} \\ &\text{by varying} && \psi_j \\ &\text{subject to} && -35^\circ \leq \psi_j \leq 35^\circ \end{aligned} \quad (3.3)$$

Where, $P_i(x_j, y_j, \psi_j)$ represents the wind farm power production for that specific wind bin direction, with x_j and y_j denoting the fixed turbine locations, and ψ_j representing the turbine yaw angle. The bounds on the yaw angle, ranging from -35° to 35° , were imposed to prevent the exploitation of nonphysical solutions that may arise when highly yawed configurations are considered.

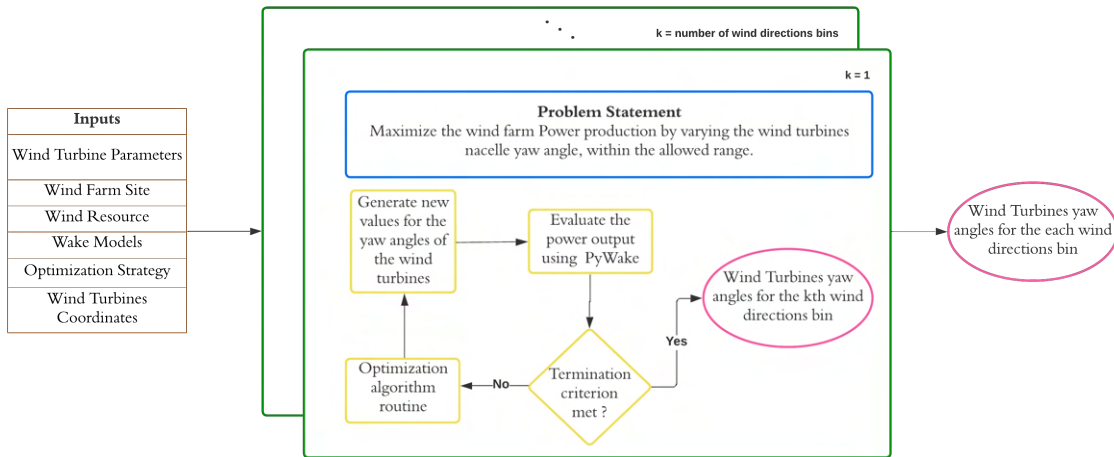


Figure 3.2: Workflow chart of the Yaw Optimization.

Figure 3.2 shows the input, the output as well as the optimization problem workflow for this scenario.

As shown in the image the inputs involve the wind turbine parameters, the wind farm site, the wind resource, the wake models, the optimisation strategy and the turbine coordinates. Once the turbine coordinates are given as input, for each k^{th} wind direction, the wind turbine's yaw angle is changed in accordance with the problem constraints. Each optimization process iterates until the termination criteria of the algorithm are satisfied. It has been chosen to use a tolerance on the improvement of the power production as a termination criterion (rather than e.g. a number of iterations). This choice allows focusing the analyses on the potential gains in wind farm efficiency without taking into account the computational differences (and thus the required number of iterations to get the best value) that may arise within different wake mitigation strategies when coupled with the optimization algorithm. This choice is common to all the scenarios, even if the value of the tolerance is different in each case. The resulting output is the wind turbines' yaw angle for each wind direction of the wind farm that achieves an optimal AEP in accordance with the optimizer and wakes models' performances.

Scenario 3: Static layout optimization

The main goal of the static WFLO is to maximize the AEP by adjusting the coordinates of wind turbines within the wind farm boundary. In this scenario, all turbines are oriented with their rotors perpendicular to the incoming wind direction, which means they are yawed in the mean wind direction, denoted by $\psi = 0$ for all turbines. The problem can be formulated as follows:

$$\begin{aligned}
 & \text{maximize} && AEP(x_j, y_j) && j = 1, \dots, n_{wt} \\
 & \text{by varying} && x_i, y_j \\
 & \text{subject to} && x_j^2 + y_j^2 \leq R_B^2
 \end{aligned} \tag{3.4}$$

where:

- AEP represents the Annual Energy Production.
- n_{wt} is the total number of wind turbines.
- x_j denotes the x-coordinate of the j-th wind turbine.
- y_j denotes the y-coordinate of the j-th wind turbine.
- n_X denotes the number of design variables.
- R_B represents the radius of the boundary of the wind farm.

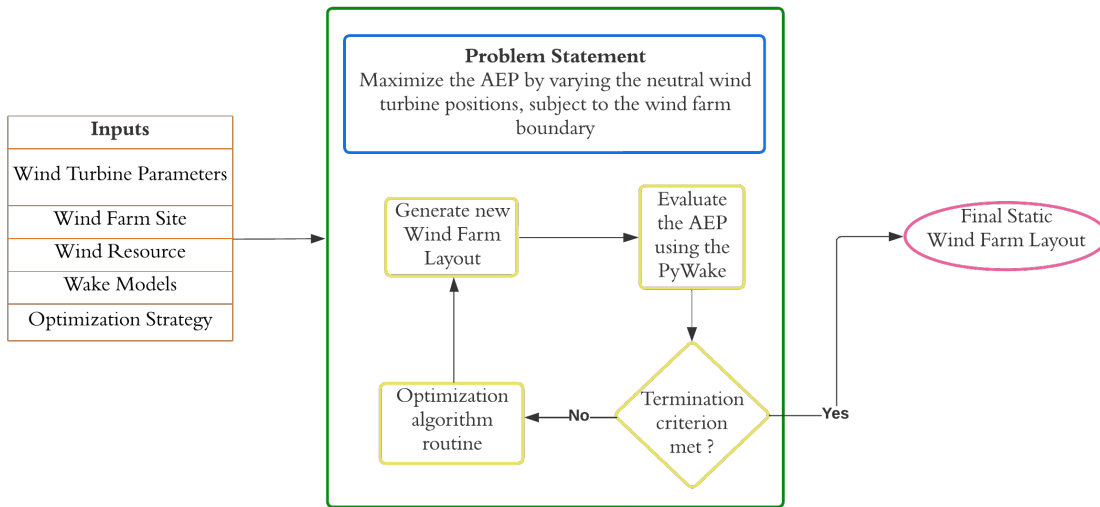


Figure 3.3: Workflow chart of the Layout Static Optimization.

Figure 3.3 shows the input, the output as well as the optimization problem workflow for this scenario.

As shown in the image the inputs involve the wind turbine parameters, the wind farm site, the wind resource, the wake model and the optimisation strategy. Once the original turbine coordinates are given as input, the wind turbine's position is changed in accordance with the circular wind farm boundary constraints. Again, the optimization process iterates until the termination criteria for the improvement of the power production is met. The resulting output is the wind turbine's optimal position, fixed and common for each wind direction, that achieves an optimal AEP in accordance with the optimizer and wakes models' performances.

Scenario 4: Sequential static optimization

The sequential yaw static optimization aims to maximize the AEP of a wind farm through the optimization of wind turbine positions and subsequent optimization of yaw angles. The optimization process consists of two steps, each addressing a specific optimization problem.

Figure 3.4 shows the used optimisation framework and clearly underlines the sequential structure of the problem..

In the first step, the objective is to maximize the AEP of a static wind farm layout by optimizing the positions of wind turbines, taking into account constraints such as the wind farm boundary. Once the optimal static positions of the wind turbines are determined, they are used as the turbine positions in the second step. It should be noted that the optimization problem described previously is the same as the one presented for scenario 3, above.

After obtaining the turbine coordinates from the first step, the second step of the optimization is still focused on maximizing the AEP of the wind farm by optimizing the yaw angles of the wind turbines for each considered wind direction. This involves solving n_{wd} optimization subproblems, with each subproblem dedicated to a specific wind direction. As the reader may infer, the optimization problem is the same as the one described for scenario 2, with the only difference being the actual positions (coordinates) of the turbines. In this case, the x and y coordinates of each turbine result from the first step of the optimization rather than being the initial positions defined in the baseline scenario.

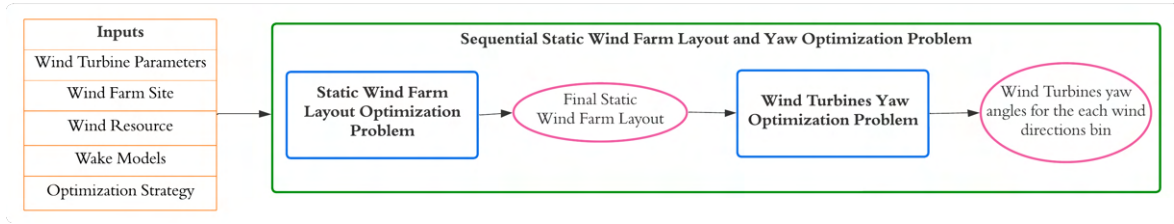


Figure 3.4: Workflow chart of the sequential static optimization.

Scenario 5: Dynamic layout optimization

The sequential dynamic layout optimization consists of two steps, representing the initial scenario in this Master's thesis project that incorporates movable turbines, allowing for the modification of turbine positions during the wind farm's lifespan. This type of layout optimization, as explained in section ??, is referred to as dynamic wind farm layout optimization.

This optimization framework is taken from the work of Ufuktan Kilinic [47]. Figure 3.5 displays the sequential framework used for this scenario. Since the static wind farm layout optimization is always conducted prior to the dynamic WFLO, it was assumed that the center of the turbine's movable range coincided with its installation position resulting from the static WFLO. It should be noted that in this work as in the previous literature, the terms "static," "installation," and "neutral" positions are used interchangeably and refer to the same position.

In the first step, the objective is to maximize the AEP of a static wind farm layout by optimizing the positions of wind turbines while considering wind farm boundary constraints, described in section 3.2.4. The optimal static positions obtained from this step correspond to the installation positions of the wind turbines.

The optimal static wind farm layout achieved in step 1 serves as input for step 2, as the movable range of the wind turbines is determined based on their installation positions. In step 2, the objective is still to maximize the AEP by optimizing the positions of wind turbines for each considered wind direction. This involves solving n_{wd} optimization subproblems, one for each considered wind direction. The optimization step is described by Equation 3.5:

$$\begin{aligned}
 &\text{maximize} && P_i(x_j, y_j) && j = 1, \dots, n_{wt} \quad i = 1, \dots, n_{wd} \\
 &\text{by varying} && x_i, y_j \\
 &\text{subject to} && x_j^2 + y_j^2 \leq R_B^2 \\
 &&& (x_{s,j} - x_j)^2 + (y_{s,j} - y_j)^2 \leq R_{mr}^2
 \end{aligned} \tag{3.5}$$

where:

- AEP represents the Annual Energy Production in GWh.
- n_{wt} is the total number of wind turbines.
- x_j denotes the x-coordinate of the j-th wind turbine.
- y_j denotes the y-coordinate of the j-th wind turbine.
- $x_{s,j}$ denotes the x-coordinate of the installation position of the j-th wind turbine.
- $y_{s,j}$ denotes the y-coordinate of the installation position of the j-th wind turbine.
- R_B represents the boundary of the wind farm.
- R_{mr} represents the movable range boundary of the wind turbine.

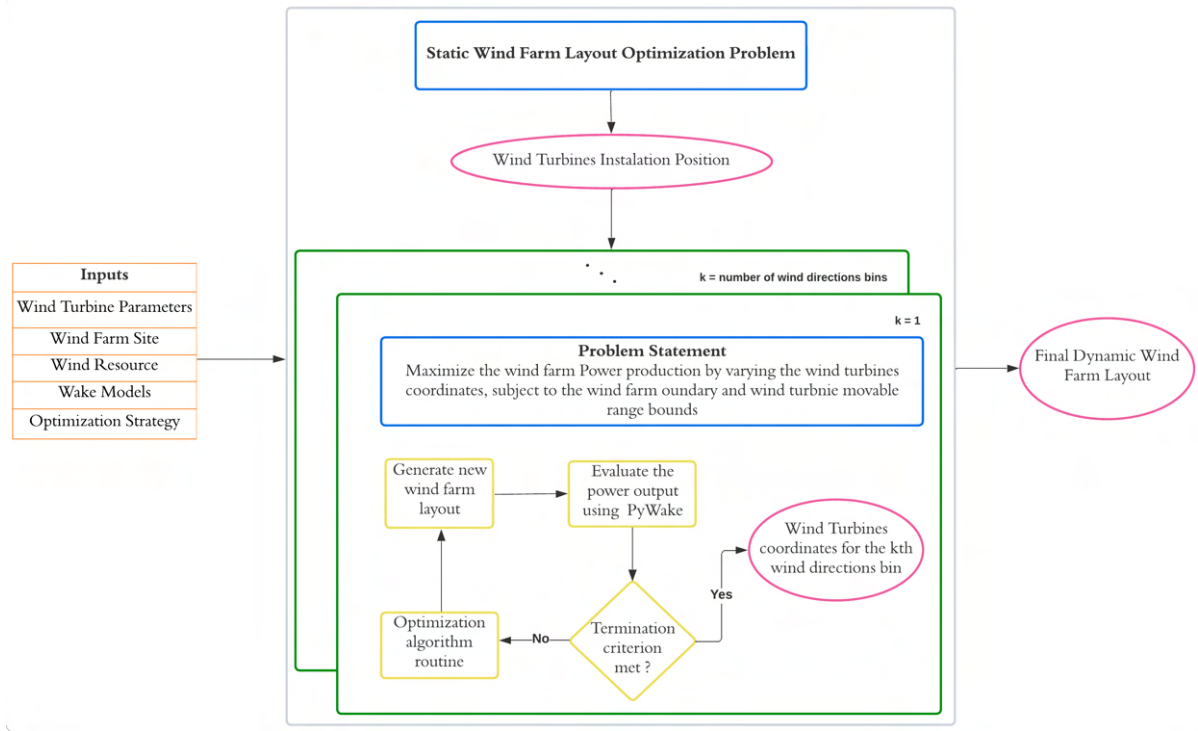


Figure 3.5: Workflow chart of the dynamic layout optimization.

Scenario 6: Sequential dynamic optimization

Sequential dynamic optimization involves maximizing the Annual Energy Production (AEP) of a wind farm through a sequential process. As shown in figure 3.6, this process consists of three steps, each addressing a specific optimization problem.

The first two steps of the sequential optimization process align with the methodology discussed in section 3.2.4. The outputs of these two steps are the installation position of the turbines and their specific location for each wind direction.

Once the optimized positions for each wind direction are determined, the third step involves adjusting the yaw angles of all turbines for each wind direction to maximize power production. This follows the optimization problem outlined in scenarios 2 and 4. The lonely regards the position of turbines. In the optimization process described above the turbines are fixed in the installation position for all the considered wind directions. However, in the third step of the sequential and dynamic layout optimization, the turbines are positioned in their optimized position, which are different for each considered wind direction.

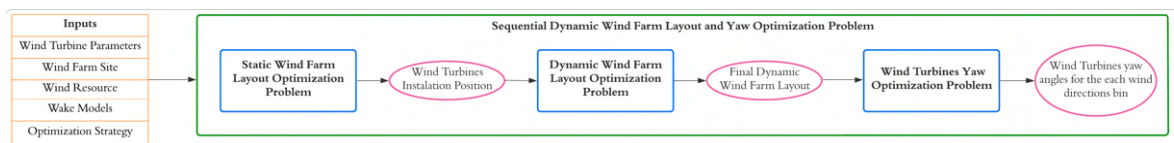


Figure 3.6: Workflow chart of the Combined Position and Yaw Static Optimization.

3.2.5. AEP calculations in Pywake

As can be seen in section 3.2.4, the majority of the optimization frameworks considered are actually divided into several optimization subproblems, one for each wind direction, that aim to maximize the power production for a specific direction bin. Additionally, for all the cases only one wind speed has

been used. With one speed only, equation 3.2 given in section 3 can be simplified to the formula presented in Equation 3.6.

$$AEP = \left(\sum_{k=1}^{n_{wd}} f_k P_k \right) 8760 \frac{\text{hrs}}{\text{yr}} \quad (3.6)$$

In a similar manner to the two-turbine case, the wind farm calculations are conducted using PyWake, a software tool. For a comprehensive introduction to the software, readers are directed to Section 2.2.3.

The approach of calculating wind farm power production for each wind direction and subsequently determining the AEP outside the PyWake environment is adopted. This enables the optimization of turbine yaw angles and turbine positions for each wind direction (when considering yaw-based wake redirection, turbine repositioning or both). It is evident that these turbine parameters depend on the incoming wind direction. In contrast, when the optimization process only needs to optimize turbine positions for fixed orientations, as described in case 3 of section 3.2.1 (static wind farm layout optimization), the AEP is computed internally in PyWake using the approach described in section 3.

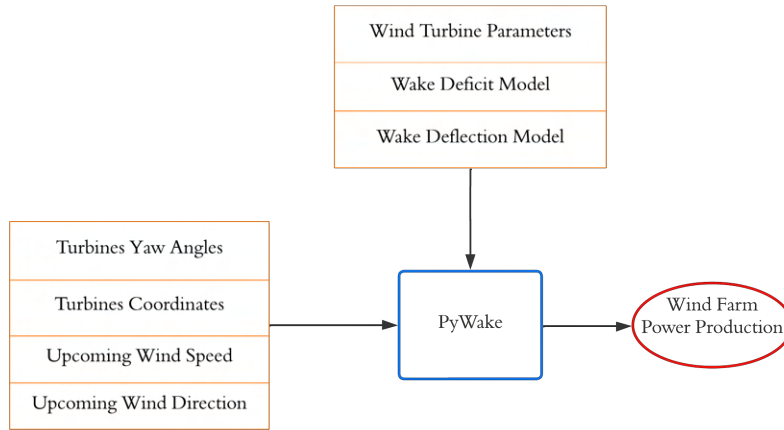


Figure 3.7: Overview of the PyWake workflow for calculating wind farm power production for different wind directions.

Figure 3.7 presents an overview of the inputs, encompassing variables and wake effect models employed, as well as the outputs and the computational tool necessary for calculating the wind farm's power production for each wind direction.

3.2.6. Wind farm efficiency

To comprehensively evaluate the impact of different wake mitigation strategies employed in various scenarios, this Master's Thesis project relies on a key metric for result comparison: wind farm efficiency. This metric is calculated by considering the AEP of the wind farm and comparing it to one of the freestanding wind turbines, which represents the energy production without any wake losses. The wind farm efficiency can be determined using equation 3.7:

$$\eta = \frac{AEP}{AEP_{\text{freestanding}}} \quad (3.7)$$

In equation ??, η represents the wind farm efficiency, AEP corresponds to the calculated annual energy production of the wind farm, and $AEP_{\text{freestanding}}$ denotes the annual energy production of an equivalent number of freestanding wind turbines, assuming no losses due to wake effects. By comparing the wind farm efficiency, the effectiveness of different wake mitigation strategies can be assessed.

3.3. Case study definition

This section presents the extended wind farm case study that was utilized in the Master's thesis project. It begins with subsection 3.3.1, which explains the rationale behind the selection of the wind farm case study. Subsequently, section 3.3.2 introduces the wind farm site. Section 3.3.3 provides the details of the wind turbines that were incorporated into the project. The wind resource considered for the study is thoroughly described in section 3.3.4. Additionally, in section 3.3.5, the movable range of the wind turbines is determined. Subsequently, in section 3.3.6, the optimization strategy employed in the optimization framework is chosen. Lastly, the wake models used for the case study are reported in section 3.3.7.

3.3.1. Wind farm case study

The optimization of wind turbine placement within a wind farm is a complex problem characterized by the presence of numerous local optima. The accurate resolution of this problem is challenging due to the involvement of a large number of interdependent variables, such as wind farm site, wind turbine type, number of wind turbines, wind resource, wake model, and optimization algorithm. To ensure the production of meaningful data, it is necessary to employ a case study that incorporate a model wind farm with characteristics that strike a balance between restrictiveness and generality. This allows for the simplicity and relevance of the case studies to complex and realistic problems. In accordance with this criterion, the wind farm scenario developed by Baker et al. (2019) [7] and utilized in the context of the International Energy Agency's Wind Task 37 (IEA37) was selected for implementation in this Master's Thesis project.

Baker et al. (2019)[7, 6] conducted a study focused on wind farm layout optimization, aiming to establish a set of best practices for optimization algorithms and wake deficit models. The study comprised two case studies to investigate the effects of Engineering Wake Models (EWM) and optimization algorithms. The first case study focused on the isolation of optimization techniques for a single simplified EWM, while the second case study sought to explore the differences that arise from combining variations in the EWM and optimization method. In this Master's Thesis project, the wind farm scenario from the first case study was chosen.

The adoption of the case study proposed by Baker et al. (2019) [7] confers two notable advantages to the dynamic Wind Farm Layout Optimization Problem (WFLOP) considered in this research. Firstly, it enables the creation and validation of a complex optimization framework for dynamic WFLOP integrated with yaw-based wake redirection. Secondly, it facilitates the comparison of the optimization results obtained from various participants in case study 1, as well as the dynamic layout outcomes achieved by Ufuktan, who developed its optimization framework based on the same case study.

It is essential to highlight that all aspects of the WFLOP considered in this research are derived from case study 1 established by Baker et al. (2019) [7]. This encompasses the wind turbine, wind farm site, number of wind turbines, wind resource, and wake model employed in the dynamic WFLOP. By keeping these factors constant, the analysis of incorporating mobility into the WFLOP is simplified. Further details regarding the selection of these factors can be found in the literature provided by the authors.

Furthermore, to the wake deficit model utilized by Baker et al. (2020)[6] has been added a wake deficit model to account for the wake deflection resulting from the wind turbine yaw misalignment with the upcoming wind speed.

3.3.2. Wind farm site

The chosen wind farm site is based on Case Study 1 proposed by Baker et al. (2019) [7], as mentioned in Section 3.3.1. Baker's study presented various wind farm sites. To focus on the optimization method and minimize the introduction of variables, the wind farms were situated on flat and level terrain. A circular farm boundary was selected to reduce the influence of the boundary on farm design. The placement of turbine hub locations was constrained within the boundary radius, and a minimum spacing of two rotor diameters between turbines was required. The turbines were arranged in evenly

spaced concentric rings. The boundary radii of the different wind farms were chosen to allow for turbine placement in concentric rings, ensuring a minimum spacing of five rotor diameters. The size of the farm radius was designed to prevent all turbines from being placed on the boundary, yet still enable meaningful turbine movement during optimization.

Three circular wind farms were specified, each with increasing size and turbine quantity:

- $n_{wt} = 16$ with $R_B = 1,300m$;
- $n_{wt} = 36$ with $R_B = 2,000m$;
- $n_{wt} = 64$ with $R_B = 3,000m$.

Here, n_{wt} represents the number of wind turbines, and R_B denotes the boundary radius of the circular wind farm.

To reduce the problem's complexity when considering the combination of a dynamic wind farm layout and wind turbines' yaw misalignment for wake redirection, only one of the three cases is studied. The scenario selected is the one with the lowest number of wind turbines ($n_{wt} = 16$), chosen to decrease computational time. The wind farm layout as well as the wind farm circular boundary that will serve as a baseline scenario are presented in figure 3.8. In the picture, the wind farm boundary is represented by the blue continuous line, while the red dots represent the turbines' coordinates.

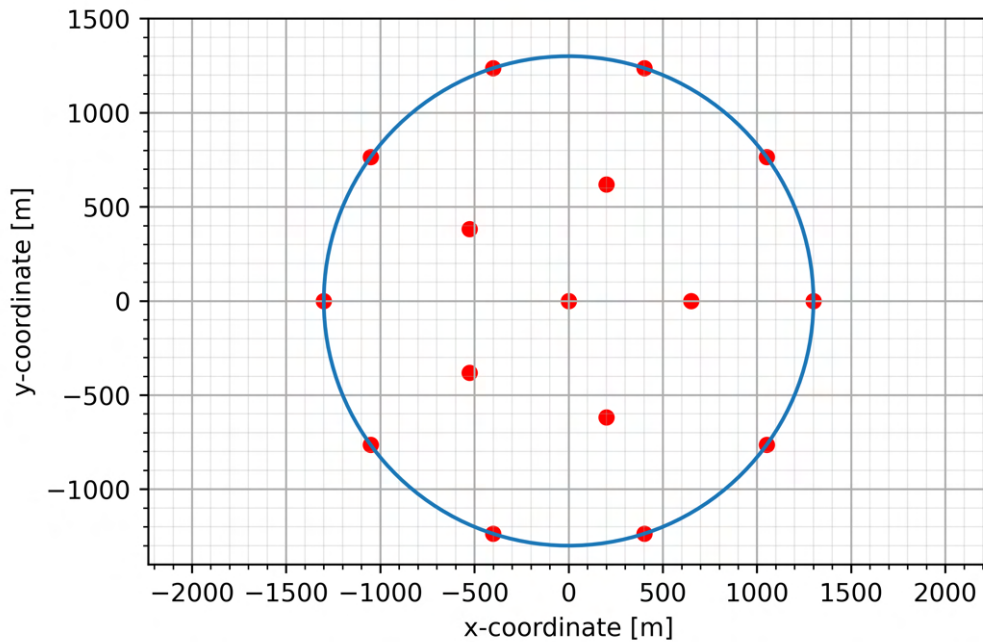


Figure 3.8: Baseline layout.

While finding a wind area with perfectly circular boundaries is challenging in practical applications, as boundaries often possess irregular shapes or consist of multiple segments rather than a single one, assuming a circular boundary helps eliminate the impact of local maxima on the optimization results that may arise due to the wind farm's irregular shape. Consistent with Baker et al.'s selection [7], the circular boundary for the wind farm is chosen to minimize the boundary's influence on the optimization outcomes.

3.3.3. Wind turbine selection

The selection of the Wind Turbine is the same as the one adopted for two turbine case described in Chapter 2. The turbine used in the simulation process is the IEA37 3.35 MW onshore reference turbine

[11]. For more information the reader is referred to Section 2.4.2.

When addressing the dynamic Wind Farm Layout Optimization Problem (WFLOP), the implementation of an onshore turbine is anticipated to have a negligible impact on the nature of outcomes. Therefore, it can be inferred that the findings obtained from the dynamic WFLO analysis for an onshore wind turbine would not significantly differ from those for an offshore wind turbine. It should be noted that the dynamic WFLOP is independent of any specific wind turbine type and is solely utilized as an input for the optimization process.

3.3.4. Wind resource selection

The wind distribution frequency and wind speed were consistent across all wind farm scenarios in the case study. The freestream wind velocity is the same for all wind directions. From the analysis of the two-turbine case discussed in chapter 2, the influence of the incoming wind speed on the potential improvement in wind farm efficiency was evident. Consequently, three wind speeds were examined: below-rated speed at 7 m/s, rated speed at 9.8 m/s, and above-rated speed at 10 m/s. This selection was made to assess the relative significance of different wake mitigation strategies for these incoming wind speed, that are representative for the different operational regime outlined in section 2.4.2. It's worth mentioning that the wind speed of 11 m/s was not included in the analysis. This decision was based on the clear indications from the results of the two turbines, which demonstrated that the optimization strategies were actually performing exceptionally well at wind speeds above the rated level. Consequently, using this wind speed for analysis might not accurately represent the potential improvements achievable through the combination of these strategies.

In contrast to the approach adopted for the two-turbine case study, the optimization procedures applied to the expanded wind farm scenario are explicitly dependent on the wind direction. Their applicability is clearly contingent upon variations in the wind direction. The variability in wind direction, in terms of selected bins and corresponding frequency, is based on the wind rose obtained from Baker et al. (2019) [7]. Figure 3.9 presents the wind rose graphically in polar coordinates. This wind rose exhibits a bi-modal off-axis wind frequency distribution, segmented into 16 directions.

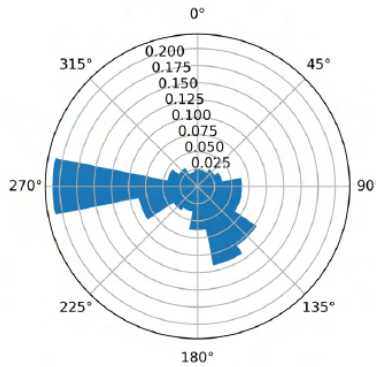


Figure 3.9: Bimodal off-axis wind frequency distribution.

3.3.5. Definition of the wind turbines' movable range size

To provide a quantitative description of the movable range size, Kilinic introduced the ratio between the boundary radius of the circular movable range and the rotor diameter, defined by Equation 3.8:

$$\frac{R_{mr}}{D_{rotor}} = C \quad (3.8)$$

Here, R_{mr} represents the boundary radius of the circular movable range shape, D_{rotor} denotes the rotor diameter, and C represents the ratio between these two variables. The size of the movable range for a wind turbine is directly proportional to the value of C . In this Master's Thesis project, various movable range sizes were investigated, ranging from $C = 0.01$ to $C = 0.75$ with increments of 0.25.

3.3.6. Optimization strategy selection

For the optimization frameworks outlined in section 3.2.4 of this Master's thesis project, the Covariance Matrix Adaptation Evolution Strategy (CMA-ES) algorithm has been chosen as the optimization approach. The algorithm is freely available on GitHub for Python [31].

This selection is supported by two relevant studies focusing on WFLO involving movable Floating Offshore Wind Turbines (FOWTs) [47, 70]. In particular, Ufuktan Kilinic, in his Master's Thesis [47], performed static layout WFLO optimization for maximizing the Annual Energy Production (AEP) using four different optimization algorithms applied to the IEA37 wind farm case study. The algorithms employed in that study were as follows:

- Covariance Matrix Adaptation Evolution Strategy (CMA-ES)
- Constrained optimization by linear approximation (COBYLA)
- Trust-region interior point method (trust-constr)
- Sequential least squares programming (SLSQP)

Among these four optimizers, CMA-ES demonstrated superior performance in terms of achieving the best optimum. Additionally, Kilinic noted that when running the optimization case only once, CMA-ES exhibited less sensitivity to the initial evaluating point compared to the other optimization algorithms, and it performed well without exceeding the boundary constraints imposed on the turbine coordinates. The performance of CMA-ES, even with a single run, is comparable to the top-ranked algorithms reported in Table 2 of Baker et al. (2019) [7].

The covariance matrix adaptation evolution strategy (CMA-ES) is a specific approach utilized for numerical optimization. It falls under the category of evolution strategies (ES), which are stochastic methods designed for optimizing non-linear or non-convex continuous problems without the need for derivatives. ES belongs to the broader field of evolutionary algorithms and evolutionary computation, both of which draw inspiration from the principles of biological evolution.

In evolutionary algorithms, the optimization process involves repeated cycles of variation (through recombination and mutation) and selection. Each generation produces new candidate solutions (represented as "x") by introducing variations, typically in a stochastic manner, to the existing parent individuals. These individuals are then selected for the next generation based on their fitness or objective function value (denoted as "f(x)"). As a result, successive generations yield individuals with increasingly better fitness values.

By convention, CMA-ES is an optimizer that minimizes the objective function it is provided with. Hence, a negative sign is applied to the AEP production in order to effectively maximize it.

The CMA-ES optimizer requires an initial guess, denoted as x_0 , for the design variables to initiate the optimization process. The specific value of x_0 varies depending on the specific optimization case being executed. CMA-ES also requires an initial standard deviation, σ_0 , which is suggested to be set to one-fourth of the design space [32]. Therefore, σ_0 is determined as one-fourth of the wind farm boundary diameter ($2 \times R_B$) for the static layout optimization, one-fourth of the wimovable range diameter ($2 \times R_{mr}$) for the dynamic layout optimization, and one-fourth of the predefined variability range of the yaw angles ($2 \times 35^\circ$) when the design variables pertain to the yaw settings of the turbines.

To terminate the algorithm, two different tolerance values are applied depending on the design variables. This termination criterion is met once the difference between the worst and best function value from the population in an iteration is smaller than the tolerance in the function value ('tolfun'). The population size is dependent on the number of design variables, which is 32 for 16 wind turbines. For 32 design variables, the population size calculated by CMA-ES is 14. Each candidate in this population has a function value. That means that there are 14 function values. For turbine coordinate variability, the tolerance relative improvement is set to 10^{-3} , while for the yaw turbine operational parameters, the tolerance is set to 10^{-6} . Simply put, the optimization is terminated if the range of these function values is smaller than 0.001 GWh for the layout optimization and 0.000001 GWh for the layout optimization. The

choice to adopt a stricter tolerance for the yaw optimization is motivated by the limited existing studies regarding the optimal optimization algorithm to employ specifically for yaw optimization. Due to the high multimodality of the problem, using a stricter tolerance value for the yaw optimization helps minimize the risk of prematurely terminating the optimization when encountering local maxima or minima in the yaw parameter optimization problem.

3.3.7. Wake models selection

The wake deficit model and wake deflection model chosen in this study are consistent with those adopted in Chapter 2. Specifically, the Simplified Bastankhah's Gaussian is used as the adopted wake deficit model, while the Jimenez wake deflection model is employed as the adopted wake deflection model. For further details regarding these two models and their respective significance in relation to the current study, readers are referred to Section 2.3.1.

In the case of a turbine positioned within multiple wakes, the total velocity deficit is determined by calculating the square root of the sum of the squares, as indicated in Equation 3.9.

$$\left(\frac{\Delta V}{V_\infty}\right)_{\text{total}} = \sqrt{\left(\frac{\Delta V}{V_\infty}\right)_1^2 + \left(\frac{\Delta V}{V_\infty}\right)_2^2 + \left(\frac{\Delta V}{V_\infty}\right)_3^2 + \dots} \quad (3.9)$$

The rotor-average model establishes one or more points at downstream wind turbine rotors, computes the velocity deficit at these points, and determines the average wind speed at the rotors. On the other hand, the rotor center model solely utilizes a single point, namely the rotor center, to ascertain the average wind speed at the rotor. Ideally, employing multiple points distributed across the rotor would yield a more accurate approximation of the rotor's average wind speed. However, it is important to note that incorporating a greater number of points also entails increased computational costs. Thus, in this Master's thesis project a rotor center model has been adopted.

3.4. Results analyses

This section presents the simulation results for the scenarios described in Section 3.2.1. Firstly, an efficiency comparison of the wind farm across all cases is conducted in Section 3.4.1. Subsequently, the influence of wind direction, wind speed, and the size of the movable range on the yaw optimization layer is discussed in Sections 3.4.3, 3.4.2, and 3.4.4, respectively.

3.4.1. Comparison of the wind farm efficiency

Figure 3.10 illustrates a comparison of wind farm efficiency across different wind speed cases and simulation scenarios at below-rated wind speed, rated wind speed and above-rated wind speed. The y-axis represents wind farm efficiency, while the x-axis displays the size of the allowed movable range of the turbines (denoted by C). This value of C , defined in Section 3.3.5, represents the ratio between the diameter of the turbine rotor and the radius of the turbine’s movable range. For instance, a C value of 0 indicates that the turbines are not allowed to move, thus excluding turbine repositioning.

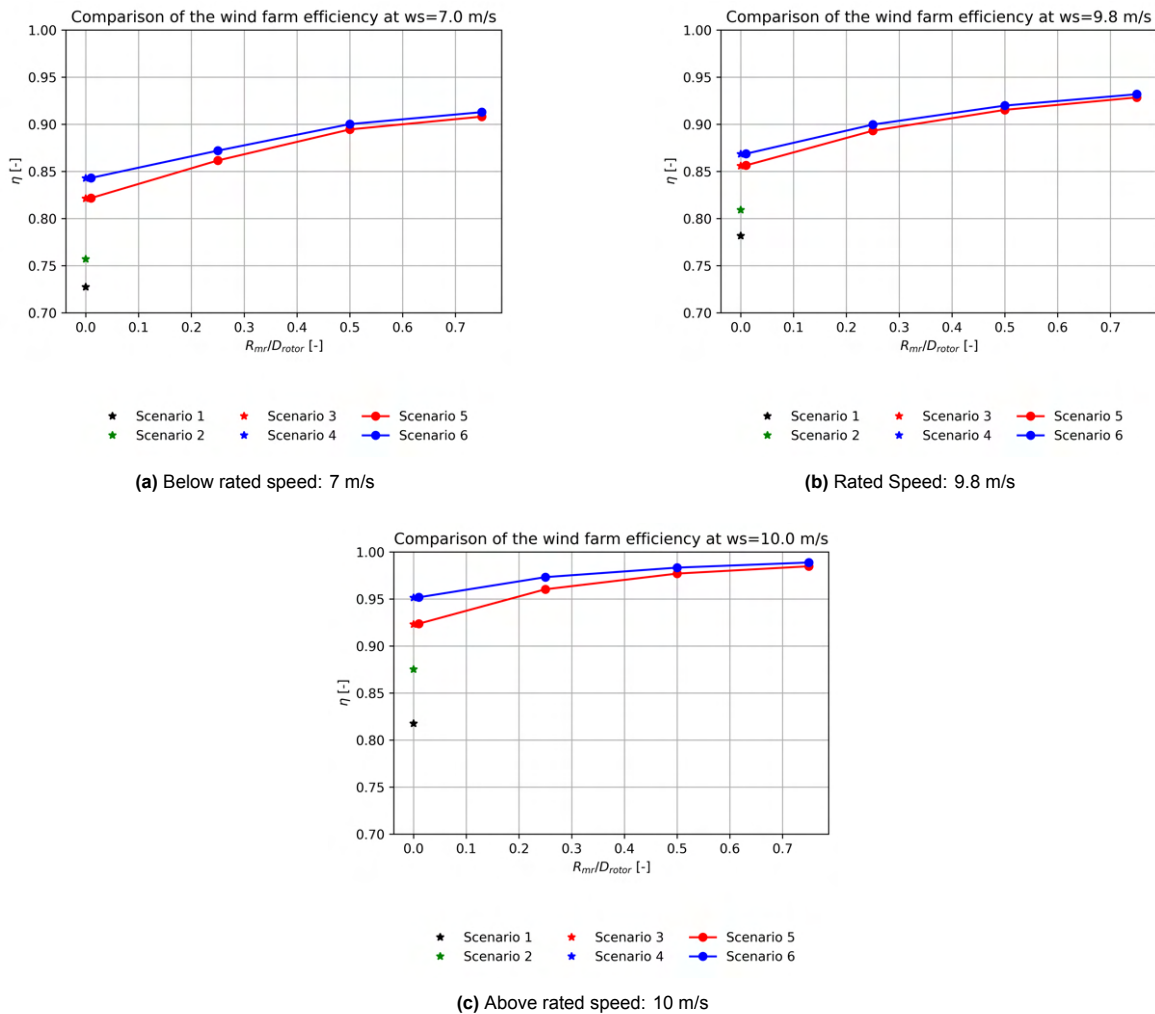


Figure 3.10: Comparison of the wind farm efficiency for different optimization scenarios at different wind speeds.

The scenarios to which the legged refers to are presented in section 3.2.1 and for convenience reported subsequently:

1. Baseline: Fixed (original) turbine positions with all turbines yawed in the mean wind direction.
2. Yaw optimization: Fixed (original) turbine positions with turbines optimally yawed for each wind direction.
3. Static layout optimization: Position optimized considering all wind directions, with all turbines yawed in the mean wind direction.

4. Combined static optimization: position optimized for all wind directions and yaw sequentially optimized for each wind direction.
5. Dynamic layout optimization: Position optimized for each wind direction, with all turbines, yawed in the mean wind direction.
6. Combined dynamic optimization: position optimized for each wind direction and yaw sequentially optimized for each wind direction.

It is shown that the combination of yaw-based wake redirection, turbine repositioning, and wind farm layout optimization ensures the highest wind farm efficiency compared to other analyzed cases. Consistent with the results of the two-turbine simulation and yaw optimization, the highest efficiency gains are achieved in the above-rated wind speed case at 10 m/s. Additionally, as the movable range of the turbine increases, the incremental efficiency gains obtained with the yaw optimization decrease. This can be understood by examining the two-turbine case: the more the downstream turbine can be repositioned in the crosswind direction, the less the upstream turbine needs to be yawed to achieve the same wake overlapping within the downstream turbine's rotor and the wake generated by the upstream turbine.

However at 10m/s , as the yaw optimization becomes more effective with increasing free stream velocity above rated wind speed, figure 3.10c demonstrates that it is possible to attain the same wind farm efficiency as the dynamic wind farm layout optimization with $C = 0.75$ by combining turbine repositioning with a movable range of $C = 0.25$ and yaw optimization. This implies that especially above rated wind speed, it is possible to reduce the required movable range of the wind turbines by combining turbine repositioning and yaw-based wake redirection.

Tables ?? show the wind farm efficiency values for the different simulation scenarios as well as the efficiency gains compared to the baseline scenario at the correspondent wind speed. It can be observed the yaw optimization on the baseline (referred to as scenario 2) guarantees nearly double the efficiency gains at 10 m/s (above the rated wind speed) compared to the cases below and at rated wind speed. This phenomenon can be explained by considering the mechanics of the yaw-based wake redirection strategy. When the turbine operates above the rated wind speed region, it is possible to yaw the turbine and reduce the effective wind speed without affecting the turbine's power production. The efficiency gains presented in table ?? align with those reported in the literature [23]. Additionally, the results of the dynamic WFLO problem at 9.8 m/s are in line with the work conducted by Kilinic [47].

These findings suggest two considerations: firstly, the combination of these two wake mitigation strategies may reduce the initial cost required for the turbine repositioning mechanism, as a smaller movable range translates to lower cost investments for actuators and mooring systems. Secondly, such a combination may occur within a specific range of conditions, specifically when the movable range of the turbine does not exceed 1D and the wind speed is above the rated wind speed. It is reasonable to assume that the higher the wind speed is above the rated wind speed, the more the yaw optimization of the turbines may guarantee high-efficiency gains on top of the dynamic wind farm repositioning.

	Without Yaw optimization		With Yaw optimization	
	$\eta[-]$	$\Delta\eta[-]$	$\eta[-]$	$\Delta\eta[-]$
Baseline	0.728	0	0.757	0.029
Static WFLO	0.821	0.093	0.843	0.115
Dynamic WFLO with C=0.25	0.862	0.134	0.872	0.144
Dynamic WFLO with C=0.50	0.894	0.166	0.900	0.172
Dynamic WFLO with C=0.75	0.908	0.180	0.912	0.184

Table 3.1: Wind farm efficiency values and gains for different simulation scenarios at 7 m/s

	Without Yaw optimization		With Yaw optimization	
	$\eta[-]$	$\Delta\eta[-]$	$\eta[-]$	$\Delta\eta[-]$
Baseline	0.781	0	0.809	0.028
Static WFLO	0.856	0.075	0.951	0.170
Dynamic WFLO with C=0.25	0.893	0.112	0.899	0.118
Dynamic WFLO with C=0.50	0.915	0.134	0.919	0.138
Dynamic WFLO with C=0.75	0.928	0.147	0.931	0.150

Table 3.2: Wind farm efficiency values and gains for different simulation scenarios at 9.8 m/s

	Without Yaw optimization		With Yaw optimization	
	$\eta[-]$	$\Delta\eta[-]$	$\eta[-]$	$\Delta\eta[-]$
Baseline	0.818	0	0.875	0.057
Static WFLO	0.923	0.105	0.951	0.133
Dynamic WFLO with C=0.25	0.960	0.142	0.973	0.155
Dynamic WFLO with C=0.50	0.977	0.159	0.983	0.165
Dynamic WFLO with C=0.75	0.984	0.166	0.989	0.171

Table 3.3: Wind farm efficiency values and gains for different simulation scenarios at 10 m/s

3.4.2. Effect of the wind direction on the yaw optimization

Figure 3.11 presents the sequential static WFLO combined with yaw optimization at a wind speed of 10 m/s. Given that the movable range sizes examined in this study fall within the range where the installation position significantly impacts wind farm power production [47], the effect of wind direction on the potential efficiency gains resulting from yaw optimization remains evident even when combined with dynamic wind farm optimization. However, it was decided to display the results when the turbine repositioning is not active as the effects are then more clearly visible.

In figure 3.11, the wind is coming in four different wind directions: 0°, 90°, 180°, and 270°. In accordance with the wind rose to represent the wind resource used in this study, as described in section 3.3.4, 270° represents the bin with the highest probability of occurrence, 90° corresponds to opposite wind direction, while 0° and 180° corresponds to the perpendicular wind directions perpendicular to 270°. It is important to underline that the turbine positions are more favourable for the dominant wind direction (i.e 270°).

Since the static wind farm layout is optimized based on the probability of wind direction bins, it is observed that when the wind comes from 270° and 90°, the turbine yaw angle is almost zero due to the optimized turbine positions for these wind directions. Note that the zero yaw angles for 90 degrees are because of the mirror symmetry of the situation with 270 degrees, which has dominated the static layout optimisation. In essence, the optimal positions designed for the 270-degree direction are inadvertently advantageous for the 90-degree direction as well. Conversely, when the wind blows from directions for which the optimized layout is less beneficial, the yaw optimization returns higher yaw angles for a greater number of wind turbines. In that case, redirecting the wake can enhance the wind farm's efficiency.

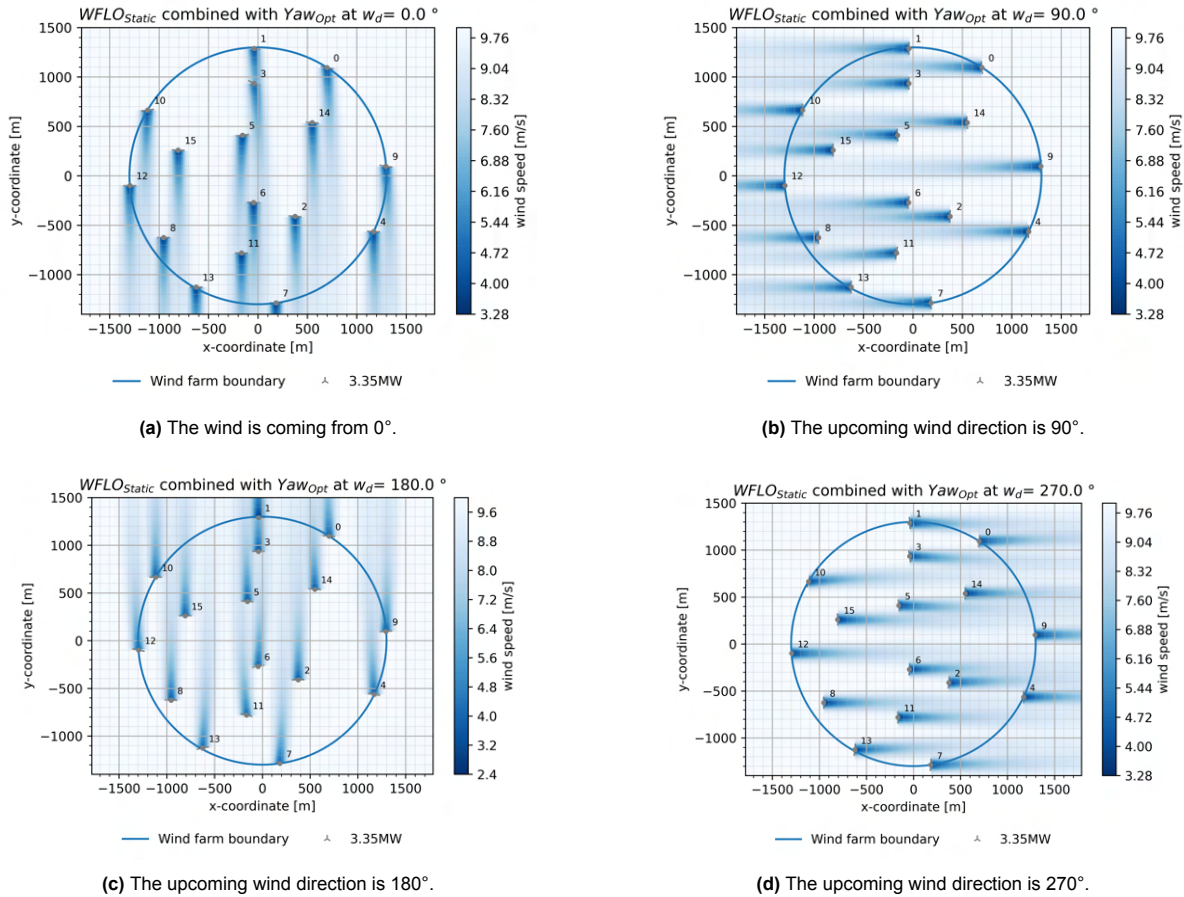


Figure 3.11: Combined static optimization results for different wind directions.

In summary, Figure 3.11 demonstrates that yaw-based wake redirection is most effective when the wind blows from directions with a lower occurrence rate. Consequently, the subsequent subsections will present the wind farm layout results for the case when the wind comes from 180° to qualitatively describe the effect of other simulation variables on the effectiveness of combining yaw-based wake redirection with other wake effect mitigation strategies.

3.4.3. Effect of the wind speed on the yaw optimization

Figure 3.12 illustrates two wind farm layout results obtained from sequential dynamic WFLO with a movable range size coefficient of 0.5 ($C=0.5$) and yaw optimization. The wind speeds considered for this analysis are 9.8 m/s and 10 m/s, with the wind originating from 180°. The purpose of presenting these two results is to visually highlight the impact of wind velocity on the outcomes of the yaw optimization layer.

In figure 3.12b, where the wind speed exceeds the rated wind speed, it is evident that the upstream turbines are yawed, resulting in the noticeable redirection of their wake. Conversely, in figure 3.12a, it can be observed that the yaw angle behind the turbines is almost unaffected, indicating that a majority of the turbines are not yawed.

To better interpret these results, insights from the analysis of the two-turbine case in chapter 2 are valuable. This analysis demonstrates that yaw-based wake redirection is more effective at wind speeds above the rated speed compared to cases below or at the rated wind speed. Scaling up this wind farm control method to an extended wind farm scenario yields consistent patterns, as turbines are yawed at wind speeds above the rated speed due to the optimization process, while they remain unyawed at wind speeds below the rated speed.

Similar observations are made observing all cases with yaw optimisation. As other cases with yaw optimisation showed similar behaviour it can be concluded that the effect of the wind speed on the yaw optimization is always similar regardless of the fact that the wind farm layout is optimized (either statically, dynamically) or not.

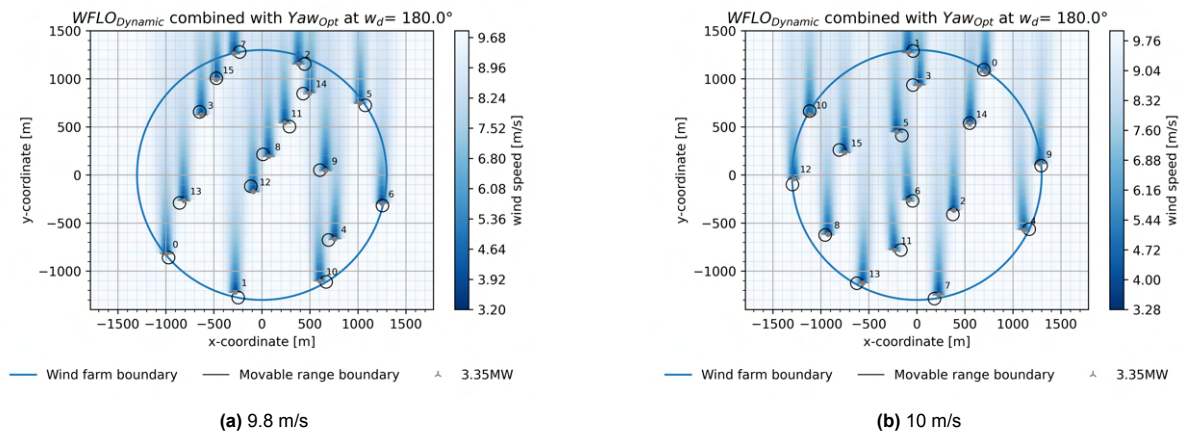


Figure 3.12: Sequential Dynamic WFLO and Yaw Optimization for different upcoming wind speeds.

3.4.4. Effect of the movable range size on the yaw optimization

Figure 3.13 illustrates the impact of movable range size on the results of yaw optimization. Specifically, it depicts the outcomes of sequential dynamic WFLO and yaw optimization for varying movable range sizes when the wind speed originates from 180° at 10 m/s (above-rated wind speed).

The figure demonstrates that when the turbine's movement is restricted, the yaw angle of the upstream turbines is not zero for the majority of cases (evident in Figure 3.13a, turbines 7, 11, 13, and 6). As the movable range of the turbine increases, the previously mentioned turbines become increasingly free to be repositioned, resulting in diminished effectiveness of yaw control (and thus both fewer yaw turbines with smaller yaw angles). The diminishing effectiveness of yaw control at a movable range characterised by a size coefficient C value of 0.75 suggests that the benefits gained from relocating the turbines outweigh the advantages derived from increased yawing in terms of overall power production, as anticipated by the two turbine analyses. This phenomenon may be explained by the hierarchy of sequential combination optimization, which prioritizes repositioning over yawing.

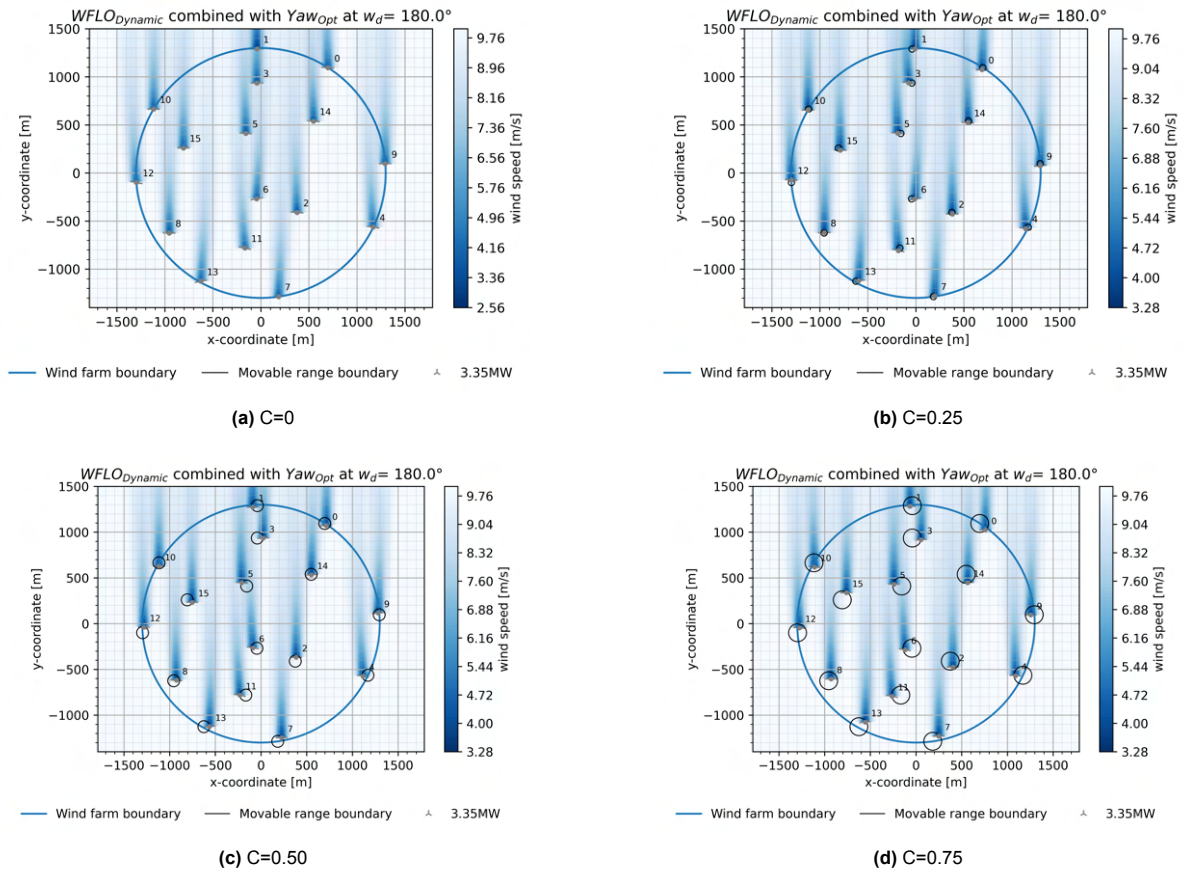


Figure 3.13: Sequential Dynamic WFLO and Yaw Optimization for different movable range sizes.

In conclusion, the combination of wind turbine repositioning and yaw-based wake redirection reveals that as the movable range size of the turbines increases, the significance of the yaw mechanism diminishes compared to the contributions ensured by turbine repositioning.

4

Mooring lines analyses

The chapter commences with an introduction concerning wind turbine positioning and the relocation mechanisms proposed in the literature, presented in section ???. Among these mechanisms, position mooring is chosen for further in-depth analysis in future studies. Additionally, section ??? delves into the examination of the impact of yaw on the translational equilibrium of the turbine. Hereafter, section 4.2 presents the methodology employed to assess the movability and station-keeping performance of the wind turbines as well as the mathematical definitions and the software tools used to perform the calculations. Subsequently, a case study is selected to apply the proposed methodology in section 4.3, and the results are subsequently analyzed in section 4.4.

4.1. Introduction to position mooring movability and station-keeping performances assessment

??? This section provides background information on various mechanisms used to reposition the turbine, as discussed in section 4.1.1. It also offers insights into the position mooring technique, as explored in section 4.1.2. Subsequently, section ??? analyzes the impact of yaw on the translational equilibrium of the turbine. Finally, in section 4.1.4, a comprehensive definition of the problem addressed in this chapter is presented.

4.1.1. Selection of the repositioning mechanism

This report discusses four different repositioning mechanisms for movable floating offshore wind turbines:

1. Yaw-Induced Turbine Repositioning (YITuR);
2. Position Mooring (PM) with mooring line length adjustment capability ;
3. Thruster Assisted Position Mooring (TAPM);
4. Dynamic Positioning (DP).

The YITuR technique controls the aerodynamic thrust force on the rotor by adjusting the nacelle yaw angle and the axial induction factor. This variation allows the wind turbine's position to be changed. While actuators already present in the wind turbine can be used for this purpose, additional costs are incurred for the mooring system to provide movable range for the turbine [33, 30].

Position mooring (PM) involves varying the length of mooring lines using winches to move the wind turbines by several rotor diameters. The change in line length creates an imbalance in mooring line tensions, leading to the turbine's displacement. PM is an energy-efficient technique that enables the turbine to have a wider movable range compared to YITuR, but it comes with increased capital and operational costs [19, 70, 47].

Thruster Assisted Position Mooring (TAPM) combines the mooring system with thrusters to reduce mooring line tensions and vessel displacements, particularly in harsh environmental conditions [48, 60].

Dynamic Positioning (DP) relies solely on thrusters to maintain a specific position and heading without a mooring system. It is commonly used in low-speed operations but requires continuous power [78].

In the Master's thesis report of Ufuktan Kilinic[47] the advantages and disadvantages of each mechanism to gain insights into their potential applications in movable offshore wind turbines are explored.

While all mechanisms have the potential to move to and maintain the desired position, PM is the only option that does not counteract the mooring line restoring forces (like YITuR or TAPM) or environmental loads (like DP). This allows the floating offshore wind turbine to move to more distant positions than YITuR or TAPM and maintain these positions at a lower cost compared to DP. Therefore, PM is chosen as the repositioning mechanism for further analysis.

4.1.2. Position Mooring for turbine repositioning

In this section, the concept of position mooring for turbine repositioning is explored in greater depth. The functioning of the repositioning mechanism is explained and elaborated upon.

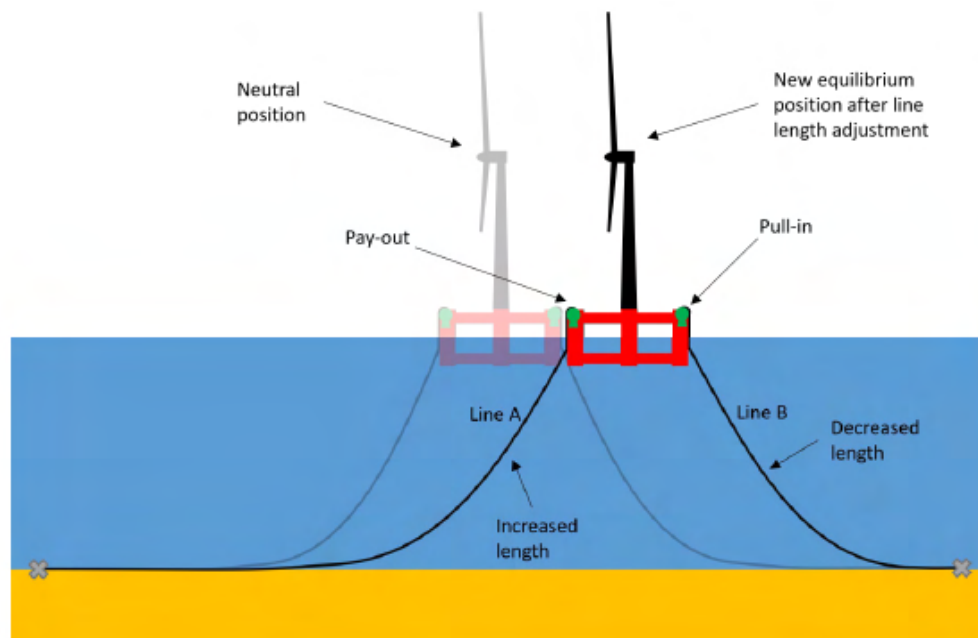


Figure 4.1: Position mooring repositioning mechanism concept for a movable floating offshore wind turbine[47].

The position mooring system for a movable wind turbine is illustrated in Figure 4.1. By manipulating the lengths of the mooring lines, the wind turbine can be shifted from its neutral position to a new equilibrium position. This adjustment is achieved by lengthening mooring line A and shortening mooring line B. Specifically, an additional mooring line is deployed from the onboard supply for line A, while the mooring line for line B is hauled in and stored on the turbine. Each mooring line is connected to a winch responsible for the payout or haul-in process.

The lengths of the mooring lines play a crucial role in determining the movement of the wind turbine. Increasing the length of line A while decreasing the length of line B causes the turbine to move to the right. This movement results from the changes in mooring line tensions, which introduce an imbalance in the forces acting on the system. As a result, the turbine is displaced until a new equilibrium point is reached, at which the line tensions stabilize, leading to the turbine's repositioning.

Notably, there is a lack of prior studies on the design of a position mooring system for a movable

floating offshore wind turbine. This design involves various aspects, such as mooring configuration, mooring line number, mooring line type, mooring line length, mooring tensioning system, mooring line storage, anchor placement, anchor type, floating platform layout, and power cable. Additionally, these design choices are highly dependent on the location's characteristics, including water depth, regulations, and environmental conditions. [70] previously proposed this concept as a means of achieving mobility in a wind farm. In their work, the repositioning mechanism consists of taut mooring lines, one end attached to the seabed and the other end to a winch. Similar mechanisms using catenary mooring lines have been proposed for other applications besides FOWTs [91]. Other technologies, such as chain jacks and in-line tensioners, exist for adjusting mooring line length but are not considered in this project [54, 88].

The movable range of the floating offshore wind turbines indicates the groups of positions that the turbine can move to and maintain. The shape of the movable range is directly influenced by the mooring system configuration. Clearly, the size and shape of the movable range are influenced by other mooring line system characteristics, as displayed in section 4.3.2.

4.1.3. The impact of the yaw on the translational equilibrium of the turbine

When examining the translational equilibrium of a Floating Offshore Wind Turbine (FOWT) in the presence of thrust force, the utilization of the yaw angle gives rise to two distinct applications:

1. The implementation of yaw angle control is employed with the primary objective of steering the wake to maximise power production, without considering its potential impact on the FOWT's position.
2. The adjustment of the yaw angle is utilized as a means to attain the desired equilibrium position by modifying the thrust force components in the x- and y-directions.

In this Master's thesis, only case one, which focuses on maximizing power production through yaw angle control, will be investigated.

The general research focus specifically is on investigating the combination of position mooring and yaw-based wake redirection wind farm control methods. If case two were also investigated, it would involve studying only one wind farm control method (turbine repositioning) with two different types of strategies to move the turbine: mooring line forces (position mooring) and aerodynamic forces (Yaw and Induction-based Turbine Repositioning (YITuR)). However, this scenario is not the primary focus of this thesis, and further exploration of this aspect could be considered in future research.

4.1.4. Problem analyses

The existing literature on position mooring for mooring line systems is almost non-existent. Only Kilinic's work partially assesses the impact of position mooring on turbine repositioning or significant movements of FOWT and its effects on the mooring system parameters [47]. However, this work disregarded all environmental forces acting on the turbine and floater system. As a result, there is no prior literature on the combination of position mooring and yaw-base wake redirection.

This Master's thesis project aims to conduct preliminary analyses of the performance of the position mooring mechanism, providing valuable preliminary information for designing a system capable of accommodating significant FOWT displacements. Additionally, it investigates whether the introduction of a yaw base wake redirection strategy may impact this design process.

To achieve this objective, a series of quasi-static analyses is performed under various simulation scenarios. These analyses are more suitable at this stage, considering dynamic analyses require more computational time and higher fidelity and may be conducted in a more advanced development stage of a mooring system specifically designed for wind turbine repositioning.

The analysis considers the thrust force acting on the wind turbine under different wind speeds and directions, aligned with the yaw settings determined at the wind farm control level. Wave and current

forces, and other environmental loads like ice, and marine growth were neglected for simplicity, as their mean values were negligible compared to the aerodynamic forces and to avoid complicating the problem.

The main objectives of these analyses are:

1. To determine the effectiveness of using position mooring for relocating and maintaining the wind turbine at different positions under varying wind scenarios.
2. To gain a better understanding of mooring lines' performance differences, including allowed displacement, mooring lines' tension, and stiffness, as the floater's position and wind turbine yaw angle change.

4.2. Methodology for position mooring performance assessment

This section introduces the methodology utilized to evaluate the movability and station-keeping performance of a position mooring system when combined with wind turbine nacelle yawing for power maximization.

The workflow is presented at a general level in Section 4.2.1, outlining the main concept and structure without delving into specific mathematical formulations. Subsequently, in Section 4.2.2, the geometrical definitions and interconnections for the floater's position and mooring lines parameters are discussed.

In Section 4.2.3, the optimization loop used to determine the ideal mooring lines lengths for each position within the movable range is presented. Finally, in Section 4.2.5, the general hypotheses on which the proposed methodology is based are reiterated.

4.2.1. Workflow and general structure

This section presents the proposed methodology for evaluating the station-keeping performance of position mooring systems for FOWT, with a focus on accounting for the impact of wind forces in achieving equilibrium.

The analysis assumes knowledge of the wind turbine's movable range and the nacelle yaw angle in advance. The shape and size of this movable range are dependent on the choice of the floater and its mooring line system. For this purpose, certain parameters are known beforehand, including the neutral position of the wind turbine, the anchor positions, and the geometry of the floater.

To assess the feasibility of maintaining equilibrium within the movable range while accounting for varying wind forces, multiple positions within the range and different wind scenarios are investigated. A discrete approach is used, selecting various positions and turbine nacelle yaw angles to explore the overall area of the movable range.

For each chosen position and turbine nacelle yaw angle, the mooring lines' lengths are adjusted to achieve equilibrium at the desired position. An optimization loop is employed to find their values. Initially, the mooring lines' lengths are randomly selected within predefined bounds for each position. The iteration process continues until the objective function, which measures the distance between the desired and actual equilibrium positions, remains unchanged in consecutive iterations within a specified tolerance. This ensures that the newly obtained equilibrium position remains in close proximity to the desired position.

Two possible scenarios can arise: either the system reaches an equilibrium state at the desired position (i.e. where the objective function reaches zero), or there remains an error between the desired position and where the system is equilibrated (i.e. where the objective function is non-zero). Although the desired floater position may not be precisely attained in the latter scenario, the actual equilibrium position may still be in close proximity to the desired position.

Challenges may arise near the boundaries of the movable range, where sufficient tensions in the mooring lines are required for equilibrium. In such cases, variations in mooring line lengths during the optimization loop may suggest inputs that do not lead to equilibrium. The algorithm halts, and the last valid mooring line lengths are taken as output.

If none of the mooring line combinations tried by the optimizer achieve equilibrium (i.e., the initial guess does not result in equilibrium), it is assumed that equilibrium cannot be reached at that specific point for the given wind scenario.

4.2.2. Definition of the position of the FOWT and of the mooring lines parameter

This section recalls the research conducted by Ufuktan Kilinic [47] to establish clear definitions for the floater's position within its movable range and any relevant geometric interconnections. These definitions are crucial for evaluating the position mooring and understanding the proposed workflow.

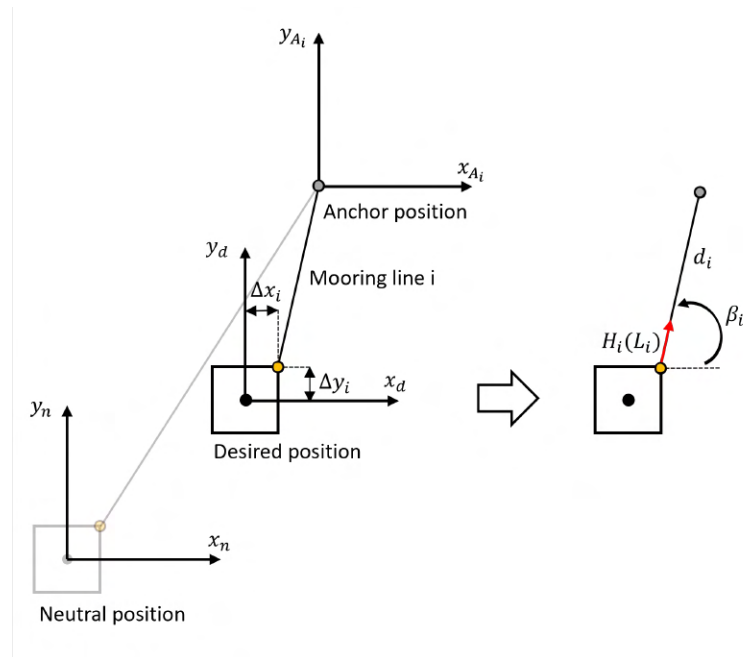


Figure 4.2: Definitions for a moored floater to assess position mooring. [47].

Figure 4.2 consists of two sections. The left part focuses on defining the significant positions of the moored floater, while the right part provides the necessary definitions to calculate the horizontal forces in the xy -plane.

It is essential to emphasize that the rectangular shape of the floater in the illustration is chosen for explanatory purposes and does not restrict the consideration of other shapes. Any other shape can be utilized as well. Additionally, $x_n y_n$ represents the global reference coordinate system.

In the left part:

- x_n and y_n are the floater's neutral coordinates.
- x_d and y_d are the floater's desired coordinates.
- x_{A_i} and y_{A_i} are the mooring line anchor (in grey) coordinates.
- Δx_i and Δy_i are the distances from the floater centre to the fairlead (in yellow).
- i is the mooring line number.

In the right part:

- L_i is the total mooring line length from fairlead to anchor.
- $H_i(L_i)$ is the horizontal component of the mooring line tension at the fairlead as a function of the mooring line length.
- d_i is the horizontal distance (xy -plane) from fairlead to anchor.
- β_i is the mooring line orientation.

In addition to the predetermined neutral and anchor positions, it is possible to predefine and select desired positions within the movable range. This allows for evaluating the station-keeping performance specifically at the desired locations, rather than considering all positions within the movable range. With all positions either fixed or predetermined, it becomes feasible to calculate the parameters d_i and β_i using geometric calculations. The horizontal distance from the fairlead to the anchor can be determined

by applying the following procedure.

The horizontal distance from fairlead to anchor can be determined as follows:

$$d_i = \sqrt{(x_{F_i} - x_{A_i})^2 + (y_{F_i} - y_{A_i})^2}, \quad (4.1)$$

where x_{F_i} and y_{F_i} are the fairlead coordinates given by:

$$\begin{aligned} x_{F_i} &= x_d + \Delta x_i \\ y_{F_i} &= y_d + \Delta y_i \end{aligned} \quad (4.2)$$

Therefore, we can write:

$$d_i = \sqrt{(x_d + \Delta x_i - x_{A_i})^2 + (y_d + \Delta y_i - y_{A_i})^2} \quad (4.3)$$

The mooring line orientation can be computed with the following function:

$$\beta_i = \arctan 2((y_{A_i} - y_{F_i}), (x_{A_i} - x_{F_i})) \quad (4.4)$$

The remaining variable that can be adjusted is the length of the mooring line (L_i). By modifying this length, the horizontal component of the mooring line tension (H_i) can be changed accordingly.

4.2.3. Mooring lines length optimization loop

Figure 4.3 depicts a representation of a single catenary mooring system, illustrating both the mooring line length (L_i) and the horizontal tension component (H_i).

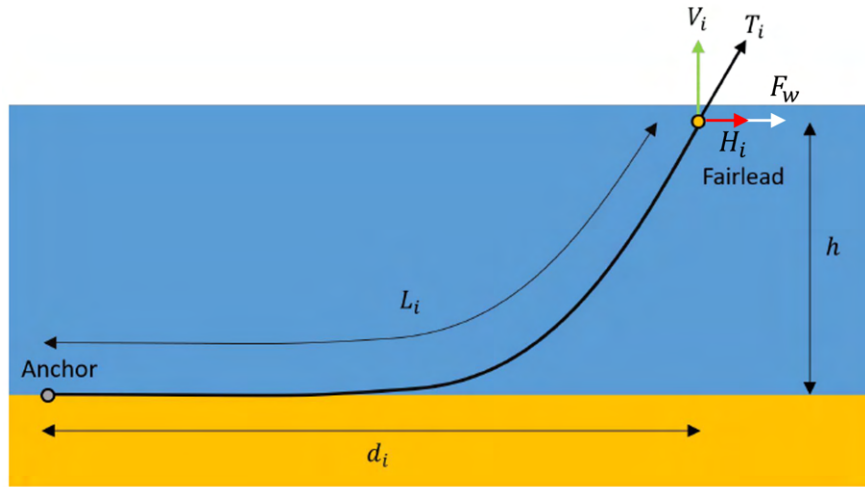


Figure 4.3: Illustration of a single catenary mooring line, modified from [47].

In this diagram, the following information is already known or determined in advance:

- anchor coordinates;
- fairlead coordinates;
- horizontal distance from fairlead to anchor (d_i);
- vertical distance from fairlead to seabed (h);
- thrust force component (F_w).

Once the properties of the mooring lines (d_i) and the aerodynamic load (F_w) are known the mooring line length (L_i) for each individual mooring line can be calculated. The catenary mooring line model [63] is used for this purpose.

This calculation to achieve equilibrium at the desired wind turbine position, is performed following the optimization problem formulated in the equation 4.5.

$$\begin{aligned} & \text{minimize } \sqrt{(x_{des} - x_{eq})^2 + (y_{des} - y_{eq})^2} \\ & \text{by varying } L_{\min}(d_i) \leq L_i \leq L_{\max}(d_i) \quad i = 1, \dots, n_{ml} \\ & \text{subject to } H_{\min} - H_i(L_i) \leq 0 \quad i = 1, \dots, n_{ml} \end{aligned} \quad (4.5)$$

Where:

- x_{des} and y_{des} are the coordinates of the desired position of the floater;
- x_{eq} and y_{eq} are the coordinates of the equilibrium position of the floater;
- n_{ml} is the number of mooring lines;
- L_{\min} is the minimum mooring line length;
- L_{\max} is the maximum mooring line length;
- H_{\min} is the minimum horizontal mooring line tension at the fairlead.

Efforts to determine the appropriate values for L_{\min} and L_{\max} are crucial to avoid encountering an ill-defined problem in the mooring system design.

The determination of the minimum and maximum lengths of the mooring line is based on the horizontal distance from the fairlead to the anchor, denoted as d_i . This distance serves as a reference point for establishing the bounds of the mooring line length. The maximum length corresponds to the situation when the mooring line is completely slack (i.e. $d_i + h$), where h represents the anchor depth.)

In contrast, the minimum length of the mooring line needs to be carefully defined to ensure that there is no vertical load applied to the anchor. This is because a vertical load at the anchor is not permissible according to established guidelines [35]. The minimum length may be determined by considering a taut mooring line (i.e. $\sqrt{d_i^2 + h^2}$), but in this case there will be a vertical load at the anchor. Thus, to determine the minimum length, two approaches can be followed. One approach involves progressively reducing the line length while monitoring for the presence of a vertical anchor load. The other approach involves solving a constraint optimization problem, where the objective is to minimize the mooring line length while enforcing constraints that prevent any vertical load at the anchor.

To prevent a scenario where all mooring lines are slack, it becomes crucial to incorporate an inequality constraint on the horizontal mooring lines' tension. This constraint guarantees the maintenance of a minimum tension in the lines, thereby averting extremely low horizontal stiffness and thus excessive displacements resulting from external forces. The minimum line tension, designated as H_{\min} , corresponds to the horizontal component of the initial tension in the mooring line when the floater assumes its equilibrium position and no thrust force is applied to the system. Generally, the chosen pretension value is approximately 0.1 to 0.2 times the breaking strength of the line [63]. This establishes an initial level of tension in the mooring lines, preventing them from becoming entirely slack and enabling enhanced control and stability of the system.

The problem does not have a unique solution, as there can be multiple combinations of mooring line lengths that can eventually achieve equilibrium for the floater in a random position. However, considering the applied thrust force, the resultant tensions in the mooring lines should be at least of a magnitude capable of balancing the wind force. This prevents that the output of the optimization is an excessively long mooring line. On the other hand, the constraints on the mooring line lengths, particularly the lower bound, ensure that extremely high tensions in the mooring system are avoided. For this reason, the chosen optimization loop is assumed to be sufficiently restrictive. However, further studies could explore more advanced strategies to determine the necessary mooring line lengths for wind turbine repositioning.

4.2.4. MoorPy for mooring lines performance calculation

The computation of the Floating Offshore Wind Turbine's (FOWT) equilibrium states under varying wind thrust forces was conducted using MoorPy, a Python-based quasi-static mooring analysis tool [76]. In MoorPy, the FOWT and the floater were implemented as six degrees of freedom (DOF) solid body, considering the latter hydrostatic characteristics.

The following results are obtained after solving the optimization problem:

- mooring line length (L_i);
- horizontal tension at the fairlead (H_i);
- distance between the desired and actual positions;
- vertical tension at the fairlead (V_i);
- tension at the fairlead (T_i);
- absolute error in the yaw angle (rotation around the z-axis) of the floater;
- stiffness matrix of the mooring line system.

For brevity and relevance, it was chosen to not display all of these results.

The aerodynamic loads were represented as a constant force vector acting on the FOWT. To simplify the analysis, the aerodynamic force vector exerted on the rotor was directly applied to the floater at the seawater level, disregarding the aerodynamic moment on the platform resulting from the hub height and the aerodynamic drag of the tower, which was assumed to be rigid. Whenever there was a change in wind direction or wind turbine nacelle's yaw angle, the aerodynamic force vector acting on the FOWT was updated accordingly.

4.2.5. General Hypotheses

It is important to acknowledge that this methodology relies on certain assumptions concerning the position mooring system. As a specific mooring system designed for position mooring is not available yet, and the geometrical modelling is taken from the work of Kilinic [47], all the hypotheses mentioned below, apart from the one relating to the wind load, are common to the work of Kilinic itself. The assumptions are:

- the tensioning system on the floater is able to pull-in and pay-out the mooring line. In other words, the on-board mechanism can provide the force needed to move the turbine;
- the excess mooring lines can be stored on the floater;
- there is enough extra mooring line on board to reach any position in the movable range;
- the mooring line is fixed to the anchor at one end and to the fairlead at the other end;
- the mooring line follows a straight path from fairlead to anchor. In other words, the projection of the line on the seabed is a straight line;
- the direction and speed of the upcoming wind are stationary, which means that the force exerted by the wind remains constant as well;
- the dynamic power cable (required to export power) is of sufficient length.

4.3. Case study definition

The methodology described in Section 4.2 is applied to a case study aimed at assessing the performance of position mooring in combination with yaw-based wake redirection. This section presents the case study, starting with an introduction to the selected wind turbine in Section 4.3.1. Subsequently, Section 4.3.2 presents details about the floater used for setting up the platform and mooring systems, along with considerations about its impact on the movable range of the wind turbine. In Section 4.3.4, a comprehensive explanation is provided on how the selected case study aligns with the proposed methodology. Finally, in Section 4.3.3, the different thrust force scenarios used in the simulations are presented.

4.3.1. Wind turbine selection

The selected wind turbine for the case study is the IEA Wind 15-Megawatt Offshore Reference Turbine. It is a publicly accessible resource that serves as a suitable benchmark for this thesis. Its publicly available design parameters make it an ideal baseline for exploring new technologies and operational methodologies [1]. The size of the IEA 15-MW reference turbine aligns with the industry's trend towards larger offshore wind turbines with higher power ratings.

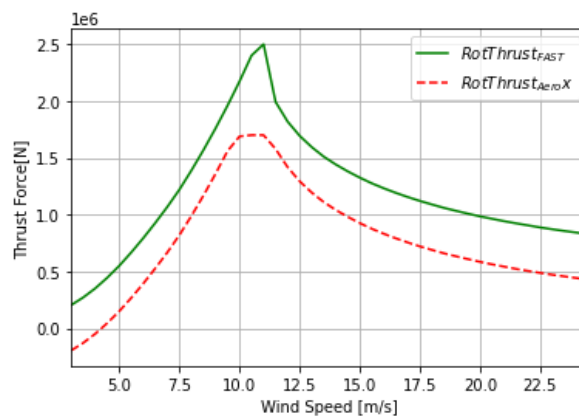


Figure 4.4: IEA Wind 15-Megawatt thrust curve.

Figure 4.4 illustrates the steady-state performance of the rotor with respect to wind speed. The green line represents the thrust calculations extrapolated from the report [1] computed using OpenFAST, while the red dotted lines represent only the aerodynamic component of the total thrust exerted on the rotor. OpenFAST incorporates gravitational loads, such as the weight of the rotor and a portion of the nacelle, in its thrust force calculations. Therefore, in order to isolate the actual aerodynamic force, the OpenFAST curve was adjusted. This adjustment involved reducing the curve by a constant offset equal to the gravitational load and applying peak shaving based on the controller settings.

The corrected thrust curve, which accounts for the aerodynamic force acting on the rotor, was employed to determine the aerodynamic force based on the incoming wind speed and direction and the yaw angle of the turbine. Once the thrust force and its components in the x and y directions of the general reference system were determined, they were used as inputs in MoorPy to calculate the necessary mooring lines' lengths to reach equilibrium at the desired position. This calculation was carried out following the optimization process described in Equation 4.5.

When the turbine undergoes yawing, the resultant thrust force exerted on the rotor is determined by incorporating the effective wind speed. This is calculated by multiplying the incoming wind speed by the cosine of the yaw angle. Subsequently, this computed value is utilized to extrapolate the updated thrust force from the red curve depicted in Figure 4.4. Notably, for the sake of maintaining simplicity and avoiding undue complexity in the analysis, the impact of yaw on the diminished rotor area is omitted.

4.3.2. Floater selection and movable range shape

The selected floater is the UMaine VoltturnUS-S, which was a floating semisubmersible platform specifically designed to support the IEA 15MW turbine [29]. This reference design, developed by UMaine, serves the wind industry by providing a publicly accessible design benchmark for the exploration of new technologies. The UMaine VoltturnUS-S consists of a floating semisubmersible platform, a chain catenary mooring system, a tower specifically designed for floating applications, and a modified controller tailored to floating platforms. The comprehensive description of the catenary mooring system within this reference floater is particularly relevant to the case study at hand. This inclusion allows for a focused investigation of the objectives outlined in section 4.1.4.

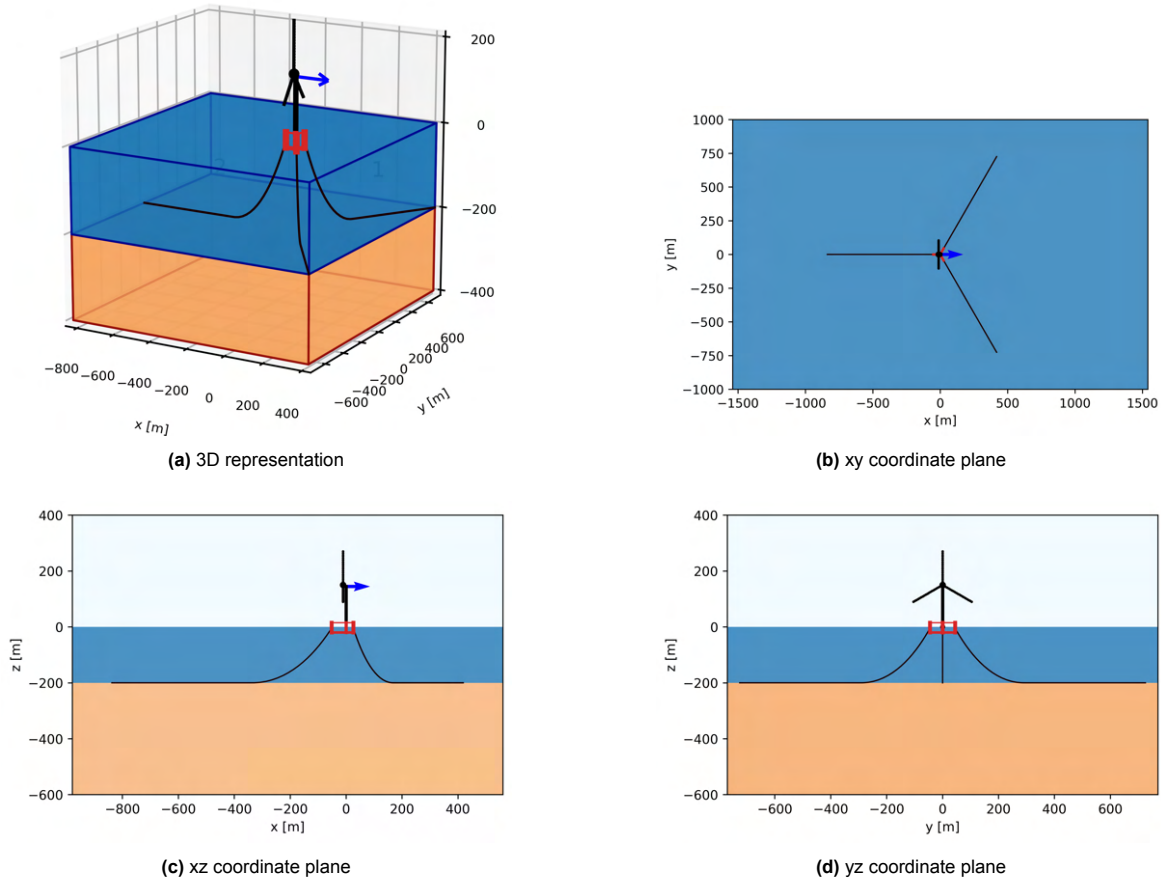


Figure 4.5: Illustrations of the UMaine VoltturnUS-S floater for the IEA 15MW turbine, modified from [47].

Figure 4.5 provides visual representations of the floater, including the wind turbine and the thrust force vector applied on the rotor, used in the study. The mooring system employed consists of three catenary mooring lines, with each line positioned at 120-degree intervals around the floater. The length of each mooring line (L_i) is set at 850 meters. The vertical distance from the fairlead to the anchor (h) measures 186 meters, while the horizontal distance (d_i) spans 779.6 meters. For more detailed information regarding other characteristics of the mooring system, please refer to Table 6 in the work by Allen et al. (2020) [29].

As stated in section 4.2, the determination of the wind turbine's neutral position (initial installation position) and the specific anchor locations play a pivotal role in defining the shape of the range within which the turbine can be moved. The selection of the UMaine VoltturnUS-S floater and of its mooring system determine the movable range shape and size. It is depicted as a triangular region in Figure 4.6. It should be noted that the vertices of the movable range triangle do not correspond to the positions of

the anchors due to the influence of the floater geometry.

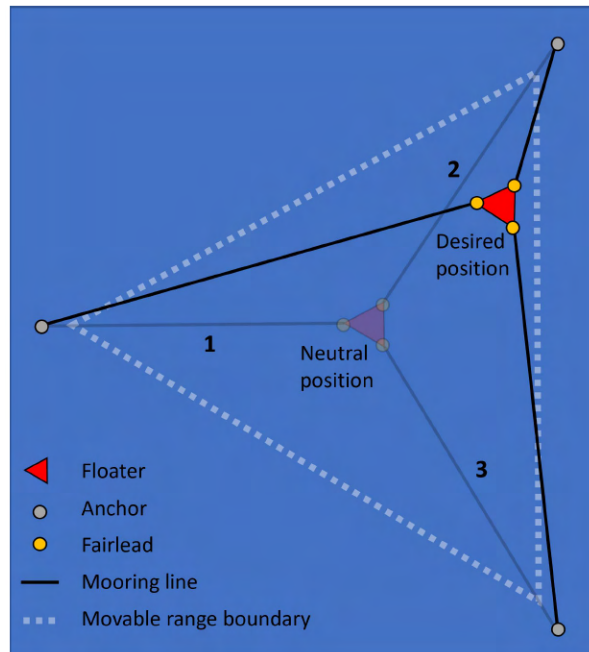


Figure 4.6: Illustration of the position mooring repositioning mechanism concept for the UMaine VoltturnUS-S floater[47].

4.3.3. Wind resource selection

In accordance with the methodology described in section 4.2, the evaluation of the station-keeping performance of FOWT position mooring considers the influence of wind force in the equilibrium. To capture the impact of wind speed and direction on the force equilibrium, different wind scenarios are selected and examined.

Only the case at rated wind speed is investigated as it corresponds to the maximum thrust force magnitude, which has the most significant impact on the equilibrium of forces acting on the floater. It is reasonable to assume that the effect of thrust force on the station-keeping performance may be scaled down (or up) at wind speeds different from the rated one.

Regarding different wind direction cases, considering the relationship with the orientation of the mooring lines system can be beneficial. Specifically, three extreme configurations are examined for each mooring line:

- Case 1, shown in figure 4.7a: the wind is blowing from west to east, resulting to be aligned with mooring line 1 and tension it when the turbine is in its neutral position ;
- Case 2, shown in figure 4.7b: the wind is blowing from south to north, resulting to be perpendicular to mooring line 1 when the turbine is in its neutral position;
- Case 3, shown in figure 4.7c: the wind is blowing from west to east, resulting to be aligned with mooring line 1 and slack it when the turbine is in its neutral position (i.e the center of the movable range).

Two different wind turbine yaw angles are investigated for each of the aforementioned cases: 0° and 15° . The selection of two cases aims to capture different scenarios representative of operational conditions when the yaw-based wake redirection is employed. The first case, with a yaw angle of 0° , is chosen as the baseline scenario. In this case, the thrust force is always aligned with the wind speed, providing a reference for comparison. The second case, with a yaw angle of 15° , represents a realistic operational set point for a yawed wind turbine aiming for wake deflection. Higher yaw angles may

significantly reduce power production, while smaller yaw angles may not effectively steer the wind turbine. The 15° yaw angle provides a practical scenario to assess the station-keeping performance. To support that, the optimization results from the previous chapters ?? relative to both the two turbine and extended wind farm case, shows that the optimizer yaw angles are typically no larger than 15 degrees.

To enhance the referencing of specific wind direction and turbine nacelle yaw angle combinations, a structured notation "case x.y" will be employed. Here, "x" signifies the case concerning the upcoming wind direction, while "y" pertains to the case involving the turbine's nacelle yaw angle. Specifically, when "y" equals '1', it corresponds to a wind turbine yaw angle of 0 degrees, and '2' denotes a yaw angle of 15 degrees. The "x" notation will follow the previous case definition. For instance, "case 1.1" corresponds to the wind blowing from west to east with the turbine's nacelle yaw angle set at 0° .

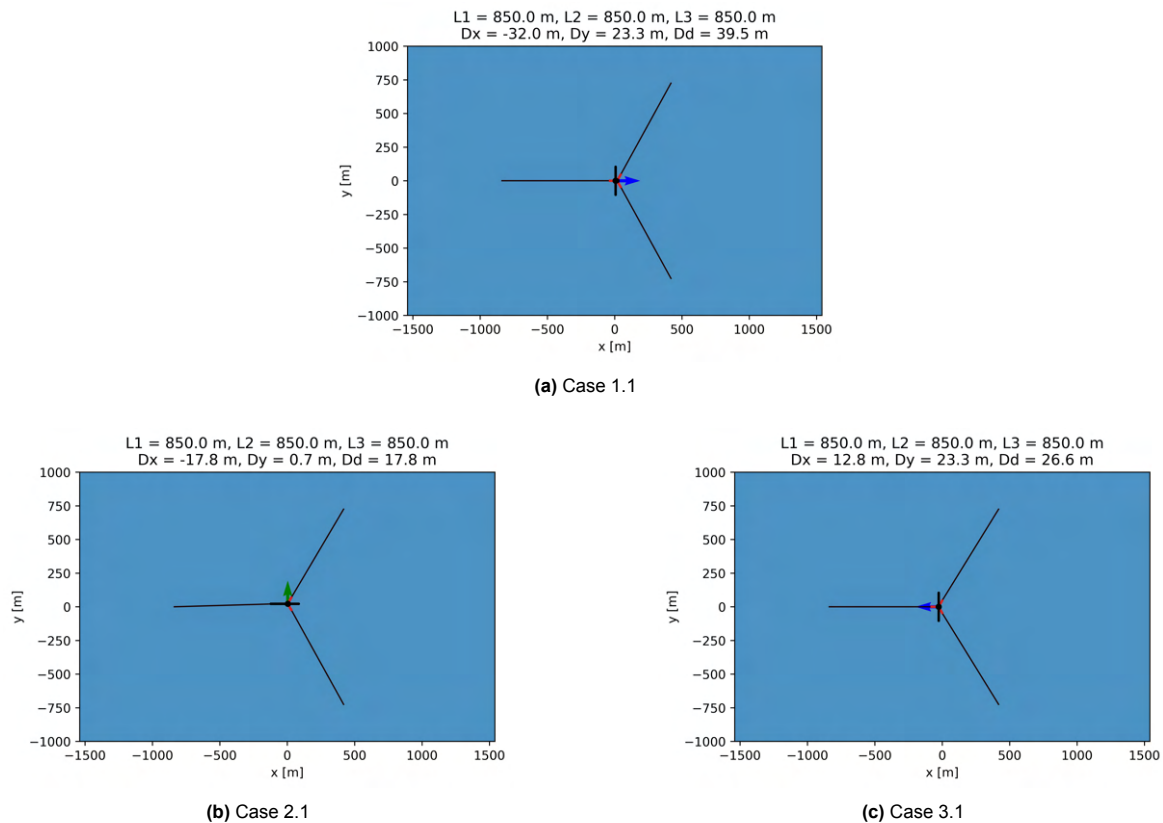


Figure 4.7: Aerial view of the considered wind direction cases.

By investigating these six combinations of wind directions (aligned with one mooring line upwind, aligned with one mooring line downwind and perpendicular to one mooring line) and operational configurations (yaw angles of 0° and 15°), a comprehensive understanding of the performance parameters of the mooring line system can be obtained. This analysis allows for the evaluation of how the mooring system behaves under different wind conditions and operational settings while keeping other input parameters constant.

4.3.4. Implementation of the methodology in the case study

As stated in section 4.2, multiple positions within the range are selected to explore the movability and station-keeping performance across the entire movable range. This is achieved by creating a 30 by 30 point mesh grid of desired floater positions. By evaluating which coordinates fall within the movable range, as illustrated in Figure 4.8, a comprehensive understanding of the feasible turbine positions is obtained, with each black dot representing a desired coordinate.

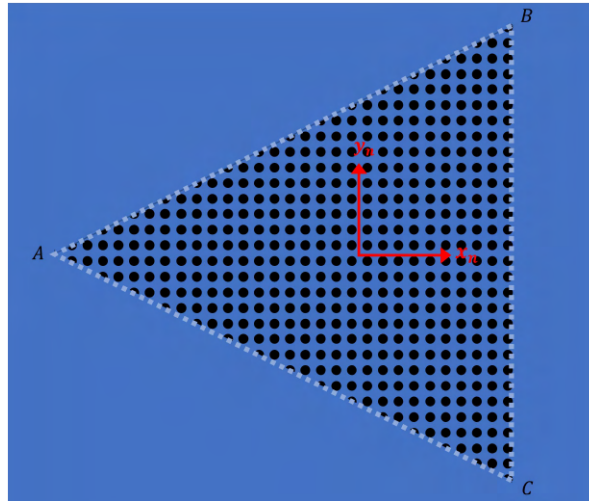


Figure 4.8: Desired coordinates for the UMaine VoltturnUS-S floater [47].

For each desired position the horizontal distances of each fairlead from the anchor (d_1 , d_2 , and d_3) and the mooring lines' orientation (β_1 , β_2 , and β_3) are calculated. These calculations are performed using Equations 4.3 and 4.4, respectively, while considering the floater's geometry. To provide a visual representation, Figure 4.9 illustrates the distance and orientation of the floater for one of the chosen positions in the case study.

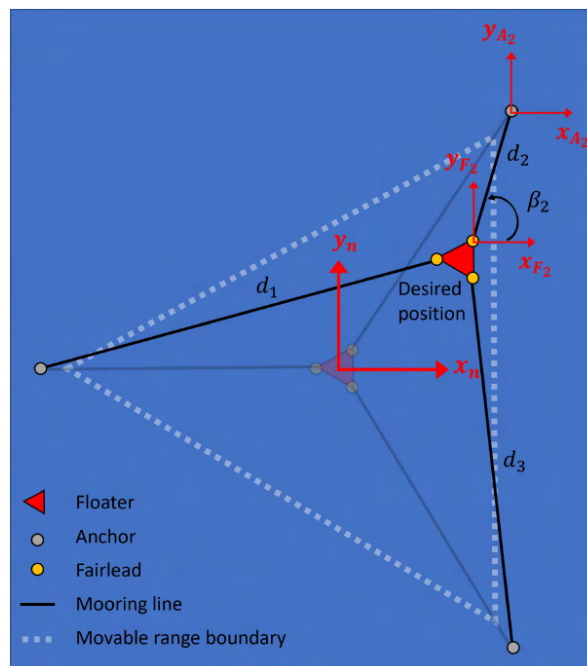


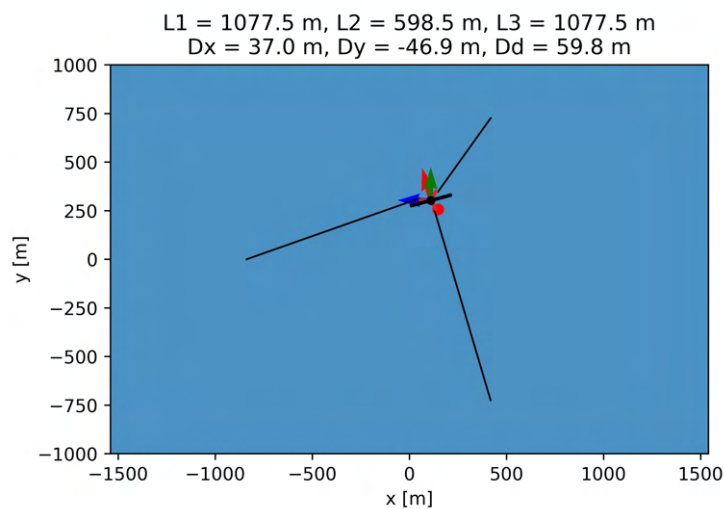
Figure 4.9: Illustration of the horizontal distances and orientation angle for an example desired UMaine VoltturnUS-S floater. [47].

At this point, the only free variables left are the mooring lines lengths L_1 , L_2 , and L_3 . These are computed by employing the optimization loop described in equation 4.5. The algorithm concludes its optimization iterations when the difference in the objective function's values (i.e. position error) between two consecutive steps becomes smaller than the threshold of 10^{-5} (m).

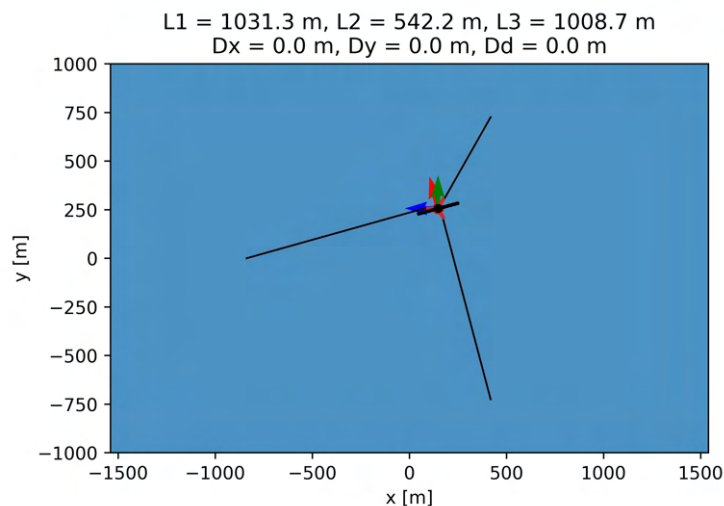
Figure 4.10 illustrates the initial and final phases of the proposed algorithm when the installation position of the floater and the desired position correspond for the specific wind case 2.2 (the reader is

referred to section 4.3.3 for the description). The red arrow denotes the total thrust force acting on the system, while the blue and green arrows represent the x and y components of the wind force. The red dot in the figure indicates the desired position for the specific iteration. Figure 4.10a presents the initial mooring line lengths (L_1 , L_2 , and L_3) and the horizontal, vertical, and overall distance, respectively (D_x , D_y , and D_d), between the equilibrium position and the desired position before the optimization loop is applied. In contrast, figure 4.10b showcases the final(i.e. resulting from the optimization loop) mooring line lengths and distances.

Initially, the mooring line lengths are computed as the mean value between the minimum and maximum length allowed for the desired position. The equilibrium position that is given by the mooring line forces corresponding to the initial lengths is clearly not the desired position. After the optimization loop, the mooring lines length is modified and the difference within the positions is reduced to zero. This can be visualized in figure 4.10b as the wind turbine and the red dot are superimposed.



(a) Initial guess for the mooring lines length for case 2.2.



(b) Final optimized result for the mooring lines length for case 2.2.

Figure 4.10: Input and output of the optimization loop for a specific position and wind scenario.

4.4. Case study results

In this section, the results obtained with the methodology described in Section 4.2 are presented. In order to better visualize the changes of each desired variable as a function of the position, the results are shown as 2D contour plots, where the x- and y-axis represent the coordinate of the floater inside the movable range.

Firstly, in section 4.4.1, the distance between the desired and actual positions is presented and discussed. Subsequently, in section 4.4.2, the findings concerning the horizontal tension of the mooring lines system are outlined. Finally, section 4.4.3 presents the results regarding the stiffness of the mooring lines.

4.4.1. Station keeping performances: position error

Figure 4.11 presents a series of contours illustrating the error between the desired and actual equilibrium positions attained by the floater for various investigated wind directions, considering the non-yawed turbine. Several observations can be made from these results:

- The station-keeping performances are satisfactory, as the error remains within the range of 0 to 10 meters in the majority of the movable range area.
- The regions where the error increases up to 90 meters are located in close proximity to the anchors. These regions' locations depend on the wind direction.

Thus, it can be inferred that the relative orientation of the mooring lines and the incoming wind direction has a relatively minor influence on the position error. It mainly affects the area where the turbine is near the anchors. However, this area constitutes only a small portion of the movable range and, as a result, it can be concluded that does not significantly impact the station-keeping performances of the mooring system.

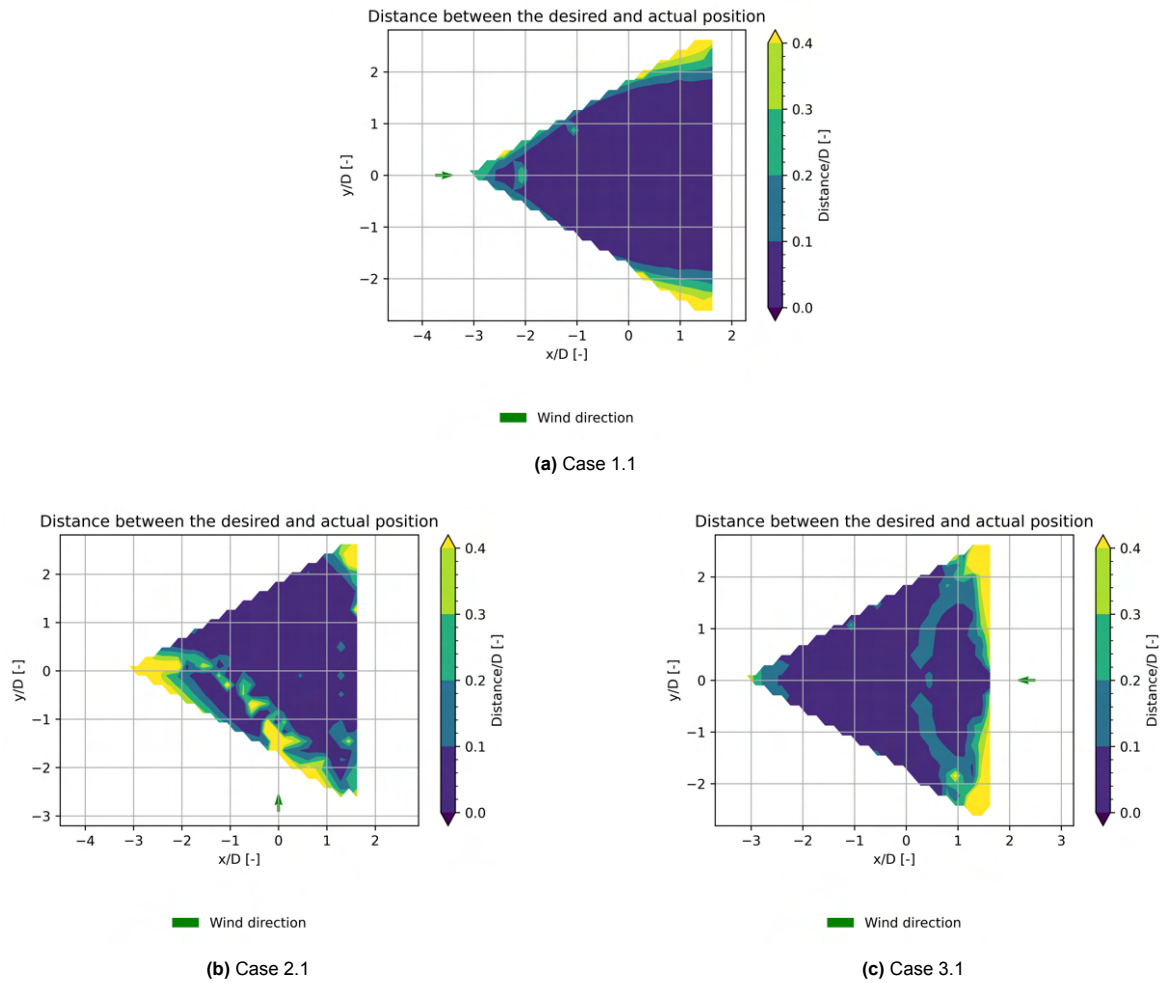


Figure 4.11: Contour plot of the difference between the desired and actual equilibrium position for different wind direction cases.

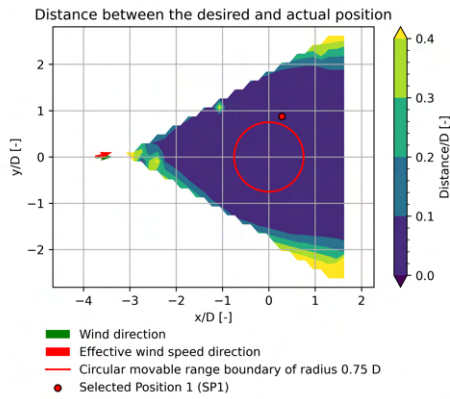
Figure 4.12 depicts a series of contour plots illustrating the variations between the intended equilibrium positions and the actual positions achieved by the floater under different wind directions, with the turbine yawed by 15° . The contours showcase the discrepancies in horizontal, vertical, and overall position errors compared to the case when the turbine is not yawed (0° yaw), considering a specific chosen location. It is important to note that the selected position varies for each investigated wind direction.

For consistency with the analyses presented in chapter 3, the selected positions are deliberately situated just outside an optimal circular movable range, having a radius equal to 0.75 times the rotor diameter. Furthermore, in these positions, the turbine has been repositioned perpendicularly to the wind direction from the installation location. The chosen positions are not precisely on the boundary of the movable range, because due to the discretized approach employed the analysed positions do not fall on the exact border. Consequently, the selected positions are the closest to the boundary that adheres to the pre-established criteria.

The disparities depicted in the figure are modest, merely a few meters, suggesting that altering the wind turbine's yaw angle does not notably influence the station-keeping performance of the system. To support this observation, readers are encouraged to compare these contours with those in figure 4.11. A qualitative comparison underscores that the differences between the 0° and 15° yaw cases are in fact minimal, a fact that is quantitatively confirmed for the chosen reference point.

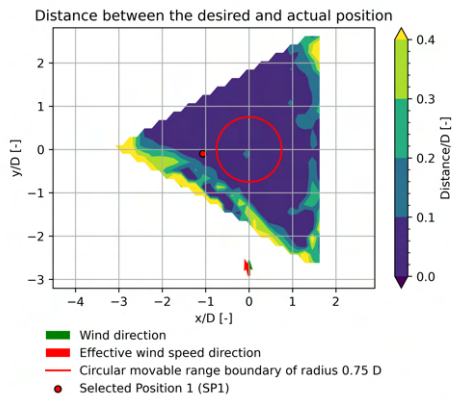
Furthermore, it's noteworthy that the areas where the greatest discrepancies arise correspond to regions with higher position errors. These areas are situated at a considerable distance from the tur-

bine's installation position. The likelihood of repositioning the turbine in these regions is low, both due to the elevated position error and the improbable necessity of such a movement, especially considering that the movable range with a radius of 0.75 times the rotor diameter excludes these positions, as illustrated in a similar manner to figure 4.12.



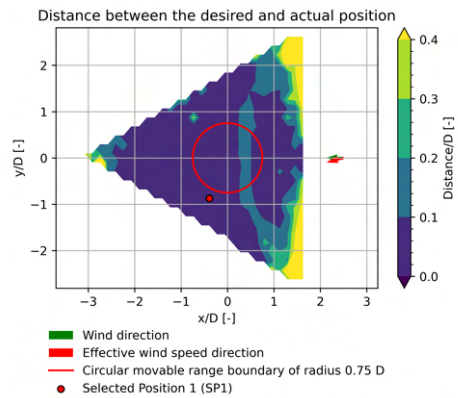
Horizontal, vertical and overall position error when the turbine is yawed of 15° at:
SP1) $D_x = 0.0$ m, $D_y = 0.0$ m, $D_d = 0.0$ m

(a) Case 1.2



Horizontal, vertical and overall position error when the turbine is yawed of 15° at:
SP1) $D_x = -0.0$ m, $D_y = -0.0$ m, $D_d = -0.0$ m

(b) Case 2.2



Horizontal, vertical and overall position error when the turbine is yawed of 15° at:
SP1) $D_x = -0.0$ m, $D_y = -0.0$ m, $D_d = -0.0$ m

(c) Case 3.2

Figure 4.12: Contour plot of the difference between the desired and actual equilibrium position for different wind direction cases when the turbine yawed of 15°.

4.4.2. Impact of the thrust force on the horizontal tension at the fairlead

In this section, the results of the horizontal tensions at the fairlead are presented. These values are chosen to be highlighted instead of the vertical and total tensions as they play a crucial role in balancing the floater under the influence of environmental forces.

It is important to note the constraint imposed on the horizontal tension, as defined in the optimization problem in equation 4.5, where the horizontal tension must be greater than or equal to the horizontal tension in the neutral position when no environmental forces are acting on the system (1.35 MN).

Figure 4.13 presents a series of contour plots illustrating the scalar sum of horizontal mooring line tensions for the three different wind direction cases when the wind turbine is not yawed. The horizontal tensions for all the combinations of positions inside the movable range and thrust force are far from the breaking parameter.

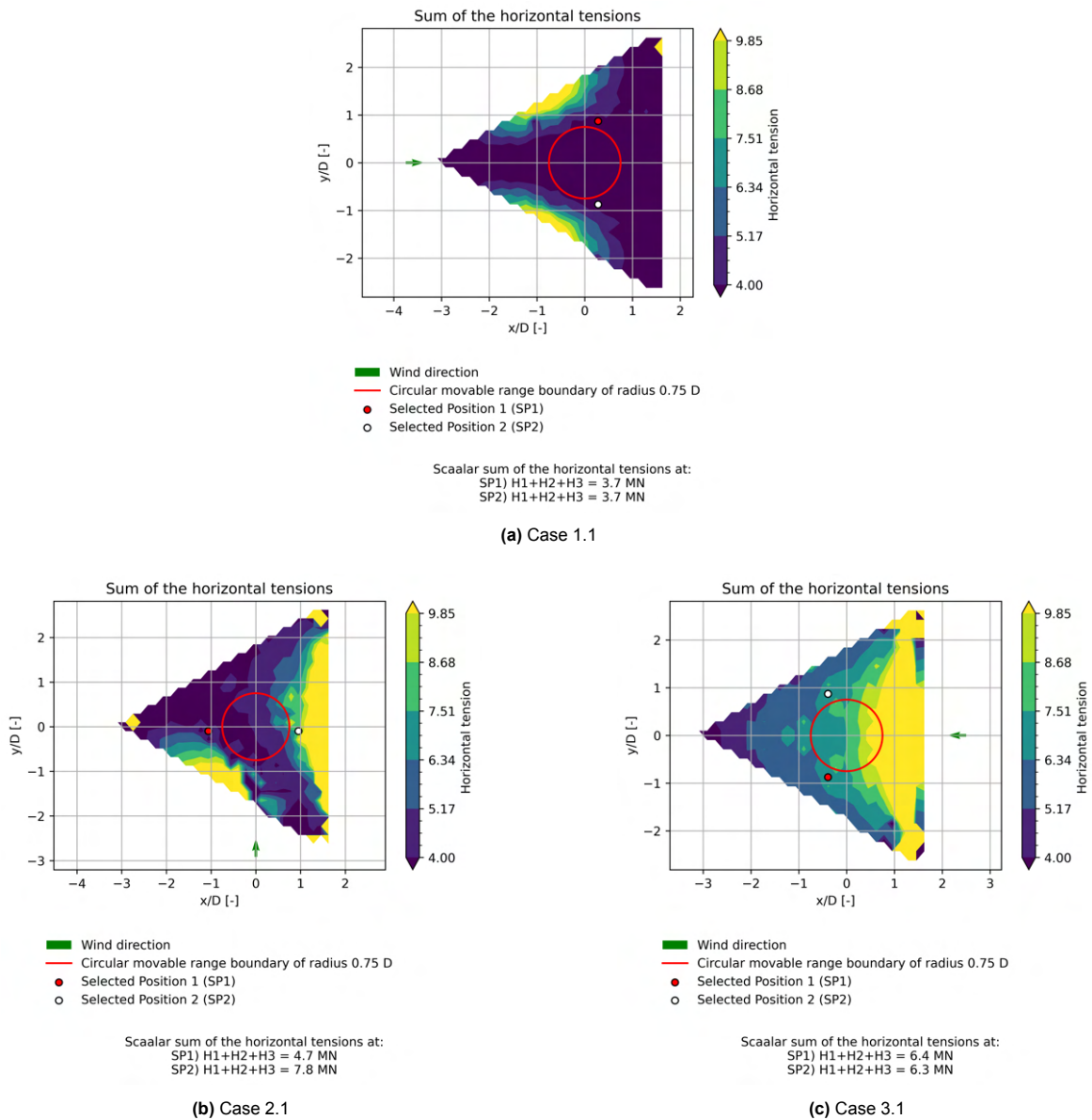


Figure 4.13: Contour plot of the scalar sum of the horizontal mooring line tension for various wind direction cases.

It is evident that the relative position of the mooring lines (i.e. the anchors' positions) and the wind direction significantly influence the contour shapes. The following observations can be made:

1. The contour plot reveals two distinct regions: one where the tensions remain relatively low and another where peaks in tension occur. The low-tension regions are situated around the center of the movable range, while the high-tension area is located near the boundaries.
2. In case 1.1 (Figure 4.13a), the tension peaks are limited to small points on the perimeter. The contour exhibits symmetry, with the mooring line 1 as the axis of symmetry. The regions of higher tension are perpendicular to the wind direction.
3. In case 2.1 (Figure 4.13b), when the wind blows perpendicular to mooring line 1, the areas of increased tension are wider compared to cases where the wind aligns with the mooring lines and the floater is downwind of the line (case 1.1). In addition, the contour loses its symmetry.
4. Case 3.1 (Figure 4.13b) displays a symmetric contour with generally higher tensions than case 1.1 and case 2.1.

These observations concerning the sum of tensions can be explained by analyzing the free-body diagram.

In case 3.1, the tension generated by the mooring line 1 and the wind direction has the same direction, and thus the contribution to the equilibrium of the mooring line 1 is minimal. To restore balance to the system, the tensions in lines 2 and 3 must increase compared to cases 2.1 and 1.1. The total tensions are most pronounced between the anchor points B and C. Within this specific region, the angles formed between the tensions provided by lines 2 and 3 and the wind direction reach their maximum values. Consequently, the component contributing to the equilibrium is minimized, resulting in higher overall tensions.

In case 1.1, the tension generated by the mooring line 1 when the turbine is positioned close to anchor A, the angle between the mooring tension generated by the mooring line 1 and the wind force increases, and the component of tension contributing to the system's equilibrium diminishes. Consequently, tensions in the other mooring lines increase to maintain the overall equilibrium of the floater, compensating both the component parallel and perpendicular to the wind direction. This phenomenon is particularly noticeable as the floater approaches the movable range's boundary, especially in the middle of the segment connecting two anchors, where tensions in the mooring lines escalate.

Figure 4.14 displays the scalar sum of the mooring lines' tension and the tension of each mooring line separately. An essential observation is that, in this case, the upwind mooring line plays a crucial role in equilibrating the floater. As shown in Figure 4.14a, it experiences higher tension compared to the other two mooring lines. On the other hand, in positions where the floater is at the midpoint of the segment between anchors A and B, and A and C the mooring line 1 and the thrust force have the highest angle between them, resulting in very high tension in mooring line 1, generating a significant tension component perpendicular to the wind. To balance this, tensions in the other mooring lines 2 and 3 increase as well. The free-body diagram approach of tensions provides a consistent strategy to explain the contours observed in the plots of horizontal tensions throughout the movable range.

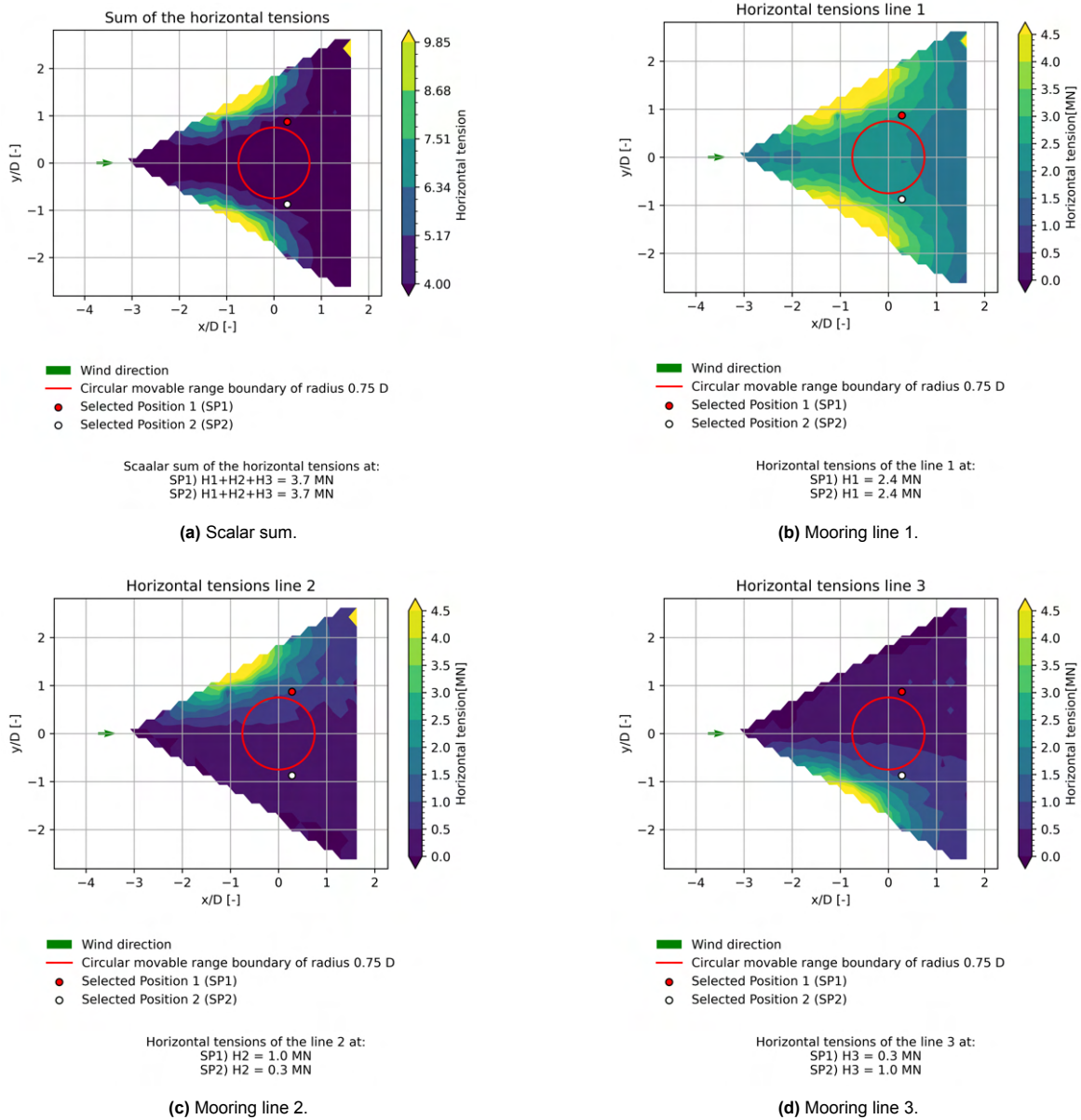


Figure 4.14: Contour plot of the mooring lines length for case 1.1.

Figure 4.15 portrays a sequence of contour plots that exhibit the scalar sum of horizontal tensions in the mooring lines. These plots are generated across various wind direction scenarios while the wind turbine undergoes a yaw angle of 15° . Accompanying these contour plots, the figure also illustrates the changes in the horizontal tensions magnitude for each individual mooring line when compared to the case where the wind turbine is yawed at 0° .

These analyses are conducted for two specific chosen positions, which vary according to each scenario. These positions are symmetrical with respect to the wind directions. The criteria for selecting these positions are in accordance with the guidelines detailed in section 4.4.1.

Upon comparing these plots with the one displayed in figure 4.13, it becomes apparent that the overall distribution of the sum of tensions within the movable range remains highly similar when the turbine is yawed and when it is not yawed. In the case of 1.2, displayed in figure 4.15a when the turbine is yawed, the contour shape is comparable to the non-yawed case, but it is no longer symmetric. The areas of peak tensions are still located close to the midpoint between anchors A and B, and between anchor A and anchor C. However, in this case, the latter zone exhibits higher tension peaks compared

to the corresponding non-yawed case, while the former zone shows smaller peaks. This behaviour can be explained using free-body diagrams.

However, the magnitude of these tensions is influenced by the yaw angle of the wind turbine, and this change in magnitude isn't consistent across all selected positions. In scenario 1.2, as shown in Figure 4.15a, when the turbine is located at position SP1, the tensions in lines 1 and 2 decrease, while the tension in line 3 increases. However, these changes are in the order of magnitude ranging from 0.2 MN to 0.7 MN. It is important to underline that the mooring lines' tension is safely smaller than the breaking line tension (22.8 MN) for all the cases when the turbine is yawed (or not). As the wind turbine yaws, the angle between the tension in mooring line 2 and the thrust force diminishes. This reduction in angle prompts the thrust force to align more closely with the mooring line 2's tension. Consequently, the tension in mooring line 2 is smaller in case 1.2 than in case 1.1 since its contribution to the equilibrium is reduced in the newly yawed turbine configuration. Conversely, the tension in mooring line 3 increases due to the yaw of the wind turbine, which tends to misalign mooring line 3 with the thrust force. This misalignment causes the angle between the tension in mooring line 3 and the thrust force to increase.

When the turbine is positioned in SP2, the mooring lines tension increases for all three lines compared to the zero yaw case. The biggest increase is recorded for mooring line 3, as the angle between the turbine and the line increase as explained before.

In case 2.2 a similar pattern is shown, as when the turbine is in position SP1 the mooring line tensions decrease, while in position SP2 the tension increases. In case 3.3 the tensions of the mooring lines increase when the turbine is yawed in both positions SP1 and SP2. These results can be again explained by means of the free body diagram.

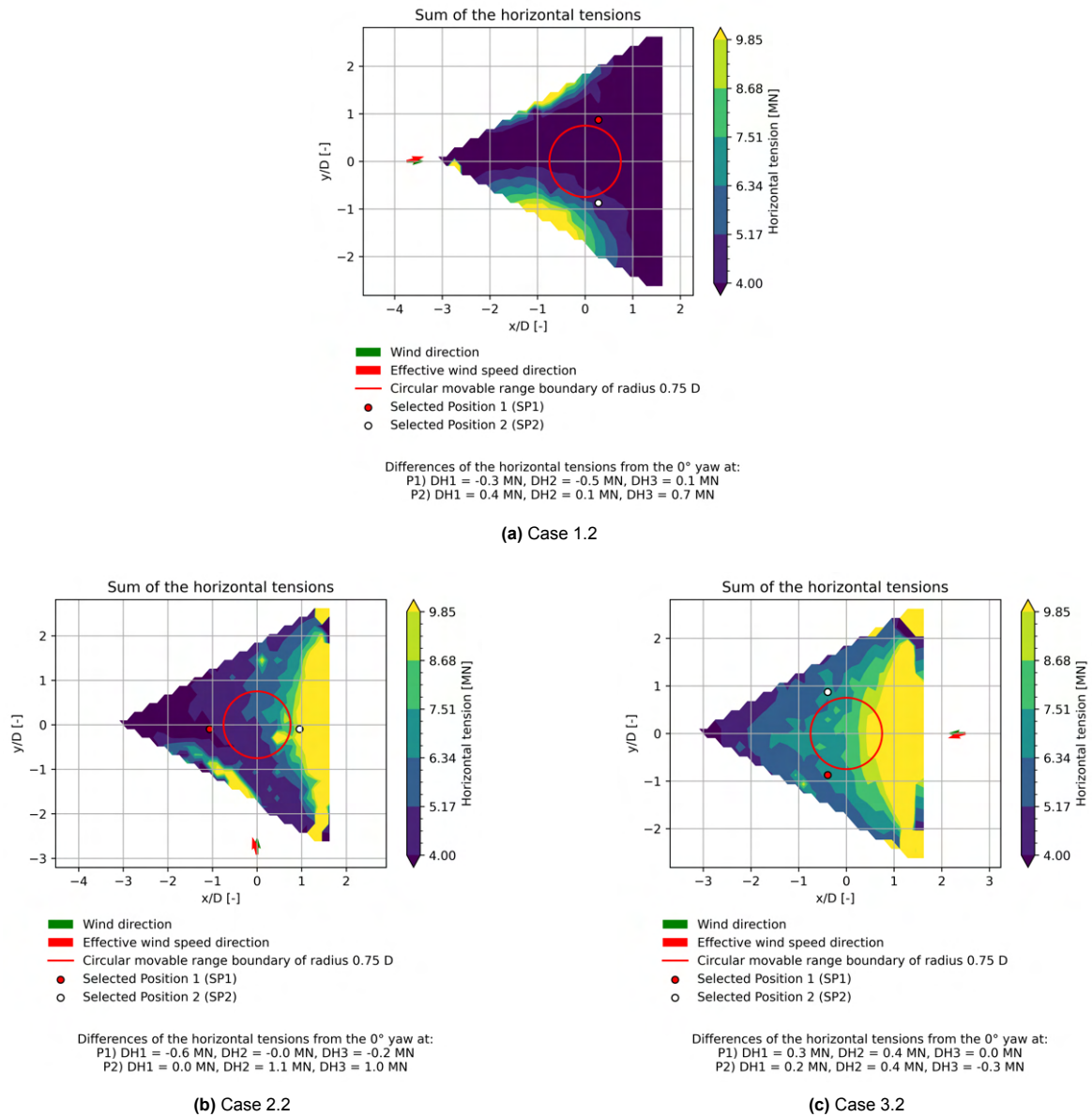


Figure 4.15: Contour plot of the sum of the horizontal mooring line tension for various wind direction cases when the turbine is yawed of 15°.

4.4.3. Effect of the wind direction and turbine yaw on the surge stiffness term

Typically the mooring systems provide a semi-submersible platform stiffness in the surge, sway and yaw degrees of freedom [53, 77]. It is essential to underline that natural periods of the semi-submersible are greatly influenced by the mooring system characteristics, as its characteristics in the horizontal plane clearly depend on the mooring system stiffness. The natural periods in heave, roll and pitch degrees of freedom are barely influenced by the mooring system [90].

In this section, only the results of the static surge stiffness of the mooring system are presented, referred to as K_{11} . It was chosen to display the results only for this component of the stiffness matrix as the analyses of the results for the sway and yaw stiffness terms won't add any insights to the ones addressed with the surge analyses. For completeness, the results relative to the sway and yaw cases are reported in the appendix.

When designing the mooring lines system is imperative to ensure that the natural frequency of the floater falls beyond the frequency ranges encompassed by the exerted loads on the structure. The loads acting on the structure can be categorized as follows:

- **Steady loads:** These encompass mean wind, current, and mean wave forces, which cause a displacement from the equilibrium position of the structure. This displacement is counteracted by the restoring force of the mooring lines.
- **Low-frequency loads:** These include wave-drift second-order forces, which emerge due to the frequencies of wave groups occurring in irregular waves.
- **First-order wave-frequency loads:** These contribute to maximum tensions in the mooring lines and induce fatigue damage.
- **Operational loads:** These are segmented into wind load, 1P (rotor rotational speed), and 3P (blade passing frequency).

Increasing the length of a mooring line results in a reduction of the stiffness contributed by the mooring system. However, it's important to consider that excessive mooring line length can render it ineffective in anchoring the floating buoy, potentially leading to significant drifting. This elongation can magnify both the mean and amplitude of the surge experienced by the floating platform due to the diminished stiffness of the mooring system. Additionally, a reduction of the floater stiffness will reduce its natural frequency, and thus potentially elevates the risk of resonant excitation at low frequencies due to second-order waves. Conversely, opting for shorter mooring lines can noticeably mitigate horizontal motions, but this could result in overly tight lines. Such tightness not only escalates the risk of high mooring tension, which in turn heightens the possibility of fracture but also exacerbates the heave motion.

The calculation of the static restoring stiffness is based on a presumed 0.1 meter displacement of the floater in the surge and sway degrees of freedom (DOFs), along with a 0.1 radians displacement for the yaw DOF. This choice is anticipated to significantly influence the outcomes, given that the loading scenarios under consideration align with the surge (X) direction for cases 1 and 3, and with the sway (Y) direction for case 2. Consequently, it's reasonable to expect that the static stiffness pertaining to the sway DOF will be notably low for cases 1 and 3, while the static stiffness related to the surge DOF in case 2 will be similarly diminished. Even if this simulation scenario may not be realistic, the results will nevertheless provide initial approximations regarding how the static stiffness changes within the movable range and the influence of yawing the turbine on this distribution.

Figure 4.16 presents contour plots illustrating the surge term of the static mooring line stiffness matrix for three different wind direction cases when the wind turbine remains unyawed. The following observations can be made:

- The contour plots reveal two distinct zones of stiffness distribution, where the stiffness of the system is either notably higher or similar to its stiffness in the installation position.
- The pattern of high stiffness areas is generally consistent with the pattern observed in the horizontal forces, as discussed in Section 4.4.2.

- The surge stiffness of case 2.1 is very low across all the movable ranges (in line with the comments above).
- High-stiffness areas tend to emerge in close proximity to the anchors.

The presence of high-stiffness areas near the anchors can be attributed to the varying length of the mooring lines. As the floater moves closer to zones near the anchor, the length of the relative mooring line decreases, leading to an overall increase in system stiffness.

The emergence of high stiffness zones when the turbine is positioned at the boundaries of the movable range raises some noteworthy considerations. While these zones may offer the greatest benefits for wind turbine repositioning, it is important to recognize that they only represent a small region within the overall movable range.

As highlighted in the analyses of the horizontal tension case, careful consideration should be given to the placement of anchors with respect to the prevalent wind direction. This is crucial to limit the occurrence of high stiffness (and tension) when the turbine is repositioned.

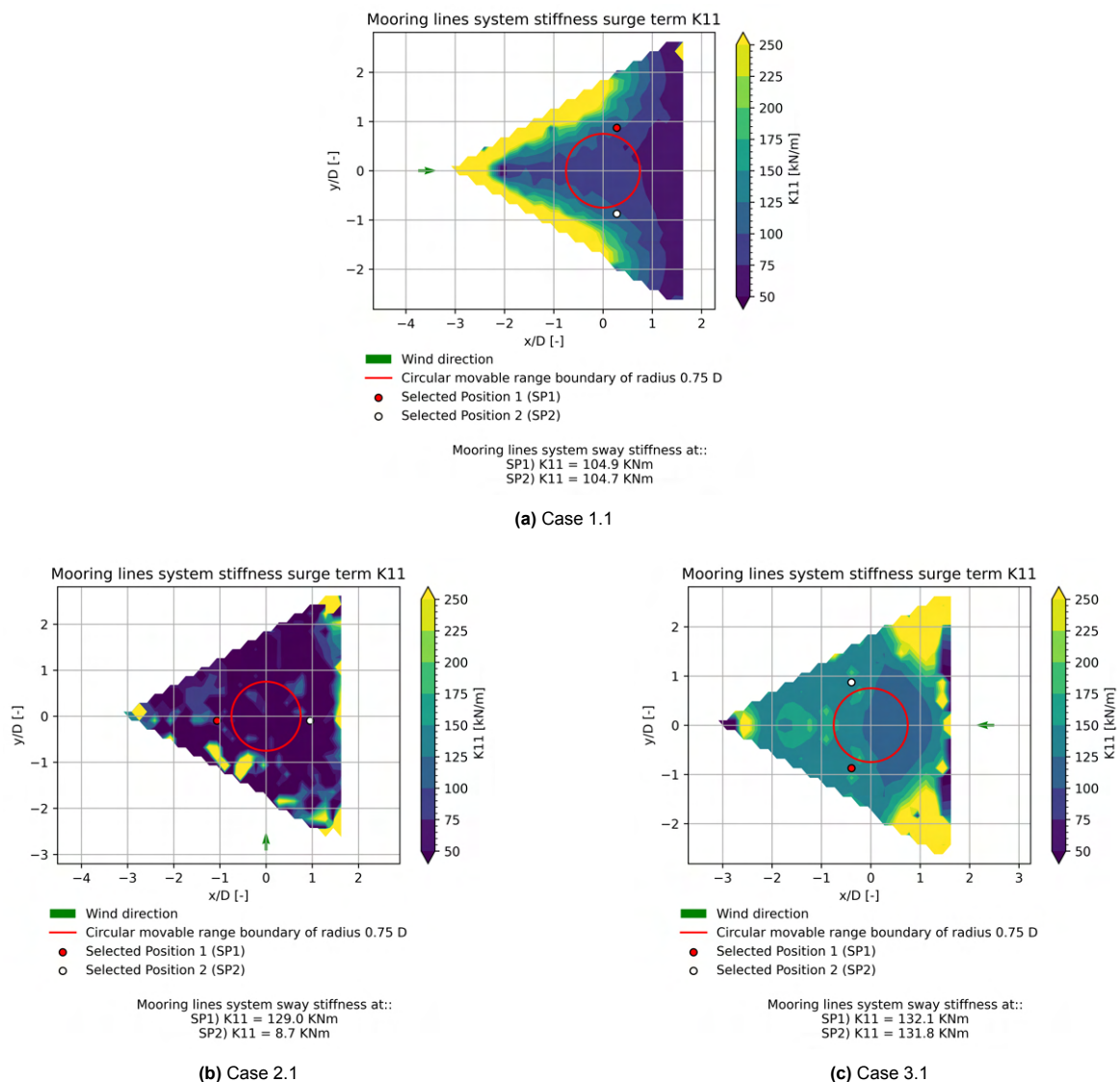


Figure 4.16: Contours plot of the surge mooring system stiffness term when the turbine yaw is 0° for different upcoming wind scenarios

The surge stiffness increases significantly as the length of one of the mooring lines decreases. This

effect is again evident when the floater approached the positions where it is necessary to increase the mooring line tension due to the high angle between the thrust force and the mooring lines that are majorly providing the equilibrium. This result is consistent with the literature [53], as shorter mooring lines result in higher stiffness. While this can be beneficial for station-keeping performances, in dynamic loading situations it may cause issues such as high tension in the mooring lines. Extremely short mooring lines can lead to excessively large horizontal restoring forces, and thus mooring lines tensions that may have a non-beneficial effect on the accumulated lifetime damage of the mooring system (i.e. fatigue).

Increasing (or decreasing) the length of mooring lines decreases (or increases) the stiffness of the mooring system in regard to certain degrees of freedom (especially surge and sway), modifying the dynamics of semi-submersible floating offshore wind turbines (FOWTs) motion. It is reasonable to expect that the mean amplitude of the floating platform surge and sway motion will increase with the increase of the length of the mooring line, as it will decrease the stiffness of the mooring system.

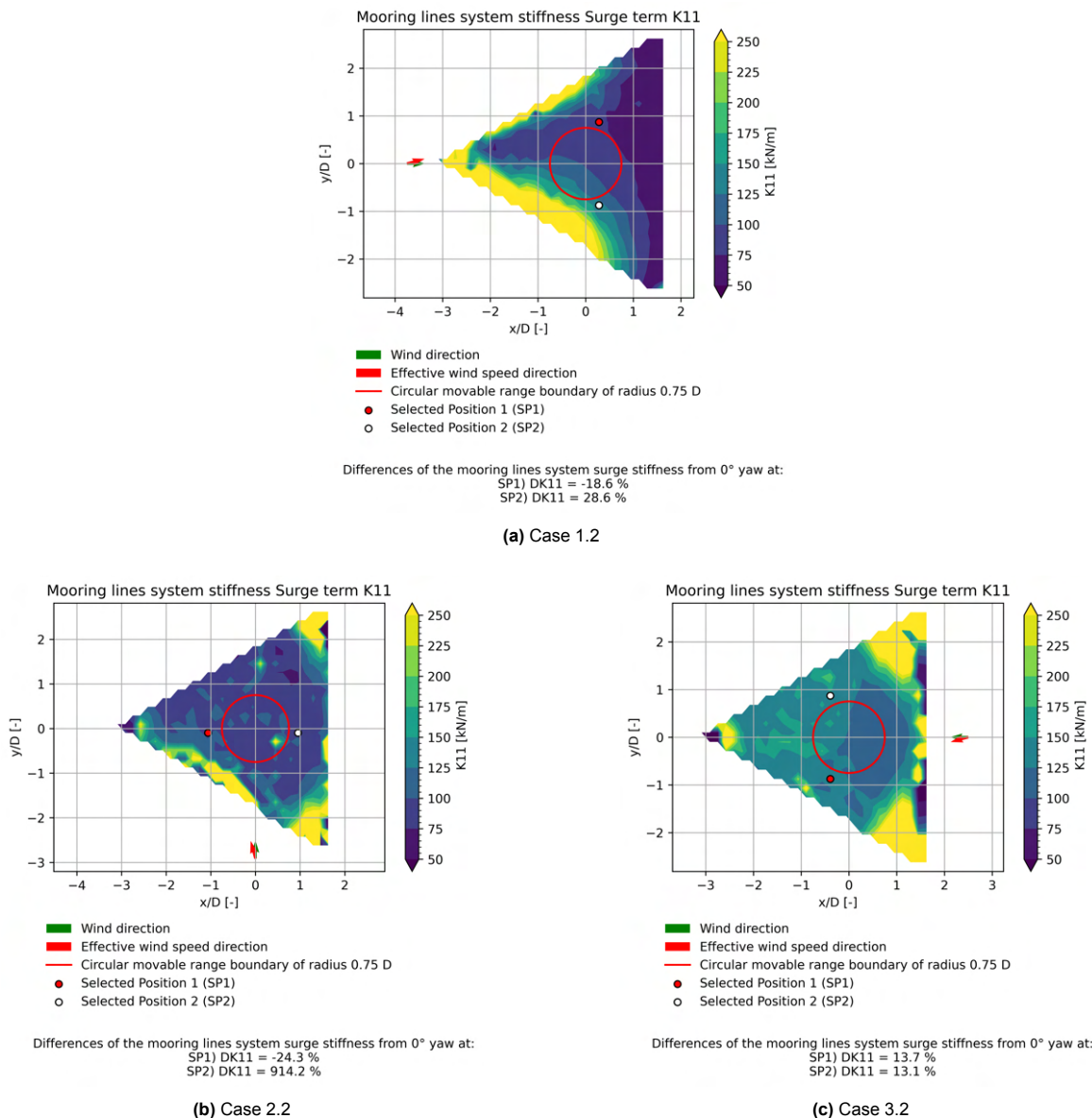


Figure 4.17: Contour plot of the mooring system stiffness for various desired positions.

Figure 4.17 displays a series of contours for all the different wind directions analysed when the wind turbine is yawed at 15°. Upon these contour plots, the figure also illustrates the percentage deviations

in stiffness term (K11) for each individual mooring line when compared to the case where the wind turbine is yawed at 0°. The differences are shown for two selected positions, the same illustrated in the previous section regarding the horizontal stiffness. The percentage changes have been defined as:

$$DK11(x, y) = \frac{K11_{15}(x, y) - K11_0(x, y)}{K11_0(x, y)} \cdot 100 \quad i = 1, 2, 3 \quad (4.6)$$

Where:

- x is the turbine x coordinate;
- y is the turbine x coordinate;
- $K11_{15}(x, y)$ is the surge stiffness term when the turbine's yaw is 15° in the turbine position;
- $K11_0(x, y)$ is the surge stiffness term when the turbine's yaw is 0° in the turbine position;

It is apparent that the effect of yaw on the stiffness term is similar to its impact on tensions. The overall contour shape remains quite similar to the non-yaw case. When the load becomes non-symmetric, as in cases 1.2 and 3.2, the stiffness distribution within the movable range becomes asymmetrical. In fact, for case 1.2 in SP1 the surge stiffness decreases by 18.6%, while in position SP2 increases by 28.6%. Additionally, for case 3.2 in SP1 the surge term increases for both SP1 and SP2 by 13%.

On the other hand, for case 2.2 the increase of the surge term for SP2 is almost a thousand per cent. This huge increase is correlated to the fact that when the turbine is yawed introduces a load component that is perpendicular to the surge (x) direction. In fact in the turbine zero yaw case, the surge stiffness for case 2.1 was an extremely low value, as can be seen in figure 4.17b.

5

Discussion

This chapter serves as a comprehensive review and emphasis of the outcomes derived from the prior analyses, aiming to provide a thorough grasp of the thesis. Each section is structured into two subsections. Initially, the primary findings corresponding to each preceding chapter are delineated and examined. Subsequently, the principal limitations of the conducted analyses are deliberated upon.

Section 5.1 is allocated to the examination of the two-turbine analyses. Following this, in section 5.2, focus is shifted to the extended wind farm scenario. Finally, section 5.3 delves into the presentation of the mooring lines analyses.

5.1. Preliminary Analyses

5.1.1. The interpretations and implications of key findings

The following interpretations and implications are derived from the key findings of the two turbine analysis:

- This study investigates the possibility of increasing power production in a two-turbine wind farm by combining turbine repositioning with yaw-based wake redirection. Specifically, when the second turbine is repositioned and the upstream turbine is yawed, it becomes feasible to achieve the same power production as the case where the upstream turbine remains stationary and the second turbine is displaced to a much greater extent.
- The results clearly indicate that the upcoming wind speed plays a crucial role in the potential gains achieved through the combination of turbine repositioning and yaw-based wake redirection. When the upcoming wind speed is below the rated wind speed, the potential power gains from this combined approach are limited. However, as the upcoming wind speed exceeds the rated wind speed, the effect of yawing the stream turbine becomes more pronounced, leading to more favourable outcomes. Throughout the analyses of the results, this outcome is due to the fact that above rated wind speed the efficiency losses of the upstream turbine when is yawed in the full load region are neglectable.
- It is noteworthy that lateral repositioning substantially outperforms longitudinal repositioning in optimizing power generation across various wind speed scenarios, aligning with prior research. Furthermore, the integration of yawing allows for a reduction in the required displacement of the upstream turbine. This reduction ranges from 0.2 to 0.5 times the rotor diameter for lateral displacement, and from 1 to 4 times the longitudinal movement for the same power efficiency achieved when the upstream turbine is not yawed. These outcomes emphasize the potential of combining both strategies, not only to enhance power output but also to lower costs associated with turbine repositioning. The addition of yaw-based wake redirection can minimize necessary turbine movements, consequently reducing repositioning costs.

5.1.2. Limitations

The main limitations that are considered for the two turbine analyses can be outlined as:

- The assumption of an ideal power curve for the wind turbine implies a sharp transition from below to above-rated wind speed, which may not be entirely realistic. Thus the results showed at 9.8 m/s and at 10 m/s are sensibly different from the conducted simulations, but that is not clearly what will happen in reality. However, the results give a good indication of what are and in what conditions the advantages of adding the yaw-based wake redirection are evident.
- The selected engineering wake models, while fast, may not offer the highest accuracy. As just two wind turbines are analysed, it could be considered to conduct advanced CFD analyses that would provide more precise assessments of the mechanics involved. However, for the sake of this master project, a fast analysis that may guarantee qualitative insights on the combinations of yaw-based wake redirection and turbine repositioning proves to be enough.

5.2. Optimized Combined Layout

5.2.1. The interpretations and implications of key findings

The following interpretations and implications are derived from the key findings of the extended wind farm analysis:

- The investigation examined a range of strategies, encompassing yaw-based wake redirection, dynamic wind farm optimization, and turbine repositioning, all aimed at enhancing wind farm efficiency. The most notable outcome was observed when all three methods were combined, resulting in the highest efficiency gains, surpassing the outcomes achieved by individual strategies. This underscores the potential of synergizing various strategies to maximize wind farm power production.
- Particularly noteworthy was the substantial influence of wind speed on the effectiveness of yaw-based redirection across all scenarios. The findings consistently aligned with the results from the analysis involving two turbines, revealing that yaw-based wake redirection primarily enhanced efficiency within the full load region and when dealing with limited movable ranges. However, below rated wind speed and with big most effective movable ranges, the benefits of introducing yaw were modest. Nevertheless, given that the costs associated with employing the yaw strategy are minimal (as it requires no extra actuators), its implementation remains justifiable.

5.2.2. Limitations

The main limitations that are considered for the extended wind farm analyses can be outlined as:

- The optimization process did not account for minimum separation distances between turbines. However, due to the relatively compact size of the considered movable range, the optimization scenarios did not lead to turbine movable ranges overlapping. Given this practical perspective, it is reasonable to assume that efficiency gains calculated with turbine repositioning would remain unchanged even if constraints on turbine separations were introduced.
- The analysis disregarded the effect of yaw on turbine repositioning (referred to as the undesired YITuR effect). The mooring lines analyses, presented in Chapter 4, demonstrated that the position mooring relocation strategy effectively maintains the desired position against environmental loads, even when turbines experience lateral loading during yawing.
- The study assumed instantaneous turbine repositioning and yaw changes. This assumption neglects the losses incurred during the transitional segments when turbines move. These losses are expected to be present in reality.
- The considered case study assumed a circular movable range. However, determining whether a relocation mechanism can ensure a specific shape (and size) for the movable range introduces numerous uncertainties. Nonetheless, the investigated movable range sizes were relatively modest compared to larger ranges explored in prior studies. This approach was chosen to exclude anchor placement from the optimization loop, a requirement for more realistic movable ranges (such as triangular or rectangular shapes, which would necessitate fewer mooring lines).

5.3. Mooring Lines System

5.3.1. The interpretations and implications of key findings

The following interpretations and implications are derived from the key findings of the mooring lines analysis:

- The optimization of mooring line lengths, considering the alterations in the thrust force direction, offers a solution to maintain the desired wind turbine position within a wide portion of the movable range, regardless of the turbine's yaw angle. This outcome underscores that position mooring effectively mitigates undesired YITUR effects, which can arise from lateral loads resulting from turbine yawing. When correlated with the findings from the analyses of the extended wind farm power maximization, it can be concluded that the power optimization results are valid in assuming that the turbine will maintain its desired position even during yawing.
- Although position mooring for turbine repositioning proves highly effective in achieving and maintaining turbine positions, it also leads to variations in tension and stiffness across different positions within the movable range. These factors are notably influenced by the turbine's specific position, wind direction, and turbine's yaw angle.
 - The most substantial changes stem from the turbine's position across the movable range. Consequently, it is prudent to acknowledge that while the floater's position can be appropriately adjusted, certain regions within the movable range may not be suitable due to elevated tensions and stiffness. Hence, an effective movable range should consider the potential inclusion of constraints on positions that experience excessive tension and stiffness.
 - Both tension and stiffness are sensitive to the relative alignment of mooring lines and the wind direction. This underscores the importance of considering anchor placement during dynamic wind farm layout optimization. This not only ensures that the movable range is optimally oriented for turbine repositioning to maximize power production but also prevents the occurrence of high tensions and stiffness in mooring lines when turbines are repositioned away from their initial installation positions.
 - The wind turbine's yaw angle indeed impacts mooring line tension and stiffness. However, these changes are negligible within the regions covered by the largest movable range analyzed in the extended wind farm assessments. The most significant changes occur in regions where tensions and stiffness are already high due to the turbine position. Consequently, considering that in these positions is less likely the turbine will be positioned, the influence of yawing becomes negligible when compared to the turbine position and mooring line orientation.

5.3.2. Limitations

The main limitations that are considered for the mooring lines analyses can be outlined as:

- It is assumed that the projection of the mooring lines on the seabed forms a straight line. However, there's limited understanding of how catenary mooring lines behave during significant displacements of floating structures. Given that a substantial section of the mooring lines rests on the seabed, the interaction between the chain and the soil becomes a factor. After relocating the floater to the desired position, the portion resting on the seabed might not move in tandem. The potential impact of this on mooring system performance remains uncertain.
- The conducted simulations adopt a quasi-static approach, and stiffness is computed with static equilibrium, based on minor body displacements. Analysis of the results highlights the pronounced sensitivity of stiffness to adjustments in mooring line length required for turbine repositioning. Dynamic analyses are necessary to discern how changes in stiffness will influence simulation dynamics, particularly in terms of design and the arrangement of the floater's natural frequencies.
- An assumption is made that mooring line length can be instantaneously adjusted in response to variations in the thrust force direction caused by wind turbine yawing. Improper correction of mooring line length when the turbine yaws can lead to modification of the floating position due to the lateral component of the thrust force.

- The wind is treated as stationary; however, potential changes in wind conditions can impact both the direction and magnitude of the thrust force, introducing complexities in controlling the position and yaw angle of the floater. Accounting for these dynamics can lead to additional design challenges.

6

Conclusion and Further Analyses

6.1. Conclusion

In this Master's thesis project, the objectives are two-fold: to provide valuable insights into the implications of combining yaw misalignment and turbine repositioning on enhancing the efficiency of a wind farm, and insights into the impact of yaw-based wake redirection when combined with position mooring on the mooring system of floating offshore wind turbines.

The results demonstrate that adding yaw-based wake redirection to turbine repositioning is most effective for wind speeds in the full-load region. The analysis of the two turbines cases revealed that this is caused by the negligible loss in the upstream, yawing turbine. In contrast, the wind speed deficit at typical distances for a downstream turbine can be significantly reduced. The results of the extended wind farm confirmed that the effect remains significant for multiple turbines, with several percent-point efficiency improvements for small movable ranges. For larger, more effective movable ranges, the contribution of yaw control drops quickly to one per cent-point or less. By adding yaw control, movable ranges can be reduced by 10 to 50%, while maintaining the same wind farm efficiency. However, the larger reduction is achieved to the smaller, less effective movable ranges. For lower wind speeds, at and below rated conditions, the effectiveness of adding yaw control quickly disappears.

Environmental loads do not significantly affect the desired positions, within the accuracy needed for AEP optimisation by repositioning, not even when the turbines get laterally loaded by yawing. The analyses of the results demonstrated that position mooring is an effective relocation strategy, as the difference between the desired position and the actual equilibrium position is the order of percent-point times the rotor diameter for a wide portion of the movable range. The more the turbine is repositioned close to the anchor, the more is difficult to maintain the required accuracy for AEP optimization. Altering the wind turbine's yaw angle does not notably influence the station-keeping performance of the system for a large region of the movable range. However, by confronting the movable range sizes explored, moving the turbine in such positions may not be required.

However, adjusting the length of the mooring lines to achieve equilibrium in different positions within the movable range significantly affects the tensions and stiffness of these lines. Specifically, for a chosen position, mooring line tension is influenced by three key factors: wind direction, the specific position of the turbine, and the turbine's yaw angle. The analysis emphasizes that the position of the turbine has the most substantial impact on mooring line tension. As the turbine moves farther from its initial installation position, the tension in the lines increases significantly, even up to five times the original tension. The relative alignment of the mooring lines and the wind direction play a crucial role in how tensions are distributed across the movable range. This implies that placing anchors strategically should consider the turbine's positions over its operational lifespan to avoid unfavourable tension and stiffness regions. The turbine's yawing does lead to minor tension changes, in the order of 5% of the mooring lines breaking tension. In light of this finding, the reduction of the movable range size to maximize power production that the addition of the yaw of the turbine for power maximization guarantees is ben-

eficial. It can be useful to avoid the need to reposition the turbine far from the installation position, in unfavourable regions due to the occurrence of high tensions.

6.2. Further Analyses

- The mooring system used to reposition the turbine has a design that is not intended to support large displacement of the platform. The following are identified gaps and may be considered in future works:
 - the effect of repositioning the floater on the soil-chain interaction and thus on the shape of the mooring line;
 - the effect of adjusting the mooring lines' length on the natural frequencies of the platform;
 - the dynamic response of the platform and the lifetime behaviour of the mooring line system and the wind turbine and floater assembly itself (i.e, fatigue behaviour);
 - only catenary mooring has been investigated. Taut mooring lines, as well as a combination of catenary and taut mooring lines, can be investigated;
 - other environmental loads apart from the wind force have been disregarded. Wave loads, especially second-order frequency loads, are expected to play a role in the platform equilibrium and thus on the performances of the mooring system;
- In the case studies considered in this Master's thesis project, the upcoming wind speed was considered stationary, and the transition of the wind from one direction to one another occurred smoothly (i.e., instantaneously). Future work may consider instationary wind speeds, which may represent a more realistic case compared to other ones analyzed in this master thesis and impact the results outlined in this project.
- Once the mooring system used for position mooring is established, an optimization strategy that may account for the costs associated with position mooring and yaw-based wake redirection may be designed and performed.
- In the literature, it is shown that the yaw-based wake redirection strategy was more effective for a different optimization function. Further studies may consider exploring a different optimization function.
- The yaw base wake redirection strategy will clearly impact the lifetime damage of the turbine yawed as it will cause an imbalance load on the rotor itself. The investigation regarding the fatigue damage of the yaw turbine may be included in a metric capable of capturing this effect.

References

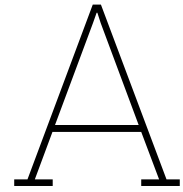
- [1] Gaertner Evan Jennifer Rinker Latha Sethuraman Frederik Zahle Benjamin Anderson Garrett Barter Nikhar Abbas Fanzhong Meng Pietro Bortolotti Witold Skrzypinski George Scott Roland Feil Henrik Bredmose Katherine Dykes Matt Shields Christopher Allen and Anthony Viselli. “Definition of the IEA 15-Megawatt Offshore Reference Wind. Golden, CO: National Renewable Energy Laboratory.” In: (2020).
- [2] Olimpo Anaya-Lara et al. “Offshore wind energy technology”. In: (2018). URL: <https://www.wiley.com/en-us/Offshore+Wind+Energy+Technology-p-9781119097761>.
- [3] Cristina L. Archer and Ahmad Vassel-Be-Hagh. “Wake steering via yaw control in multi-turbine wind farms: Recommendations based on large-eddy simulation”. In: *Sustainable Energy Technologies and Assessments* 33 (June 2019), pp. 34–43. ISSN: 22131388. DOI: 10.1016/J.SETA.2019.03.002.
- [4] Dirk Assmann, Ulrich Laumanns, and Dieter. Uh. *Renewable energy : a global review of technologies, policies and markets*. Earthscan, 2006, p. 320. ISBN: 9781138985124. URL: <https://www.routledge.com/Renewable-Energy-A-Global-Review-of-Technologies-Policies-and-Markets/Assmann/p/book/9781138985124>.
- [5] K. Atias and S.P. Ladany. “Optimal economic layout of turbines on windfarms”. In: *Wind Eng* 30.2 (2006), pp. 141–151.
- [6] N Francesco Baker. “Instructional Case Studies in the Field of Windfarm Optimization”. In: *Theses and Dissertations* (2020), pp. 2020–2032. URL: <https://scholarsarchive.byu.edu/etd>.
- [7] Nicholas F Baker et al. “Best Practices for Wake Model and Optimization Algorithm Selection in Wind Farm Layout Optimization”. In: (2019). DOI: 10.2514/6.2019-0540. URL: <https://scholarsarchive.byu.edu/facpub>.
- [8] M. Bastankhah and F. Porté-Agel. “A new analytical model for wind-turbine wakes”. In: *Renewable energy* 70 (2014), pp. 116–123.
- [9] S. Boersma et al. “A tutorial on control-oriented modeling and control of wind farms”. In: *Proceedings of the American Control Conference* (June 2017), pp. 1–18. ISSN: 07431619. DOI: 10.23919/ACC.2017.7962923.
- [10] S. Boersma et al. “A tutorial on control-oriented modeling and control of wind farms”. In: *Proceedings of the American Control Conference* (June 2017), pp. 1–18. ISSN: 07431619. DOI: 10.23919/ACC.2017.7962923.
- [11] Pietro Borlotti et al. *Systems Engineering in Wind Energy - WP2.1 Reference Wind Turbines*. 2019. URL: <https://www.nrel.gov/docs/fy19osti/73492.pdf>.
- [12] L.Rebecca Busby. *Wind power : the industry grows up | WorldCat.org*. 2012. URL: <https://www.worldcat.org/it/title/wind-power-the-industry-grows-up/oclc/820829209>.
- [13] Naima Charhouni, Mohammed Sallaou, and Khalifa Mansouri. “Realistic wind farm design layout optimization with different wind turbines types”. In: *International Journal of Energy and Environmental Engineering* 10 (3 Sept. 2019), pp. 307–318. ISSN: 22516832. DOI: 10.1007/S40095-019-0303-2/FIGURES/6. URL: <https://link.springer.com/article/10.1007/s40095-019-0303-2>.
- [14] Søren Christiansen, Thomas Bak, and Torben Knudsen. “Damping Wind and Wave Loads on a Floating Wind Turbine Damping Wind and Wave Loads on a Floating Wind Turbine”. In: 6 (2013), pp. 4097–4116. ISSN: 1996-1073. DOI: 10.3390/en6084097. URL: www.mdpi.com/journal/energiesArticle.
- [15] C. Cossu. “Evaluation of tilt control for wind-turbine arrays in the atmospheric boundary layer”. In: *Wind Energy Science* 6.3 (2021), pp. 663–675. DOI: 10.5194/wes-6-663-2021. URL: <https://wes.copernicus.org/articles/6/663/2021/>.

- [16] P.A. Crosby. "Application of a Monte Carlo optimization technique to a cluster of wind turbines". In: *J Sol Energy Eng Trans ASME* 109.1987 (), pp. 330–336.
- [17] Wilson D. et al. "Evolutionary computation for wind farm layout optimization". In: *Renewable Energy* 126 (2018), pp. 681–691. ISSN: 0960-1481.
- [18] H. S. Dhiman, D. Deb, and A. M. Foley. "Bilateral Gaussian wake model formulation for wind farms: A forecasting based approach". In: *Renewable and Sustainable Energy Reviews* 127 (2020), p. 109873.
- [19] DNV-OS-E301. 2021. URL: <https://rules.dnv.com/servicedocuments/dnvpmp/>.
- [20] C.N. Elkinton, J.E. Manwell, and J.G. McGowan. "Optimizing the layout of offshore wind energy systems". In: *Mar Technol Soc J* 42.2 (2008), pp. 19–27.
- [21] Equinor. *Floating wind - Equinor*. <https://www.equinor.com/energy/floating-wind>. 2022.
- [22] Paul Fleming et al. "Simulation comparison of wake mitigation control strategies for a two-turbine case". In: *Wind Energy* 18 (12 2015). ISSN: 10991824. DOI: 10.1002/we.1810.
- [23] Paul A. Fleming et al. "Wind plant system engineering through optimization of layout and yaw control". In: *Wind Energy* 19 (2 Feb. 2016), pp. 329–344. ISSN: 1099-1824. DOI: 10.1002/we.1836. URL: <https://onlinelibrary.wiley.com/doi/full/10.1002/we.1836> <https://onlinelibrary.wiley.com/doi/abs/10.1002/we.1836> <https://onlinelibrary.wiley.com/doi/10.1002/we.1836>.
- [24] S. Frandsen and et al. "Analytical modelling of wind speed deficit in large offshore wind farms". In: *Wind Energy: An International Journal for Progress and Applications in Wind Power Conversion Technology* 9.1-2 (2006), pp. 39–53.
- [25] X. Gao, H. Yang, and L. Lu. "Optimization of wind turbine layout position in a wind farm using a newly-developed two-dimensional wake model". In: *Applied Energy* 174 (2016), pp. 192–200.
- [26] M. Gaumond et al. "Evaluation of the wind direction uncertainty and its impact on wake modeling at the Horns Rev offshore wind farm". In: *DTU Wind Energy, Risø Campus, Roskilde, Denmark* (2020).
- [27] S.A. Grady, M.Y. Hussaini, and M.M. Abdullah. "Placement of wind turbines using genetic algorithms". In: *Renew Energy* 30 (2005), pp. 259–270.
- [28] Damien Haberlin, Alfonso Cohuo, and Thomas K. Doyle. *Ecosystem benefits of floating offshore wind*. Cork: MaREI – Science Foundation Ireland Centre for Energy, Climate and Marine, University College Cork, 2022.
- [29] Allen Christopher Anthony Viselli Habib Dagher Andrew Goupee Evan Gaertner Nikhar Abbas Matthew Hall and Garrett Barter. "Definition of the UMaine VoltturnUS-S Reference Platform Developed for the IEA Wind 15-Megawatt Offshore Reference Wind Turbine". In: ().
- [30] Chenlu Han and Ryozo Nagamune. "Platform position control of floating wind turbines using aerodynamic force". In: *Renewable Energy* 151 (May 2020), pp. 896–907. ISSN: 18790682. DOI: 10.1016/j.renene.2019.11.079.
- [31] N. Hansen, Y. Akimoto, and P. Baudis. "CMA-ES/pycma on Github". In: *Zenodo* (2019). DOI: 10.5281/zenodo.2559634.
- [32] N. Hansen and S. Kern. "Evaluating the CMA Evolution Strategy on Multimodal Test Functions". In: *Computational Science and Engineering Laboratory (CSE Lab), Swiss Federal Institute of Technology (ETH) Zurich, Switzerland* (2010). {nikolaus.hansen,skern}@inf.ethz.ch. URL: <http://www.icos.ethz.ch/cse/>.
- [33] Jeffrey R. Homer and Nagamune R. Han C. "Position Control of an Offshore Wind Turbine with a Semi-submersible Floating Platform Using the Aerodynamic Force". In: *2016 IEEE Canadian Conference on Electrical and Computer Engineering (CCECE)* (2017). URL: <https://ieeexplore.ieee.org/stamp/stamp.jsp?tp=&arnumber=7726687&tag=1>.
- [34] Michael F. Howland, Sanjiva K. Lele, and John O. Dabiri. "Wind farm power optimization through wake steering". In: *Proceedings of the National Academy of Sciences of the United States of America* 116 (29 2019), pp. 14495–14500. ISSN: 10916490. DOI: 10.1073/PNAS.1903680116/-/DCSUPPLEMENTAL. URL: www.pnas.org/cgi/doi/10.1073/pnas.1903680116.

- [35] *Handbook of Offshore Engineering (2-volume set)*. Elsevier, 2005. - Cerca con Google. Elsevier, 2005.
- [36] IEA. "IEA Report 2022". In: *Wind Electricity (2022)*. URL: <https://www.iea.org/reports/wind-electricity>.
- [37] IEA Wind TCP Task 37: Systems Engineering in Wind Energy. *IEA Wind Task 37*. 2023. URL: <https://iea-wind.org/task37/> (visited on 03/06/2023).
- [38] IRENA and CPI. *Global landscape of renewable energy finance, 2023*. Tech. rep. Abu Dhabi: International Renewable Energy Agency, 2023.
- [39] T. Ishihara and G. W. Qian. "A new Gaussian-based analytical wake model for wind turbines considering ambient turbulence intensities and thrust coefficient effects". In: *Journal of Wind Engineering and Industrial Aerodynamics* 177 (2018), pp. 275–292.
- [40] T. Ishihara, A. Yamaguchi, and Y. Fujino. "Development of a new wake model based on a wind tunnel experiment". In: *Global wind power* 6 (2004).
- [41] Ángel Jiménez et al. "Application of a LES technique to characterize the wake deflection of a wind turbine in yaw". In: *WiEn* 13 (6 Sept. 2010), pp. 559–572. ISSN: 10991824. DOI: 10.1002/WE.380. URL: <https://ui.adsabs.harvard.edu/abs/2010WiEn...13..559J/abstract>.
- [42] John K. Kaldellis, Panagiotis Triantafyllou, and Panagiotis Stinis. "Critical evaluation of Wind Turbines' analytical wake models". In: *Renewable and Sustainable Energy Reviews* 144 (July 2021). ISSN: 18790690. DOI: 10.1016/j.rser.2021.110991.
- [43] F.C. Kaminsky and R.H. Kirchhoff. "Optimal spacing of wind turbines in a wind energy power plant". In: *Sol Energy* 39.6 (1987), pp. 467–471.
- [44] I. Katic, J. Højstrup, and N. O. Jensen. "A simple model for cluster efficiency". In: *European wind energy association conference and exhibition*. Vol. 1. 1986, pp. 407–410.
- [45] Ali C. Kheirabadi and Ryoza Nagamune. *A quantitative review of wind farm control with the objective of wind farm power maximization*. 2019. DOI: 10.1016/j.jweia.2019.06.015.
- [46] Ali C. Kheirabadi and Ryoza Nagamune. "Modeling and power optimization of floating offshore wind farms with yaw and induction-based turbine repositioning". In: vol. 2019-July. 2019. DOI: 10.23919/acc.2019.8814600.
- [47] Ufuktan Kilinc. *Dynamic wind farm layout optimization. To find the optimal spots for movable floating offshore wind turbines through dynamic repositioning*. 2022.
- [48] Helle Kristine et al. "Control of Thruster Assisted Position Mooring System on Floating Production Storage and Offloading". In: ().
- [49] A. Kusiak and Z. Song. "Design of wind farm layout for maximum wind energy capture". In: *Renewable Energy* 35.3 (2010), pp. 685–694.
- [50] G. C. Larsen. *A simple wake calculation procedure*. Tech. rep. Risø National Laboratory, 1988.
- [51] Gunner C. Larsen et al. "Yaw induced wake deflection - a full-scale validation study". In: *Journal of Physics - Conference Series* 1618.6 (2020), p. 062047. DOI: 10.1088/1742-6596/1618/6/062047.
- [52] P. B.S. Lissaman. "Energy Effectiveness of Arbitrary Arrays of Wind Turbines". In: <https://doi.org/10.2514/3.62441> 3 (6 May 1979), pp. 323–328. ISSN: 01460412. DOI: 10.2514/3.62441. URL: <https://arc.aiaa.org/doi/10.2514/3.62441>.
- [53] B. Liu and J. Yu. "Effect of Mooring Parameters on Dynamic Responses of a Semi-Submersible Floating Offshore Wind Turbine". In: *Sustainability* 14 (2022), p. 14012. DOI: 10.3390/su142114012.
- [54] Kai Tung Ma et al. "Mooring designs for floating offshore wind turbines leveraging experience from the oil and gas industry". In: *Proceedings of the International Conference on Offshore Mechanics and Arctic Engineering - OMAE* 1 (2021). DOI: 10.1115/OMAEE2021-60739.

- [55] Rafael Valotta Rodrigues Bjarke Tobias Olsen Mads M. Pedersen Alexander Meyer Forsting Paul van der Laan Riccardo Riva Leonardo A. Alcayaga Romà Javier Criado Risco Mikkel Friis-Møller Julian Quick Jens Peter Schøler Christiansen and Pierre-Elouan Réthoré. “PyWake 2.5.0: An open-source wind farm simulation tool”. In: (Feb. 2023). URL: <https://gitlab.windenergy.dtu.dk/TOPFARM/PyWake>.
- [56] G. Marmidis, S. Lazarou, and E. Pyrgioti. “Optimal placement of wind turbines in a wind park using Monte Carlo simulation”. In: *Renew Energy* 33 (2008), pp. 1455–1460.
- [57] Martins and Andrew Ning. *Engineering Design Optimization*. 2021. URL: <https://mdobook.github.io/>.
- [58] Andrew Moore, James Price, and Marianne Zeyringer. “The role of floating offshore wind in a renewable focused electricity system for Great Britain in 2050”. In: *Energy Strategy Reviews* 22 (2018), pp. 270–278. DOI: 10.1016/j.esr.2018.10.002. URL: <https://doi.org/10.1016/j.esr.2018.10.002>.
- [59] S.G. Mosetti, C. Poloni, and B. Diviacco. “Optimization of wind turbine positioning in large wind-farms by means of a genetic algorithm”. In: *J Wind Eng Ind Aerodyn* 51 (1994), pp. 105–116.
- [60] Dong T. Nguyen and Asgeir J. Sørensen. “Switching control for thruster-assisted position mooring”. In: *Control Engineering Practice* 17 (9 Sept. 2009), pp. 985–994. ISSN: 0967-0661. DOI: 10.1016/J.CONENGPRACT.2009.03.001.
- [61] A.G. Olabi et al. “Wind Energy Contribution to the Sustainable Development Goals: Case Study on London Array”. In: *Sustainability* 15 (2023), p. 4641. DOI: 10.3390/su15054641.
- [62] U.A. Ozturk and B.A. Norman. “Heuristic methods for wind energy conversion system positioning”. In: *Electr Power Syst Res* 70 (2004), pp. 179–185.
- [63] Jeom Kee Paik. “Mooring system engineering for offshore structures”. In: *Ships and Offshore Structures* 14 (7 Oct. 2019), pp. 788–788. ISSN: 1744-5302. DOI: 10.1080/17445302.2019.1636537.
- [64] Fernando Porté-Agel, Majid Bastankhah, and Sina Shamsoddin. “Wind-turbine and wind-farm flows : a review.” In: *Boundary-layer meteorology, 2020, Vol. 174, pp. 1-59 [Peer Reviewed Journal]* 174 (1 Jan. 2020), pp. 1–59. ISSN: 15731472. DOI: 10.1007/s10546-019-00473-0. URL: <https://doi.org/10.1007/s10546-019-00473-0>.
- [65] Guo-Wei Qian and Takeshi Ishihara. “A New Analytical Wake Model for Yawed Wind Turbines”. In: *Department of Civil Engineering, School of Engineering, The University of Tokyo* (2018).
- [66] Makbul A.M. Ramli, Housseem R.E.H. Boucekara, and Ahmad H. Milyani. “Wind farm layout optimization using a multi-objective electric charged particles optimization and a variable reduction approach”. In: *Energy Strategy Reviews* 45 (2023), p. 101016. ISSN: 2211-467X. DOI: <https://doi.org/10.1016/j.esr.2022.101016>. URL: <https://www.sciencedirect.com/science/article/pii/S2211467X22002103>.
- [67] P.-E. Réthoré. *State of the art in wind farm layout optimization*. Available from: <http://windenergyresearch.org/2010/10/state-of-the-art-in-wind-farm-layout-optimization/> [accessed Feb. 2013]. 2010.
- [68] R.A. Rivas et al. “Solving the turbine positioning problem for large offshore wind farms by simulated annealing”. In: *Wind Eng* 33.3 (2009), pp. 287–298.
- [69] A N Robertson and J M Jonkman. “Loads Analysis of Several Offshore Floating Wind Turbine Concepts”. In: (2011). URL: www.deepcwind.org.
- [70] S. F. Rodrigues et al. “Wake losses optimization of offshore wind farms with moveable floating wind turbines”. In: *Energy Conversion and Management* 89 (2015). ISSN: 01968904. DOI: 10.1016/j.enconman.2014.11.005.
- [71] Nejmi Saadallah and Erlend Randeberg. “Dynamic repositioning in floating wind farms”. In: *NORCE Energy* (2020).
- [72] M. Sawant et al. “A Review on State-of-the-Art Reviews in Wind-Turbine- and Wind-Farm-Related Topics”. In: *Energies* 14.8 (2021), p. 2041. DOI: 10.3390/en14082041.

- [73] Christopher R. Schwalm, Spencer Glendon, and Philip B. Duffy. "RCP8.5 tracks cumulative CO2 emissions". In: *Proceedings of the National Academy of Sciences* 117.33 (2020), pp. 19656–19657. DOI: 10.1073/pnas.2007117117. URL: <https://doi.org/10.1073/pnas.2007117117>.
- [74] Lucas Sens, Ulf Neuling, and Martin Kaltschmitt. "Capital expenditure and levelized cost of electricity of photovoltaic plants and wind turbines – Development by 2050". In: *Renewable Energy* 185 (Feb. 2022), pp. 525–537. ISSN: 0960-1481. DOI: 10.1016/J.RENENE.2021.12.042.
- [75] Rabia Shakoor et al. "Wake effect modeling: A review of wind farm layout optimization using Jensen's model". In: *Renewable and Sustainable Energy Reviews* 58 (May 2016), pp. 1048–1059. ISSN: 18790690. DOI: 10.1016/J.RSER.2015.12.229.
- [76] M. Hall S. Housner S. Srinivas and S. Wilson. "MoorPy: Quasi-Static Mooring Analysis in Python". In: *National Renewable Energy Laboratory* (2021). URL: <doi.org/10.11578/dc.20210726.1>.
- [77] Mohammed Khair Al-Solihat and Meyer Nahon. "Mooring and hydrostatic restoring of offshore floating wind turbine platforms". In: Jan. 2015. DOI: 10.1109/OCEANS.2014.7003269.
- [78] Asgeir J. Sørensen. "A survey of dynamic positioning control systems". In: *Annual Reviews in Control* 35 (1 Apr. 2011), pp. 123–136. ISSN: 1367-5788. DOI: 10.1016/J.ARCONTROL.2011.03.008.
- [79] Tyler Stehly and Patrick Duffy. *2021 Cost of Wind Energy Review*. Tech. rep. National Renewable Energy Laboratory, Dec. 2022.
- [80] R.J. Templin. *An estimation of the interaction of windmills in widespread array*. Laboratory Report LTR-LA-171. National Aeronautical Establishment, 1974.
- [81] A. Tesauro, P.-E. Réthoré, and G.C. Larsen. "State of the art of wind farm optimization". In: *Proceedings of EWEA 2012 – European Wind Energy Conference & Exhibition, Copenhagen, Denmark*. 2012.
- [82] Angelo ; Tesauro et al. "General rights State of the art of wind farm optimization State of the Art of Wind Farm Optimization". In: *Downloaded from orbit.dtu.dk on* (2022).
- [83] J J Thomas and A Ning. "A method for reducing multi-modality in the wind farm layout optimization problem". In: *Journal of Physics: Conference Series* 1037.4 (2018), p. 042012.
- [84] L. Tian and et al. "Development and validation of a new two-dimensional wake model for wind turbine wakes". In: *Journal of Wind Engineering and Industrial Aerodynamics* 137 (2015), pp. 90–99.
- [85] Weiyang Tong et al. "Impact of different wake models on the estimation of wind farm power generation". In: *12th AIAA Aviation Technology, Integration and Operations (ATIO) Conference and 14th AIAA/ISSMO Multidisciplinary Analysis and Optimization Conference* (2012). DOI: 10.2514/6.2012-5430. URL: <https://arc.aiaa.org/doi/10.2514/6.2012-5430>.
- [86] M. Wagner, J. Day, and F. Neumann. "A fast and effective local search algorithm for optimizing the placement of wind turbines". In: *Renew Energy* 51 (2013), pp. 65–70.
- [87] Ryan Wiser et al. "Expert elicitation survey predicts 37% to 49% declines in wind energy costs by 2050". In: *Nature Energy* 6.5 (2021), pp. 555–565. DOI: 10.1038/s41560-021-00810-z. URL: <https://doi.org/10.1038/s41560-021-00810-z>.
- [88] Yongyan Wu et al. "Mooring Tensioning Systems for Offshore Platforms: Design, Installation, and Operating Considerations". In: *Proceedings of the Annual Offshore Technology Conference* 1 (Apr. 2018), pp. 229–244. ISSN: 01603663. DOI: 10.4043/28720-MS. URL: /OTCONF/proceedings-abstract/180TC/1-180TC/179747.
- [89] S. Xie and C. Archer. "Self-similarity and turbulence characteristics of wind turbine wakes via large-eddy simulation". In: *Wind Energy* 18.10 (2015), pp. 1815–1838.
- [90] Kun Xu et al. "Design and comparative analysis of alternative mooring systems for floating wind turbines in shallow water with emphasis on ultimate limit state design". In: *Ocean Engineering* 219 (Nov. 2020). DOI: 10.1016/j.oceaneng.2020.108377.
- [91] 'Claire' Zhao et al. "Global Benefits and Operational Challenges of Vessel Relocation". In: (May 2015), V003T02A059. DOI: 10.1115/OMAE2015-41199.



Additional results for position mooring of UMaine VoltturnUS-S

Figure A.1 displays the contours plot of the sway mooring system stiffness term when the turbine yaw is 0° for different upcoming wind scenarios.

A.0.1. Sway stiffness terms

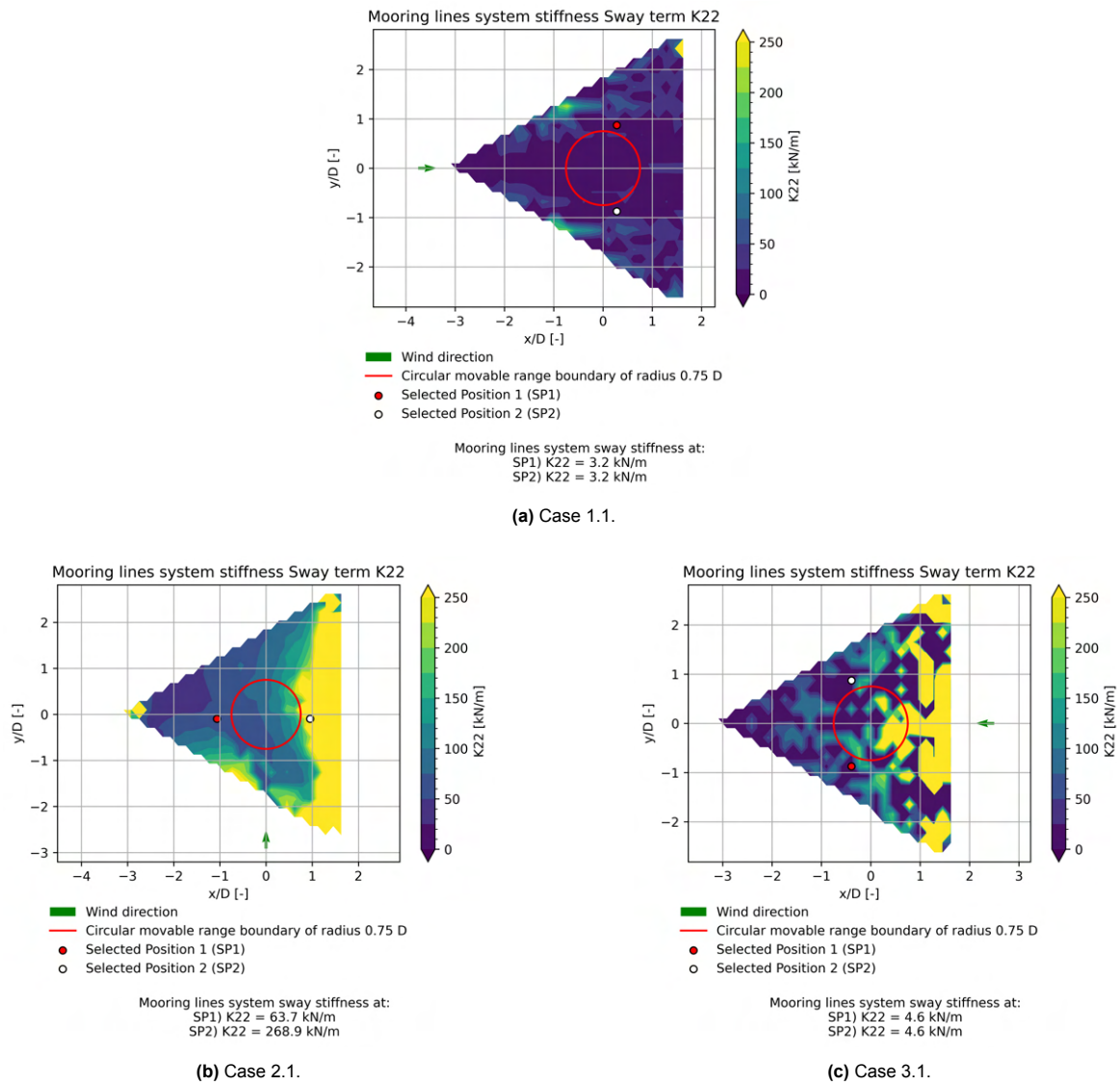
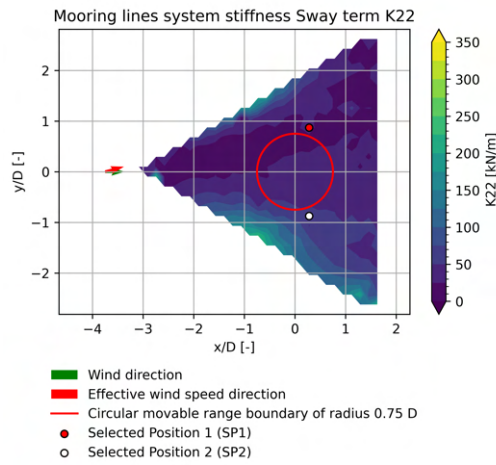


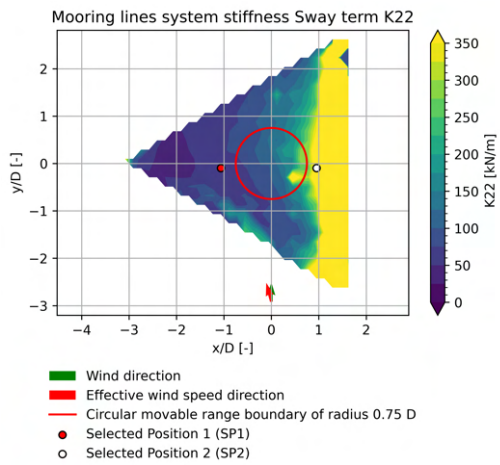
Figure A.1: Contours plot of the sway mooring system stiffness term when the turbine yaw is 0° for different upcoming wind scenarios

Figure A.2 displays the contours plot of the sway mooring system stiffness term when the turbine yaw is 15° for different upcoming wind scenarios.



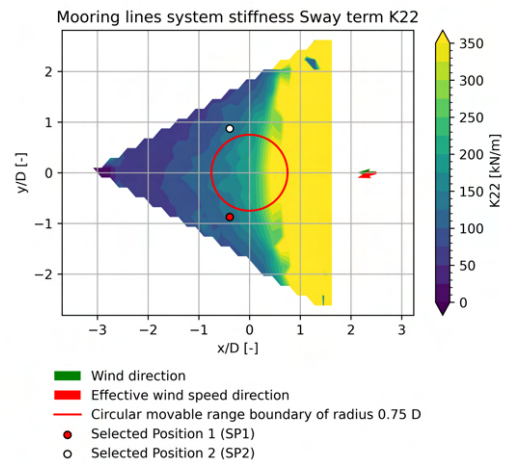
Differences of the mooring lines system sway stiffness from 0° yaw at:
 SP1) DK22 = 769.1 %
 SP2) DK22 = 1761.0 %

(a) Case 1.2.



Differences of the mooring lines system sway stiffness from 0° yaw at:
 SP1) DK22 = -11.5 %
 SP2) DK22 = 44.3 %

(b) Case 2.2.



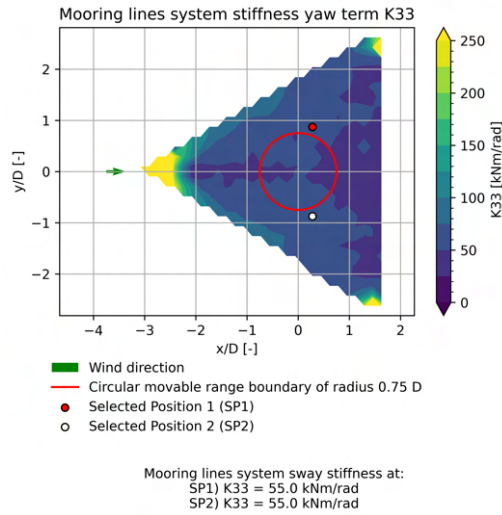
Differences of the mooring lines system sway stiffness from 0° yaw at:
 SP1) DK22 = 3064.8 %
 SP2) DK22 = 2720.2 %

(c) Case 3.2.

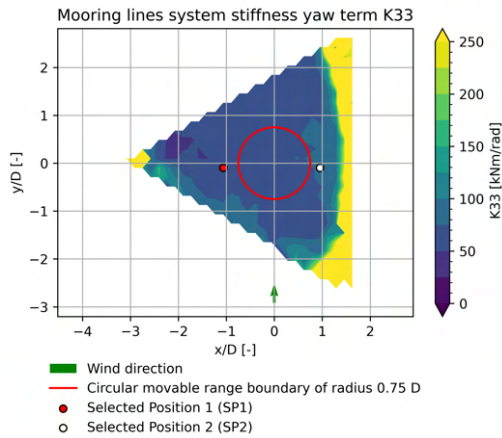
Figure A.2: Contours plot of the sway mooring system stiffness term when the turbine yaw is 15° for different upcoming wind scenarios

A.0.2. Yaw stiffness terms

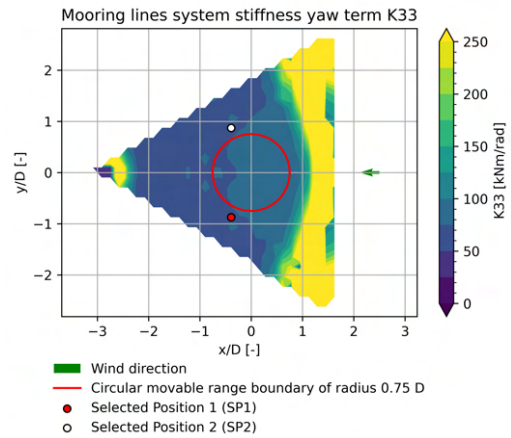
Figure A.3 shows the plots of the yaw mooring system stiffness term when the turbine yaw is 0° for different upcoming wind scenarios.



(a) Case 1.1.



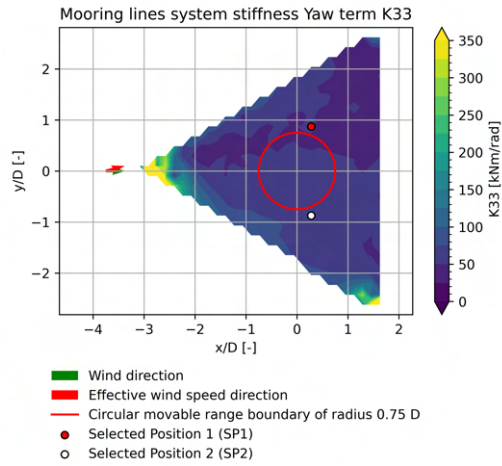
(b) Case 2.1.



(c) Case 3.1.

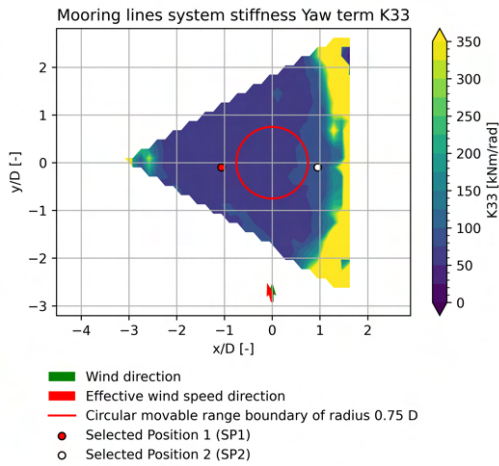
Figure A.3: Contours plot of the yaw mooring system stiffness term when the turbine yaw is 0° for different upcoming wind scenarios

Figure A.4 shows the plots of the yaw mooring system stiffness term when the turbine yaw is 15° for different upcoming wind scenarios.



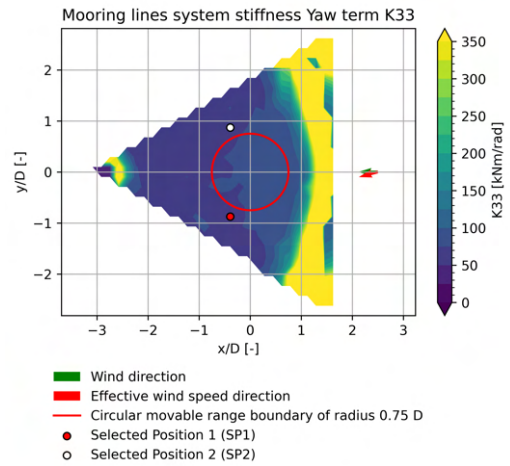
Differences of the mooring lines system yaw stiffness from 0° yaw at:
 SP1) DK33 = -6.5 %
 SP2) DK33 = 11.7 %

(a) Case 1.1.



Differences of the mooring lines system yaw stiffness from 0° yaw at:
 SP1) DK33 = -8.0 %
 SP2) DK33 = 9.7 %

(b) Case 2.1.



Differences of the mooring lines system yaw stiffness from 0° yaw at:
 SP1) DK33 = 5.1 %
 SP2) DK33 = 1.7 %

(c) Case 3.1.

Figure A.4: Contours plot of the yaw mooring system stiffness term when the turbine yaw is 15° for different upcoming wind scenarios